
Doctoral Dissertations

Student Theses and Dissertations

Spring 2012

Organoclay dispersion in linear low-density polyethylene and maleated linear low-density polyethylene via supercritical carbon dioxide processing

Matthew J. Factor

Follow this and additional works at: https://scholarsmine.mst.edu/doctoral_dissertations

 Part of the [Chemical Engineering Commons](#)

Department: Chemical and Biochemical Engineering

Recommended Citation

Factor, Matthew J., "Organoclay dispersion in linear low-density polyethylene and maleated linear low-density polyethylene via supercritical carbon dioxide processing" (2012). *Doctoral Dissertations*. 1961. https://scholarsmine.mst.edu/doctoral_dissertations/1961

This thesis is brought to you by Scholars' Mine, a service of the Missouri S&T Library and Learning Resources. This work is protected by U. S. Copyright Law. Unauthorized use including reproduction for redistribution requires the permission of the copyright holder. For more information, please contact scholarsmine@mst.edu.

ORGANOCLAY DISPERSION IN LINEAR LOW-DENSITY POLYETHYLENE AND
MALEATED LINEAR LOW-DENSITY POLYETHYLENE VIA
SUPERCRITICAL CARBON DIOXIDE PROCESSING

by

MATTHEW JOHN FACTOR

A DISSERTATION

Presented to the Faculty of the Graduate School of the
MISSOURI UNIVERSITY OF SCIENCE AND TECHNOLOGY

In Partial Fulfillment of the Requirements for the Degree

DOCTOR OF PHILOSOPHY

in

CHEMICAL ENGINEERING

2012

Approved by

Sunggyu Lee, Advisor
Douglas Ludlow, Co-Advisor
Yangchuan Xing
David Westenberg
Fatih Dogan

© 2012

Matthew John Factor

All Rights Reserved

ABSTRACT

Research into polymer-clay nanocomposites (PCN's) has been ongoing for decades as a result of the property enhancements offered by clay. To fully exploit these property enhancements, organically modified clays (organoclays) are utilized to promote clay delamination by reducing the disparity between the hydrophilicity of the clay and the hydrophobicity of the highly used polyolefin polymer. Since the organic modification of organoclays can degrade at temperatures typical to many polymers during melt-mix processing, this work utilizes the low-temperature processing fluid supercritical carbon dioxide (scCO₂) to disperse an organoclay into the highly used polymer LLDPE and ascertains the associated processing conditions for achieving this goal.

Investigations into the LLDPE resin size, scCO₂ processing time, scCO₂ capability and the processing component compatibility were undertaken to better understand the important parameters to achieving organoclay dispersion, in terms of infusion and intercalation/exfoliation behavior. A LLDPE pellet resin showed improved dispersion and obtainable information over that of a granule resin, securing the choice of resin for subsequent experiments. Experiments undertaken with pellet resin exhibited that a 1-hr processing time was insufficient for organoclay infusion into LLDPE, however when infusion occurs, intercalation/exfoliation can be affected by scCO₂. Increasing the compatibility of LLDPE with clay and the processing fluid revealed that the increased compatibility had altered the effect of scCO₂. Further analysis with the 93A-infused samples was conducted in order to gain a better understanding of the effect of scCO₂ processing, such as the quantity and size of clay particles dispersed and changes to the polymer incurred by processing.

ACKNOWLEDGMENTS

I would like to express my gratitude to those who have helped me over the course of my graduate career, aiding in the pursuit of my Ph.D. First and foremost, I would like to thank Dr. Sunggyu Lee for his moral, intellectual and financial support. His extensive wisdom enhanced my graduate experience in and out of the lab. It has been an honor to be his doctoral student and will be a privilege to have him as a confidant in my pursuit of future endeavors. Also, I would like to thank Dr. Douglas Ludlow for his advisement and his diligence in handling matters pertinent to the attainment of my Ph.D. I would like to show my appreciation to the U.S. Department of Education for awarding me the GAANN fellowship as a source of financial support. My doctoral committee deserves recognition as well for the time and effort they put forth in assessing the research I conducted for my Ph.D. Last but not least, I would like to thank my family and friends for their encouragement and the welcomed diversions they have afforded me over the years.

TABLE OF CONTENTS

	Page
ABSTRACT.....	iii
ACKNOWLEDGMENTS	iv
LIST OF FIGURES	ix
LIST OF TABLES.....	xii
SECTION	
1. INTRODUCTION.....	1
1.1. POLYMER-CLAY NANOCOMPOSITES (PCN's)	1
1.2. MOTIVATION.....	1
1.3. OBJECTIVE	3
1.4. APPROACH.....	3
2. REVIEW OF LITERATURE.....	5
2.1. POLYETHYLENE	5
2.1.1. Polymerization Methods.....	5
2.1.1.1 Free-radical polymerization	6
2.1.1.2 Coordination polymerization	8
2.1.1.3 Metallocene catalyst polymerization (single-site)	9
2.1.2. Grades.....	9
2.1.2.1 High-density polyethylene (HDPE).....	9
2.1.2.2 Low-density polyethylene (LDPE).....	10
2.1.2.3 Linear low-density polyethylene (LLDPE)	11
2.1.2.4 Other polyethylenes	12
2.2. CLAY.....	12
2.2.1. Montmorillonite (MMT)	13
2.2.2. Organoclay	16
2.3. POLYMER-CLAY NANOCOMPOSITES.....	18
2.3.1. Polymer-Clay Compatibility	19
2.3.2. Characterization.....	20
2.3.2.1 X-ray diffraction (XRD)	20

2.3.2.2	Fourier transform infrared (FTIR) spectrometry	22
2.3.2.3	Scanning electron microscopy (SEM)	23
2.3.2.4	Thermogravimetric analysis (TGA).....	24
2.3.2.5	Differential scanning calorimetry (DSC).....	24
2.4.	SUPERCRITICAL CARBON DIOXIDE (ScCO ₂).....	25
2.4.1.	ScCO ₂ Background.....	25
2.4.2.	ScCO ₂ as a Solvent.....	27
2.4.3.	ScCO ₂ as a Plasticizer	27
2.4.4.	ScCO ₂ Diffusion.....	28
2.4.5.	ScCO ₂ Intercalation/Exfoliation of Clay	29
3.	EXPERIMENTAL APPARATUS	31
3.1.	ScCO ₂ PROCESSING SYSTEM	31
3.2.	EXTRUSION SYSTEM	31
3.3.	X-RAY DIFFRACTION (XRD)	33
3.4.	FOURIER TRANSFORM INFRARED (FTIR) SPECTROMETRY	34
3.5.	THERMOGRAVIMETRIC ANALYSIS (TGA).....	35
3.6.	DIFFERENTIAL SCANNING CALORIMETRY (DSC)	35
3.7.	SCANNING ELECTRON MICROSCOPY (SEM).....	36
4.	EXPERIMENTAL MATERIALS AND PROCEDURE.....	37
4.1.	MATERIALS.....	37
4.2.	PROCEDURE.....	39
4.2.1.	Granule LLDPE Experiments	39
4.2.2.	LLDPE and LLDPE-g-MA Experiments	40
4.2.3.	LLDPE Experiments (1-hr)	40
4.2.4.	Extruded LLDPE/93A Experiments.....	41
5.	EXPERIMENTAL ANALYSIS.....	43
5.1.	DISPERSION ANALYSIS BY XRD.....	43
5.1.1.	Results	43
5.1.1.1	Resin size experiments: granule vs. pellet.....	43
5.1.1.1.1	LLDPE granules in scCO ₂	43
5.1.1.1.2	LLDPE pellets in scCO ₂	45

5.1.1.1.3 Summary	47
5.1.1.2 Processing time experiments: LLDPE in scCO ₂ for 1 hr.....	48
5.1.1.3 ScCO ₂ capability experiments: extruded LLDPE/93A.....	50
5.1.1.4 Compatibility experiments: LLDPE-g-MA	54
5.1.2. Discussion	57
5.1.2.1 Factors affecting clay gallery.....	57
5.1.2.1.1 Molecular size.....	57
5.1.2.1.2 Surfactant conformation.....	58
5.1.2.1.3 Surfactant-clay surface interaction	58
5.1.2.2 Analysis of samples	59
5.1.2.2.1 Cause of clay gallery changes.....	59
5.1.2.2.2 Effect of processing conditions.....	60
5.2. EXTENDED ANALYSIS OF 93A-INFUSED LLDPE AND LLDPE-g-MA.	61
5.2.1. Results	61
5.2.1.1 DSC.....	61
5.2.1.2 TGA	65
5.2.1.2.1 LLDPE	65
5.2.1.2.2 LLDPE-g-MA.....	68
5.2.1.3 FTIR.....	72
5.2.1.3.1 LLDPE	77
5.2.1.3.2 LLDPE-g-MA.....	77
5.2.1.3.3 Uniform dispersion analysis	77
5.2.1.4 SEM	78
5.2.1.4.1 LLDPE	78
5.2.1.4.2 LLDPE-g-MA.....	78
5.2.2. Discussion	80
5.2.2.1 Effect of scCO ₂ on the polymer.....	81
5.2.2.1.1 DSC: crystallinity.....	81
5.2.2.1.2 TGA: thermal stability	82
5.2.2.2 Quantity of 93A infused.....	83
5.2.2.2.1 TGA vs. FTIR: LLDPE.....	84

5.2.2.2.2 TGA vs. FTIR: LLDPE-g-MA	85
5.2.2.2.3 TGA vs. FTIR: accuracy analysis.....	86
5.2.2.2.4 Effect of processing conditions: LLDPE	86
5.2.2.2.5 Effect of processing conditions: LLDPE-g-MA	87
5.2.2.3 Visual inspection.....	88
5.2.2.3.1 LLDPE	88
5.2.2.3.2 LLDPE-g-MA	90
6. CONCLUSIONS	94
APPENDIX.....	97
BIBLIOGRAPHY.....	110
VITA	115

LIST OF FIGURES

	Page
Figure 2.1. Intermolecular chain transfer mechanism.....	7
Figure 2.2. Intramolecular “back-biting” mechanism.....	7
Figure 2.3. Diagram of MMT clay layers	14
Figure 2.4. Energy of attraction for van der Waals forces as a function of the interlamellar distance between two MMT clay platelets (From equation in Ngo et al. ¹⁷)	15
Figure 2.5. Configurations of clay within a polymer-clay nanocomposite.....	19
Figure 2.6. Carbon dioxide phase diagram	26
Figure 2.7. Carbon dioxide density-pressure isotherms (From Peng-Robinson equation of state with Mathias-type volume shift ³¹)	26
Figure 3.1. Schematic for the scCO ₂ processing system.....	32
Figure 3.2. Schematic for the scCO ₂ reactor.....	32
Figure 3.3. Schematic for extrusion and pelletizer system	33
Figure 4.1. Methyl dihydrogenated tallow ammonium (organic modification of 93A) ..	37
Figure 5.1. XRD patterns of granule LLDPE/93A samples	44
Figure 5.2. XRD patterns of pellet LLDPE/93A samples.....	46
Figure 5.3. XRD patterns of LLDPE/93A samples in scCO ₂ for 1 hr	49
Figure 5.4. XRD patterns of LLDPE/93A samples (– –) in scCO ₂ for 1 vs. 3-hr periods	49
Figure 5.5. XRD patterns of LLDPE/93A samples (– +) in scCO ₂ for 1 vs. 3-hr periods	50
Figure 5.6. XRD patterns of X LLDPE/93A samples.....	51
Figure 5.7. XRD patterns of X/scCO ₂ LLDPE/93A samples	52
Figure 5.8. XRD patterns of LLDPE/93A samples for X vs. X/scCO ₂ at 1 wt% 93A	52

Figure 5.9. XRD patterns of LLDPE/93A samples for X vs. X/scCO ₂ at 5 wt% 93A	53
Figure 5.10. XRD patterns of LLDPE/93A samples for X vs. X/scCO ₂ at 13 wt% 93A	53
Figure 5.11. XRD patterns of LLDPE-g-MA/93A samples	55
Figure 5.12. Example of DSC curves produced by LLDPE/93A and LLDPE-g-MA/93A samples	62
Figure 5.13. Example of integrating the area under the melting curve.....	64
Figure 5.14. TGA of pure LLDPE and LLDPE processed with 93A in scCO ₂	66
Figure 5.15. Residual weight of pure LLDPE and LLDPE processed with 93A in scCO ₂	67
Figure 5.16. Quantity of 93A infused into LLDPE estimated from TGA residual weight.....	69
Figure 5.17. TGA of pure LLDPE-g-MA and LLDPE-g-MA processed with 93A in scCO ₂	69
Figure 5.18. Residual weight of pure LLDPE-g-MA and LLDPE-g-MA processed with 93A in scCO ₂	70
Figure 5.19. Quantity of 93A infused into LLDPE-g-MA estimated from TGA residual weight (not to scale).....	71
Figure 5.20. LLDPE/93A standard spectra with absorbance peak 522 cm ⁻¹	74
Figure 5.21. LLDPE/93A standard spectra with absorbance peak 2019 cm ⁻¹	74
Figure 5.22. Calibration curve for LLDPE/93A nanocomposites with 0 to 0.25 wt% 93A loadings	75
Figure 5.23. Calibration curve for LLDPE/93A nanocomposites with greater than 0.25 wt% 93A loadings.....	76
Figure 5.24. SEM of clay particle displaying its measurement dimensions	79
Figure 5.25. SEM of clay particle exhibiting delamination.....	80
Figure 5.26. Comparison of the quantity of 93A infused into LLDPE as determined by TGA and FTIR analysis (standard deviation bars included)	84

Figure 5.27. Comparison of the quantity of 93A infused into LLDPE-g-MA as determined by TGA and FTIR analysis (standard deviation bars included)	85
Figure 5.28. SEM of LLDPE/93A sample (– –) surface	88
Figure 5.29. SEM of LLDPE/93A sample (– +) surface	89
Figure 5.30. SEM of LLDPE/93A sample (+ –) surface	89
Figure 5.31. SEM of LLDPE/93A sample (+ +) surface	90
Figure 5.32. SEM of LLDPE-g-MA/93A sample (– –) surface	92
Figure 5.33. SEM of LLDPE-g-MA/93A sample (– +) surface	92
Figure 5.34. SEM of LLDPE-g-MA/93A sample (+ –) surface	93
Figure 5.35. SEM of LLDPE-g-MA/93A sample (+ +) surface	93

LIST OF TABLES

	Page
Table 4.1. Properties of LLDPE resins used in scCO ₂ -processing experiments.....	38
Table 4.2. Conditions for processing 93A with LLDPE granule in scCO ₂	40
Table 4.3. Conditions for processing 93A with LLDPE and LLDPE-g-MA in scCO ₂ ...	41
Table 4.4. Conditions for processing 93A with LLDPE in scCO ₂ for 1 hr.....	41
Table 4.5. Conditions for processing extruded LLDPE/93A in scCO ₂	42
Table 5.1. CO ₂ density vs. d ₀₀₁ -spacing of granule LLDPE/93A samples.....	44
Table 5.2. CO ₂ density vs. d ₀₀₁ -spacing of pellet LLDPE/93A samples.....	47
Table 5.3. d ₀₀₁ -spacing values of LLDPE/93A samples for X vs. X/scCO ₂	54
Table 5.4. CO ₂ density vs. d ₀₀₁ -spacing of LLDPE-g-MA/93A samples	56
Table 5.5. Melting (T _m) and crystallization (T _c) temperatures of LLDPE and LLDPE-g-MA infused with 93A as measured by DSC.....	63
Table 5.6. Crystallinity of LLDPE samples infused with 93A	64
Table 5.7. Crystallinity of LLDPE-g-MA samples infused with 93A	65
Table 5.8. Main decomposition for pure LLDPE and processed LLDPE/93A samples..	66
Table 5.9. Main decomposition for pure LLDPE-g-MA and processed LLDPE-g-MA/93A samples	70
Table 5.10. Average weight percentage and standard deviation of 93A in LLDPE	77
Table 5.11. Average weight percentage and standard deviation of 93A in LLDPE-g-MA	78
Table 5.12. Influence of scCO ₂ -processing conditions on crystallinity (heating 1) for LLDPE/93A samples.....	81
Table 5.13. Influence of scCO ₂ -processing conditions on crystallinity (heating 1) for LLDPE-g-MA/93A samples.....	82

Table 5.14. Size distribution of clay particles in as-received 93A and LLDPE-g-MA/93A samples.....	91
--	----

1. INTRODUCTION

1.1. POLYMER-CLAY NANOCOMPOSITES (PCN's)

Since the late 1980's when Toyota reported property enhancements in nylon-6 with the addition of clay, polymer-clay nanocomposites (PCN's) have been of great interest to researchers.¹⁻³ Possessing properties initially well-suited for a wide variety of applications from food packaging to car parts,^{1,2} PCN's have been able to further expand their uses to alternative energy applications such as batteries,⁴ fuel cells⁵ and solar cells.⁶ Clay as a polymer filler can improve on a myriad of properties including stiffness, strength, flame retardancy, dimensional stability, gas permeability, solvent resistivity and UV resistivity. Abundant in nature, clays are inexpensive and non-toxic to the environment and humans. Inherently, clays are in a stacked platelet configuration and agglomerated but offer greater property enhancement when intercalated or exfoliated into individual layers as a result of their high aspect ratio facilitating greater interaction between clay and polymer. Conventional composites can require 20 to 40 vol% filler to achieve the same properties as a nanocomposite that uses 1 to 5 vol% filler. Due to low filler content, viscosity increases are not a concern for processing, which can be accomplished at similar conditions to those for the neat polymer. Most nanocomposites are prepared by melt processing, but can be made by other techniques such as in-situ polymerization or solvent casting.⁷

1.2. MOTIVATION

The motivation for this work emerges from a necessity to create PCN's by a method capable of operating at low temperatures without employing organic solvents.

Typically, PCN's are created by melt mixing polymer and clay in high shear mixing devices that utilize high temperatures to melt polymer. High temperatures can degrade the organic modification of organoclays (e.g., degradation initiates around $180^{\circ}\text{C}^{3,7}$), hindering the compatibilization of polymer and clay. Also during processing with melt-mixing devices, thermal degradation can occur with some polymers such as polypropylene (PP) and polytetrafluoroethylene (PTFE).⁸ Polymer-clay nanocomposite synthesis methods involving organic solvents, e.g., solvent-casting and in-situ polymerization, enable the low-temperature mixing of dissolved polymer and clay in solution, but can require large amounts of toxic chemicals to dissolve the polymer. These chemicals can be difficult to completely separate from the product and recycle. In addition, they are harmful to humans and the environment, requiring specialized handling and disposal, which can be costly, especially on the industrial scale.

Supercritical carbon dioxide (scCO_2) processing can be employed as an alternative method of producing PCN's. In its supercritical state, accessible at a low temperature of 31.06°C , carbon dioxide (CO_2) can possess the solvating properties comparable to that of a liquid organic solvent,⁹ capable of dissolving, swelling and plasticizing polymers. Processed at low temperatures, organoclays retain their organic modification to facilitate clay dispersion and a stable morphology, empowering greater enhancement of PCN's. In addition, select polymers can be processed without degrading. The separation of CO_2 from the PCN product is straightforward, as depressurization will revert CO_2 to a subcritical gas that can be removed and recycled. Handling and disposal are also simpler as CO_2 is non-toxic to humans and environmentally benign.

1.3. OBJECTIVE

The objective of this study is to determine if organoclay Cloisite 93A (93A) can be dispersed into linear low-density polyethylene (LLDPE) via scCO₂ processing. Dispersion is indicated by infusion and/or the enhanced intercalation/exfoliation behavior of the organoclay. This work will center around a low processing time for infusion to add to the industrial viability of the process. In addition, the processing parameters most conducive to achieving this goal are determined.

1.4. APPROACH

To accomplish the objective of dispersing organoclay into LLDPE with scCO₂ using a low infusion time, experiments were conducted to observe the effect LLDPE resin size has on the dispersion of organoclay and the associated steps of sample analysis. From these experiments, it appeared that the pellet resin could provide comparable or improved dispersion as well as additional sample information not afforded by the granule resin.

The pellet resin underwent experiments to investigate the processing time (1-hr vs. 3-hr), the capability of scCO₂ when clay is infused into the polymer and the effect of LLDPE compatibility on dispersion. The information gained from the experiments revealed that a 1-hr processing time was insufficient for infusion, infused clay could still be affected by scCO₂ and a more compatible form of LLDPE could affect dispersion kinetics. The more compatible polymer, LLDPE grafted with maleic anhydride (a.k.a. LLDPE-g-MA or maleated LLDPE), was employed to ascertain if the maleic anhydride

(MA) compatibilizing modification could enhance infusion and intercalation/exfoliation behavior of 93A.

Further analysis was conducted on the organoclay-infused polymers, LLDPE and LLDPE-g-MA, in order to obtain a better understanding of the influence of the scCO₂ treatment. The infusion, d₀₀₁-spacing, morphology and distribution of 93A in the polymers were determined analytically from X-ray diffraction (XRD) patterns and observed visually from scanning electron microscopy (SEM). The quantity of infused clay was estimated by thermogravimetric analysis (TGA) and calculated by Fourier transform infrared (FTIR) analysis, which used a method novel to PCN's. And changes in the polymer due to scCO₂ treatment were investigated with differential scanning calorimetry (DSC) and TGA.

2. REVIEW OF LITERATURE

2.1. POLYETHYLENE

Polyolefins are a class of polymers synthesized from double-bonded hydrocarbons, such as ethylene, propene, butene-1 and isobutene. Polymerized, these hydrocarbons make polyethylene, polypropylene, polybutylene-1 and polyisobutylene, respectively.¹⁰ The resulting thermoplastic polymers are solid when cool, but soften, liquefy and degrade, as they are heated to a temperature in which their covalent bonds are broken. This is in contrast to thermoset polymers where heating will not soften the hard polymer, but extreme temperatures will degrade the polymer by breaking covalent bonds.¹¹ Manufactured by the British company ICI in 1939, low-density polyethylene (LDPE) was the first polyolefin to be commercialized.¹²

Polyethylene, the most manufactured of the polyolefins, is a semicrystalline polymer available in a variety grades.¹² The most common grades are high-density polyethylene (HDPE), LDPE and linear low-density polyethylene (LLDPE). Polyethylene grades are homo- and co-polymerized to exhibit a wide range of properties in terms of density (low, medium and high), melt flow index (low, medium, and high), average molecular weight (low, medium, high and ultra-high) and molecular weight distribution (narrow and broad).¹⁰

2.1.1. Polymerization Methods. Ethylene can be polymerized by the following methods: free-radical polymerization (high-pressure process), coordination polymerization (medium- and low-pressure catalytic process) or metallocene catalyst polymerization. Each method produces a different type of polyethylene that can greatly differ in properties from one another.

2.1.1.1 Free-radical polymerization. Free-radical polymerization of ethylene is a high-pressure process (100 MPa or higher¹³) that produces highly branched homopolymers with side chains of different lengths.¹⁰ High processing pressures are important to concentrate a suitable amount of the ethylene monomer, since above 9°C ethylene is a gas, as well as increase the reaction rate. The increased reaction rates are also attributed to the high temperatures within the reactor that range from 140°C to 300°C, averaging out to 220°C.¹³

The polymerization can occur by either an intermolecular chain transfer mechanism or an intramolecular “back-biting” mechanism.^{12,13} The intermolecular chain transfer mechanism (Figure 2.1) occurs when different polyethylene chains react with one another¹³ to produce long-chain branches of hexyl or longer.¹² Shorter chains (e.g. typically ethyl and butyl¹³) are produced by the intramolecular “back-biting” mechanism (Figure 2.2) that occurs when a polyethylene chain reacts with itself.¹³ This mechanism is at higher pressures and achieves lower conversions than the chain transfer mechanism. Furthermore, crystallinity increases due to short-chains allowing a more compact structure than long-chains. By increasing polymerization pressure, the number of short-branches increases to result in a nearly linear polymer.¹²

this fashion until radicals combine to terminate the reaction. To help control polymer molecular weight, chain transfer agents are employed such as hydrogen, acetone, propane, propene, and methyl ethyl ketone.¹³

2.1.1.2 Coordination polymerization. The coordination polymerization method using medium and low pressures produces linear (reduced branching) homo- and copolymers.^{10,12} Both discovered in the early 1950's,^{14,15} two types of catalysts for this process are Phillips- and Ziegler-type catalysts.

Medium-pressure processes (3 to 4 MPa) at 85 to 180°C use Phillips-type catalysts made of an aluminum oxide (Al_2O_3) or silica-alumina base that supports chromium oxide (CrO_3).^{10,11} In Phillips-type catalysis, choosing a catalyst that favors the chain termination reaction (β -hydrogen shift reaction) is important to controlling the polymer molecular weight, thus melt flow index, since typical chain-transfer agents such as hydrogen poison the catalyst.¹³

Ziegler-type catalysts consist of titanium esters, titanium halides or aluminum trialkyls¹² for low-pressure processing (0.1 to 5 MPa) in temperatures of 20 to 150°C. Titanium tetrachloride, TiCl_4 , and triethyl aluminum, $(\text{CH}_3\text{CH}_2)_3\text{Al}$, made up the first Ziegler-type catalysts,¹² but many other variations exist.^{13,14} Ziegler-type catalysts are typically supported by Mg compounds such as $\text{Mg}(\text{OH})\text{Cl}$ or MgCl_2 . Compared to catalysts without support, a narrower molecular weight distribution is produced in polyethylene when catalysts are supported with MgCl_2 . Ziegler catalyst polymerizations employ hydrogen to help control the polymer molecular weight.¹³ Intermediate species when polymerizing in the presence of coordination catalysts are σ - and π -bonded organometallic compounds.^{13,14}

2.1.1.3 Metallocene catalyst polymerization (single-site). A third route to polyethylene, developed in 1980,¹² that allows for further tailoring of its properties is metallocene catalyst polymerization (a.k.a. single-site catalyst polymerization). Metallocene catalysts offer markedly increased activity over Ziegler-type catalysts, offsetting the higher cost of the metallocene catalyst to make them competitive.¹² Metallocene catalysts differ from coordination catalysts in that they allow polymers to be built that have a narrow molecular weight distribution and a particular monomer sequence can be specified during polymerization.^{10,12} Control over the monomer sequence is due to the stable transition metal components with distinct structures,¹³ allowing a more efficient integration of comonomers such as butene-1, hexene-1 and octene-1.¹² In addition, polymers with a wide range of densities can be produced. Methyl aluminoxane (MAO) cocatalyst activates transition metal compounds, such as Zr- or Ti-centers coupled with cyclopentadienyl residuals, to create metallocene catalysts.¹⁰ Exhibiting a narrow molecular weight distribution and a high density, the first process produced a linear polyethylene with the catalyst bis(cyclopentadienyl)zirconium dichloride (Cp₂ZrCl₂)-MAO.¹² As with Ziegler catalysis, control over molecular weight can be maintained with hydrogen and the β -shift reaction. And current processes employing Phillips- and Ziegler-type catalysts for PE production can switch to metallocene catalysts without making equipment changes.¹³

2.1.2. Grades. Different grades of polyethylene are produced by employing different processing methods.

2.1.2.1 High-density polyethylene (HDPE). High-density polyethylene is produced by coordination polymerization in either a medium- or low-pressure

environment. At pressures of 3 to 4 MPa, the medium-pressure process employs a Philips-type catalyst at 85 to 180°C to synthesize HDPE with a molecular weight of 50,000 g/mol. Ziegler-type catalysts aid in the polymerization of HDPE in a low-pressure process (0.1 to 5 MPa) at 20 to 150°C. Molecular weight of HDPE using Ziegler-type catalysts is between 200,000 to 400,000 g/mol. Exceeding that of LDPE, the crystallinity of HDPE is 60 to 80% and the density is 940 to 970 kg/m³. Trash cans, gasoline canisters, vehicle fuel tanks, crates, pails, housewares, and transportation and storage containers^{10,12} are just a few of the applications for HDPE. Special grades of HDPE are used for drinking and waste water equipment fittings, high-pressure pipes and components for the automotive and chemical industries.¹⁰

2.1.2.2 Low-density polyethylene (LDPE). Low-density polyethylene is produced by free-radical polymerization in a continuous process using pipe reactors or a discontinuous process with stirrer reactors. The ethylene polymerization reaction is initiated with 0.05 to 0.1% oxygen or peroxides and occurs at temperatures between 150 and 275°C and pressures from 100 to 300 MPa.^{10,12,13} Since ethylene has a critical temperature of 9.5°C and a critical pressure of 5.08 MPa, the polymerization reaction takes place in supercritical ethylene. The resultant polymer has a crystallinity of 40 to 50%, an average molecular weight of up to 600 kg/mol and side chains of dissimilar lengths. The density of LDPE is 915 to 935 kg/m³. This density range includes medium-density polyethylene (MDPE) that has a density of 925 to 930 kg/m³. Typical applications for LDPE include films (packaging, shrink, heavy-duty bags, agriculture), wire sheathing, pipes, pipe coatings, thermoforming boards and flexible containers and bottles.¹⁰

2.1.2.3 Linear low-density polyethylene (LLDPE). Linear low-density polyethylene is synthesized with a high-efficiency catalyst with one of the following four methods: in suspension, in solution, in gas-phase low-pressure process or modified high-pressure process. LLDPE has typically the same applications as LDPE and compared to LDPE, films made with LLDPE are stronger at low temperatures, more resistant to penetration and tearing, have a lower tendency for stress cracking and have good optical properties.¹⁰

The suspension (slurry) process is performed in either autoclave reactors or loop reactors. The autoclave reactor process that can employ multiple cascading reactors operates in a pressure range of 0.5 to 1.0 MPa and temperature range of 80 to 90°C. And at conditions of chromium-based Phillips catalysts, the loop reactor process operates at pressures ranging from 3 to 4 MPa and at a temperature of 100°C.¹³

The solution process, which can be built for LLDPE production or dual production of LLDPE and HDPE, operates at pressures near 10 MPa and temperatures from 200 to 300°C.¹³

Employing a fluidized bed reactor, a wide range of densities (890 to 970 kg/m³) and MFIs (0.01 to 100) for PE have been reported for polyethylene production in gas-phase processes that can be used to create both LLDPE and HDPE. The reaction temperature range for this process is from 80 to 100°C and the pressure ranges from 0.7 to 2.0 MPa.¹³

Autoclave or tubular reactors are used in high-pressure processes for polyethylene production. Functioning at pressures of 150 to 200 MPa, the autoclave process acts like a continuous stirred-tank reactor (CSTR) with temperatures ranging from 180°C in the first

zone to 290°C in the final zone. Operating in the regime of plug flow reactors (PFR), the tubular reactor withstands reaction pressures of 200 to 350 MPa and the reaction temperature is dependent upon the initiator. The temperature varies from peroxydicarbonate initiated polymerizations at 140°C to oxygen initiated polymerizations occurring at 190°C. This process modified specifically for LLDPE production typically employs specially designed Ziegler-type catalysts capable of withstanding the high temperatures.¹³

2.1.2.4 Other polyethylenes. Other polyethylenes have unique properties that allow them to be used for more specialized applications. Categorized as high-density polyethylenes, these include high-molecular weight high-density polyethylene (HMWHDPE) and ultra high-molecular weight high-density polyethylene (UHMWHDPE). On the low-density side of the spectrum, PE's with unique properties are very low-density polyethylene (VLDPE) and ultra low-density polyethylene (ULDPE). And polyethylenes produced with metallocene catalysts (PE-M) include MLLDPE, MMDPE, MHDPE, MVLDPE and PE-MD/HD-(M).¹³

2.2. CLAY

Clays that have a crystalline structure are categorized as smectites (phyllosilicates), serpentines, micas (illites), kaolins, chlorites and vermiculites, and other clays (glaucinite, sepiolite-palygorskite-attapulgite and mixed-layer clay minerals).^{3,16} The crystalline structure and charge characteristics (location and amount) per unit cell are the foundation for clay classification. The most commercialized clays are classified under smectites, which include hectorite (HT) and montmorillonite (MMT).³ Due to the limited

availability of HT, MMT is the most manufactured clay for use in polymer-clay nanocomposites.^{3,12}

2.2.1. Montmorillonite (MMT). Montmorillonite is a naturally occurring 2:1 phyllosilicate that can exhibit a broad range of compositions in its three different layers.^{3,12} The octahedral layer contains aluminum (Al), magnesium (Mg) and iron (Fe^{3+}) that vary in compositions of 3.0 to 4.0 wt%, 0 to 1.4 wt% and 0 to 1.0 wt%, respectively. The tetrahedral layer consists of silicon (Si), ranging in composition from 7.2 to 8.0wt%, and Al, ranging in composition from 0 to 0.8 wt%. And the interlamellar aqueous layer contains an exchangeable cation of sodium (Na^+) that exists in a composition range of 0.67 to 0.8 wt%.³ The structure of MMT is configured such that a central octahedral layer (composed mainly of Al) is located between two silica tetrahedral layers, as seen in Figure 2.3.^{3,12} Generally, each unit cell has a net negative charge (ideally -0.67) on the flat side of the platelet due to Mg^{+2} cations replacing some Al^{+3} cations. The cation-exchange capacity (CEC) is typically 0.915 meq/g, but can range from 0.8 to 1.2 meq/g.³ Present between aluminosilicate layers, hydrated Na^+ , Mg^{2+} , Ca^{2+} , Li^+ , or K^+ cations balance the negative charge, imparting a slightly positive charge at the edges of the platelets.¹²

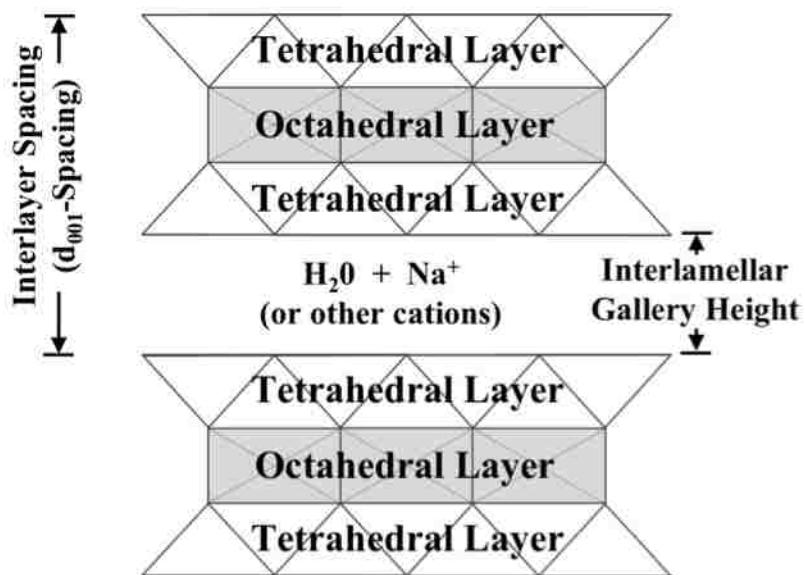


Figure 2.3. Diagram of MMT clay layers

The distance between platelets is referred to as interlamellar gallery height and the interlayer spacing is the thickness of the platelet plus the interlamellar gallery height, displayed in Figure 2.3. The interlayer spacing is the d_{001} -spacing (or basal spacing) in XRD analysis and is nominally 0.96 nm for dry MMT, corresponding to the thickness of a MMT platelet. Partially hydrated, natural MMT has a d_{001} -spacing of 1.2 to 1.4 nm. Clays consist of stacks of platelets held together by van der Waals forces that weaken as platelets are separated (Figure 2.4).³

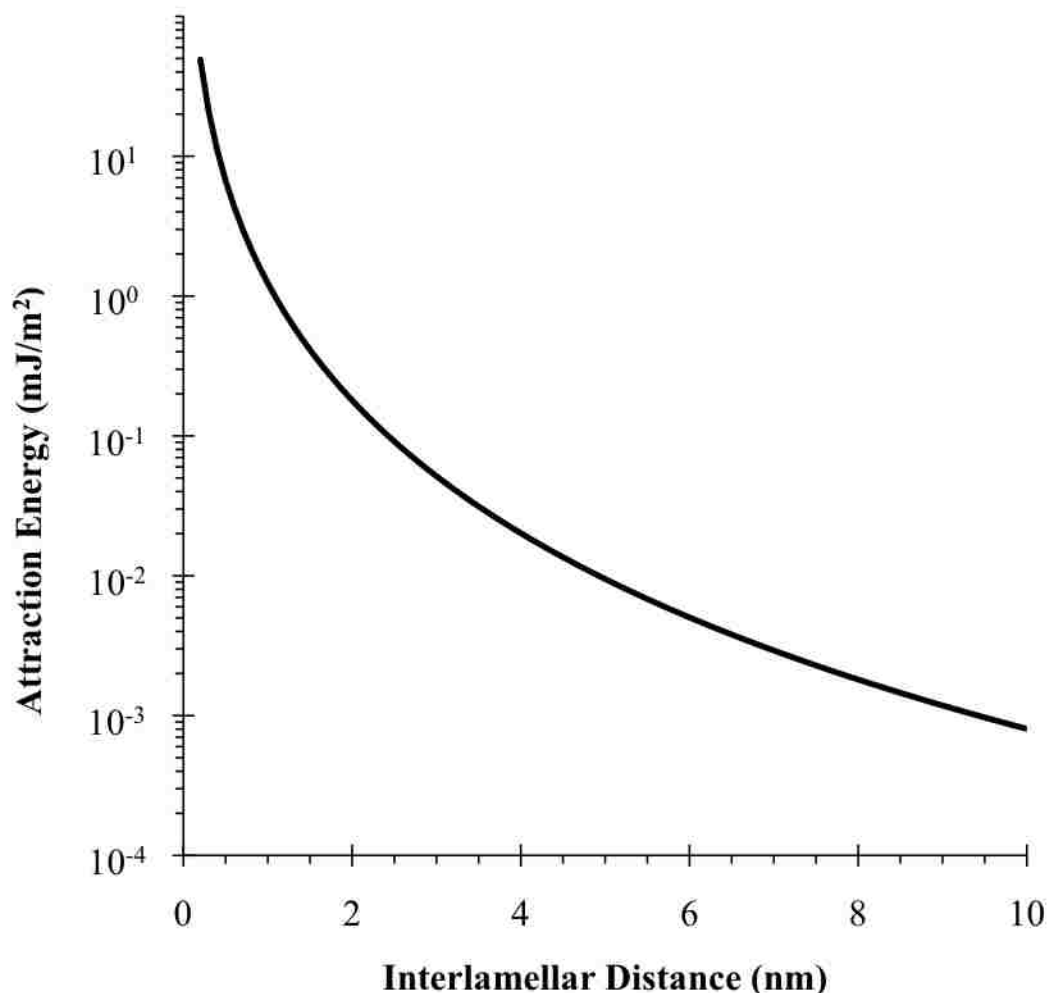


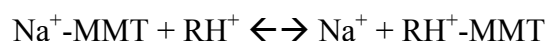
Figure 2.4. Energy of attraction for van der Waals forces as a function of the interlamellar distance between two MMT clay platelets (From equation in Ngo et al.¹⁷)

Due to its high water content (typically 23%), clay is oven dried to remove the majority of water prior to processing. Water can swell MMT up to 30 times its original volume. Montmorillonite has a specific surface area of 750 to 800 m²/g, which is below its theoretical value of 834 m²/g. Its density is typically 2.5 g/ml and it possesses a Mohs hardness (20°C) value of 1.5 to 2.0. The aspect ratio of MMT can be up to 1500, but commercially the aspect ratio is typically from 10 to 300. Commercial clays consist of

particles ($\sim 8\mu\text{m}$ in size) containing upwards of 3000 platelets. The color of clay is dictated by its composition and can range from blue-grey or pale yellow to dark red. The Fe^{3+} content affects the reddish color of clay and also alters the refractive index for certain MMT clays, ranging from 1.523 to 1.590.³

2.2.2. Organoclay. Organoclays are clays that have been converted from their natural hydrophilic state to an organophilic (hydrophobic) state. Due to their thixotropic nature and thus their ability to control the flow behavior of liquids, organoclays were initially (1940's) used as additives in paints, waxes, cosmetics, printing inks, lubricants, etc.³ Since the 1980's, the interest in organoclays has shifted toward polymeric additives.

The conversion of clay to organoclay is achieved by a cation-exchange reaction that exchanges the metal cations (Na^+) between clay layers with organic cations (RH^+) such as alkylammonium salts.^{3,12,16} The cation-exchange reaction



is a reversible process requiring excess organic cations RH^+ to ensure the reaction produces organoclay. The ease at which this is done is determined by the cation-exchange capacity (CEC), optimally between 0.8 and 1.2 meq/g for MMT (ion concentration range that deters solid-solid interactions between platelets and promotes acceptable chemical activity). A variety of factors influence the rate of reaction such as reaction medium, temperature, pressure, pH, clay type, clay concentration, clay particle geometry, exchange cation type, etc. For example, the ion exchange reaction proceeds faster in water than in alcohol (or other organic liquids in aqueous solutions) and at elevated

temperatures (recommended from 60 to 80°C). And the fastest reacting type of clay is Na-MMT.³

The physical process of exchanging cations for other cations in Na-MMT is accomplished by mechanical shear mixing of a Na-MMT aqueous slurry in the presence of excess organic cations. The shear mixing aids in the ion exchange and can be conducted in devices such as a colloid mill. Ultrasonication of the Na-MMT aqueous slurry can replace shear mixing to facilitate the ion exchange reaction.³

The choice of intercalant is dependent on its ability to diffuse between clay layers, expand the interlamellar spacing, and improve clay interactions with the organic host matrix. The organic cation is dual-functional, able to bond strongly to the clay platelets and have an organic portion that non-ionically interacts with the clay surface. The goal of the organic part is to expand the interlamellar spacing (reduces solid-solid interactions between platelets) and render the clay organophilic as to improve the clay-organic matrix interactions.³ The expansion of interlamellar spacing is in relation to the size of the organic cation, longer chains forcing clay layers further apart. Many types of exchange cations, thus organoclays, are available and chosen depending on the end-use of the clay.^{3,12,16}

Marked by clay discoloration, the organic component (intercalant) of organoclays may begin to decompose at temperatures lower than 180°C, resulting in reduced interlayer spacing. The decomposition products for commercial organoclays modified with a quaternary alkylammonium surfactant can include water, carbon dioxide, alkenes, alkanes, alcohols, carboxylic acids, aldehydes, aromatics, amines, and dialkyl sulfate.⁷

2.3. POLYMER-CLAY NANOCOMPOSITES

Clays can exist in three different configurations within a polymer matrix: immiscible (conventional), intercalated and exfoliated. Immiscible composites are microcomposites containing stacks of clay platelets surrounded by polymer chains.^{3,12} Clays in intercalated and exfoliated configurations interact with the polymer matrix via their platelets with nanometer dimensions (~1 nm platelet thickness), making them nanocomposites.¹⁶ In an intercalated configuration, stacks of clay platelets contain polymer chains between their platelets, increasing the interlayer spacing (d_{001} -spacing < 8.8 nm). If the clay stacks have been delaminated into individual platelets, the configuration is deemed exfoliated (d_{001} -spacing > 8.8 nm).^{3,12} Exfoliated clay platelets can be randomly aligned or aligned in one direction within a polymer matrix, constituting disordered and ordered exfoliated configurations.³ Most PCN's exhibit more than one configuration.¹⁶ Figure 2.5 displays the different configurations of clay within a polymer matrix.

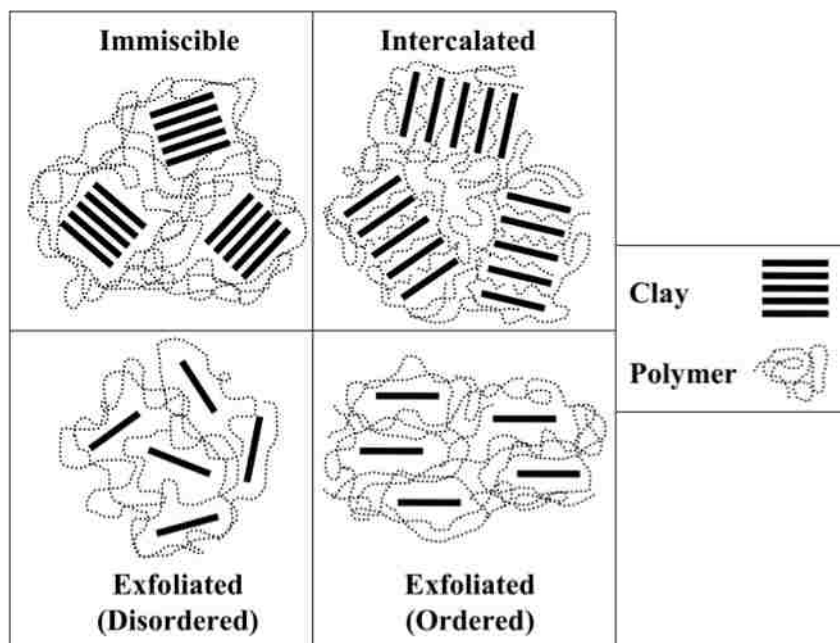


Figure 2.5. Configurations of clay within a polymer-clay nanocomposite

2.3.1. Polymer-Clay Compatibility. Compatibility between the polymer matrix and clay filler plays a significant role in the properties of the resultant composite due to its ability to affect the clay's configuration. Clay that is incompatible with the polymer matrix will favor agglomeration, resulting in a conventional clay structure.¹⁸ In addition to increasing interlamellar gallery distance, clay modifications have been motivated by the intent of increasing the material compatibility between clay and polymer for use in PCN's. Typically clays are modified by organic cations (normally alkylammonium salts) exchanged with metal cations (Na^+) intercalated between clay platelets and are commonly referred to as organoclays.^{3,12} By compatibilizing the ions between clay platelets with the polymer matrix, the polymer chains are more likely to enter the interlamellar galleries of the clay to create an intercalated structure. In many instances of PCN creation, intercalation or partial intercalation/exfoliation is the optimal configuration obtained with

the use of organoclays. The absence of complete exfoliation could be due to the still large difference between the hydrophobicity of polymers and the hydrophilicity of the organoclay. To reconcile this difference, further compatibilization can be employed in addition to the modifications offered by the organoclay. Grafting maleic anhydride (MA) onto non-polar polymers (e.g., polyolefins) adds a hydrophilic (polar) component to a hydrophobic polymer that is capable of interacting with the oxygen groups on the surface of the hydrophilic clay platelet. The hydrophilic nature of MA aids the polymer in entering the clay gallery, while the hydrophobic polymer pushes the platelets apart into an exfoliated structure. The hydrophobic nature of the polymer is important to exfoliating the clay since a polymer that is hydrophilic will be attracted to the clay platelets, holding them together as it enters the clay gallery to produce an intercalated morphology.^{19,20}

2.3.2. Characterization. Characterization of PCN's is important to determining the properties they will exhibit. The following methods use x-rays, infrared light, electrons or heat in order to obtain information about a sample.

2.3.2.1 X-ray diffraction (XRD). X-ray diffraction (XRD) analysis is a technique employed to analyze materials exhibiting crystallinity (e.g., PCN's). An XRD instrument contains an X-ray tube, a monochromator and a detector. A specimen undergoing XRD analysis is bombarded by X-rays emitted by the X-ray tube. The X-rays are created by striking a metal such as copper with accelerated electrons, transferring energy to the metal that in turn releases radiation in the form of X-rays.²¹ After impacting the specimen, the diffracted X-rays are collected by a rotating detector and are converted into a spectrum of peaks that provides details on the crystalline structure

depending on location and shape of the peak.^{3,21} Unknown materials can be identified via an XRD spectrum since each material exhibits a different pattern.²² An XRD spectrum will display the diffraction angle (2θ) on the x-axis and the intensity (of arbitrary units) on the y-axis.³ A specimen can be analyzed in the form of a thin sheet or a powder. Wide angle X-ray scattering (WAXS) and small angle X-ray scattering (SAXS) are the two types of XRD devices that typically operate in diffraction angle ranges above and below $2\theta = 2^\circ$, respectively.^{3,12} During analysis of the XRD spectrum, the peak location is used to calculate the interlayer spacing between adjacent crystallographic planes (e.g., clay platelets), a.k.a. the d-spacing, using Bragg's law:

$$d_{00n} = \frac{n\lambda}{2\sin\theta} \quad (1)$$

where n is an integer indicative of the order of reflection ($n = 1$ for principal reflection), λ is the wavelength of the incident X-ray beam ($\lambda = 0.1540562$ nm for Cu-K α_1 radiation source), and θ is the incident (or reflection) angle of the X-ray beam.³

In terms of PCN's, the typical XRD diffraction angle range for clays is $2\theta = 1$ - 12° .³ Mentioned above, Bragg's law can be used in conjunction with the peak position to determine the distance between clay platelets within a polymer matrix, which can indicate the degree of polymer intercalation or clay modifier removal. Peak shape also provides information about the clay morphology, as peak broadening can be due to the partial exfoliation of the clays (i.e., the existence of a range of d-spacing values) or defects in the crystalline structure of the clays. During exfoliation, the intensity of the

peak decreases in addition to its broadening, and completely exfoliated clays display no peak.^{3,22}

2.3.2.2 Fourier transform infrared (FTIR) spectrometry. Fourier transform infrared (FTIR) spectrometry is a useful analytical technique capable of detecting minute amounts of chemicals in solid, liquid or gaseous states. This ability enables the identification, qualification and quantification of components within a sample. An FTIR device works by focusing an infrared (IR) beam on a sample that in turn either transmits or absorbs the frequencies of the beam, depending on the vibrational and rotational energy levels of the sample's molecules to create an identifying spectrum or "fingerprint" unique to the material.^{22,23} The main components comprising a typical FTIR spectrometer are the IR source, interferometer, sample chamber, detector and computer. Beginning with the source (i.e., a glowing black-body source), an IR beam of energy is emitted that is encoded with all frequencies in the IR range by the interferometer, drastically enhancing the scanning speed as opposed to a single-frequency beam. Typical interferometers consist of a beam splitter, transmitting half of the IR beam and reflecting the other half, a fixed mirror and a mobile mirror.^{22,23} Upon leaving the interferometer, the signal-encoded beam (interferogram) is directed through the sample chamber where the sample is held typically in a nitrogen-purged environment. Mentioned above, the signals of the IR beam are either transmitted through or absorbed by the sample, depending on the composition of the sample. The signals not absorbed are collected by the detector, digitized, and sent to the computer for conversion (employing Fourier transform) into a spectrum indicative of the sample.²³

Considering PCN's, FTIR analysis is advantageous for determining polymer and clay modifier degradation⁷ due to processing conditions or the amount of clay within the sample.²⁴ As the concentration of clay increases within the sample, peaks indicative of the clay will increase accordingly. Unlike XRD, clay with any morphology can be detected by FTIR, but the morphology cannot be determined by the spectra. In addition, FTIR is a non-destructive technique, permitting a sample to be analyzed many times.

2.3.2.3 Scanning electron microscopy (SEM). Scanning electron microscopy (SEM) is an imaging technique that enables the topographic viewing of a material with a resolution of 1 to 10 nm and exhibits a large depth of focus.^{22,25,26} An SEM consists of an electron gun, electromagnetic lenses, detectors, cathode-ray tube and a charge-coupled diode (CCD).^{25,26} The electron gun emits electrons (maximum accelerating voltage is typically 30 kV) that are focused onto the specimen by electromagnetic lenses.^{22,25,26} The source of electrons is usually a tungsten filament or a lanthanum hexaboride crystal.^{25,26} The electron beam is scanned across the specimen, which in turn produces backscattered electrons, secondary electrons, X-rays and Auger electrons.^{22,25,26} The detectors collect the incident electrons and X-rays for material analysis such as surface imaging or composition determination.^{22,26} The image is produced on the cathode-ray tube, and it is captured on film or digitalized with the CCD.^{22,25,26} The SEM is kept under high vacuum (about 10^{-3} Pa) to prevent the electrons from scattering (due to collisions with air molecules) before reaching the specimen. To prevent electrons from electrostatically charging the specimen from an inadequate path to ground, materials with insufficient electrical conductivity are coated with conducting carbon or metal to make them conductive. Employing an energy-dispersive spectrometer (EDS) or wavelength-

dispersive spectrometer (WDS), SEM is capable of detecting X-rays for determining the chemical composition of a specimen.^{25,26} SEM can be used to analyze materials such as polymers, ceramics, metals and biomaterials. When analyzing the interaction of clay with the polymer matrix in PCN's, SEM can aid in revealing morphology, distribution and particle size of the clay.

2.3.2.4 Thermogravimetric analysis (TGA). Thermogravimetric analysis (TGA) is a technique that relates a sample's mass to the temperature of its environment at a given time. To conduct TGA analysis, a sample is exposed to an increasing (or decreasing) temperature at a constant rate or an isothermal environment for a set period of time and measuring the resultant change in the sample. The atmospheric gas can also be adjusted to analyze the sample in different environments, such as an inert (nitrogen) or oxidative (air) environment.^{27,28} A TGA device consists of a microbalance that relays the changing mass of the sample to a force coil, compensating for the change in terms of an electromagnetic force that is proportional to the mass change.²⁷ From the resultant thermal profile of TGA, properties of materials can be ascertained including composition, thermal stability, oxidative stability, moisture content, volatile content, kinetics of decomposition,^{27,28} material lifetime and flammability. Materials that benefit from TGA include polymers (thermoplastics and thermosets), composites, ceramics, glasses, pharmaceuticals, food coatings, organic materials, petroleum and explosives.

2.3.2.5 Differential scanning calorimetry (DSC). Differential scanning calorimetry (DSC) is a useful tool for determining a material's melting temperature, glass transition temperature, crystallization point, heat of melting, heat of fusion, degree of crystallization, composition, blend compatibility, oxidation conditions, curing conditions,

purity and phase diagrams. A DSC plot reveals endothermic and exothermic peaks due to the respective absorbing and releasing of heat by the analysis material.^{27,29} The analysis can occur with the material subjected to an increasing, decreasing or constant temperature. The DSC device functions by subjecting a sample and a reference material to the same conditions and the difference between the quantities of heat required to increase their temperatures represents the heat flow, which is plotted against temperature or time.^{27,29} Typically samples are analyzed in an inert nitrogen (or argon) environment unless oxidative studies are being conducted.²⁷ A DSC can be used for investigating polymers, such as assessing the curing process of thermosets and the phase transitions of thermoplastics. Also, the food and pharmaceutical industries benefit from the utilization of DSC.^{27,29}

2.4. SUPERCRITICAL CARBON DIOXIDE (ScCO₂)

2.4.1. ScCO₂ Background. Supercritical carbon dioxide (scCO₂) possesses properties of both gas and liquid with high diffusion rates and solublizing characteristics, respectively. Altering these density-driven properties can be accomplished by adjusting temperature and pressure, making it a tunable fluid. In addition, CO₂ is inexpensive, non-toxic, non-combustible and chemically stable. Carbon dioxide reaches its critical point at 31.06°C and 7.38 MPa, exhibiting a critical density of about 0.466 g/cm³. The phase diagram and density-pressure isotherms for CO₂ are, respectively, displayed in Figures 2.6 and 2.7. Current applications employing scCO₂ include coffee decaffeination, dry cleaning, chemical extraction and separation, fluoropolymerization,³⁰ low-temperature polymer processing, and biological and pharmaceutical processing.

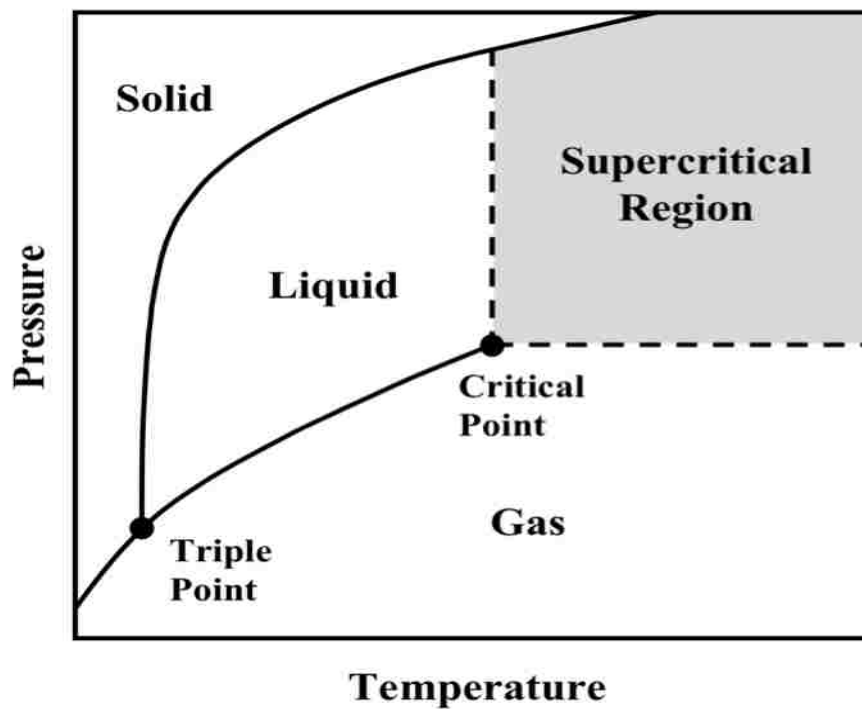


Figure 2.6. Carbon dioxide phase diagram

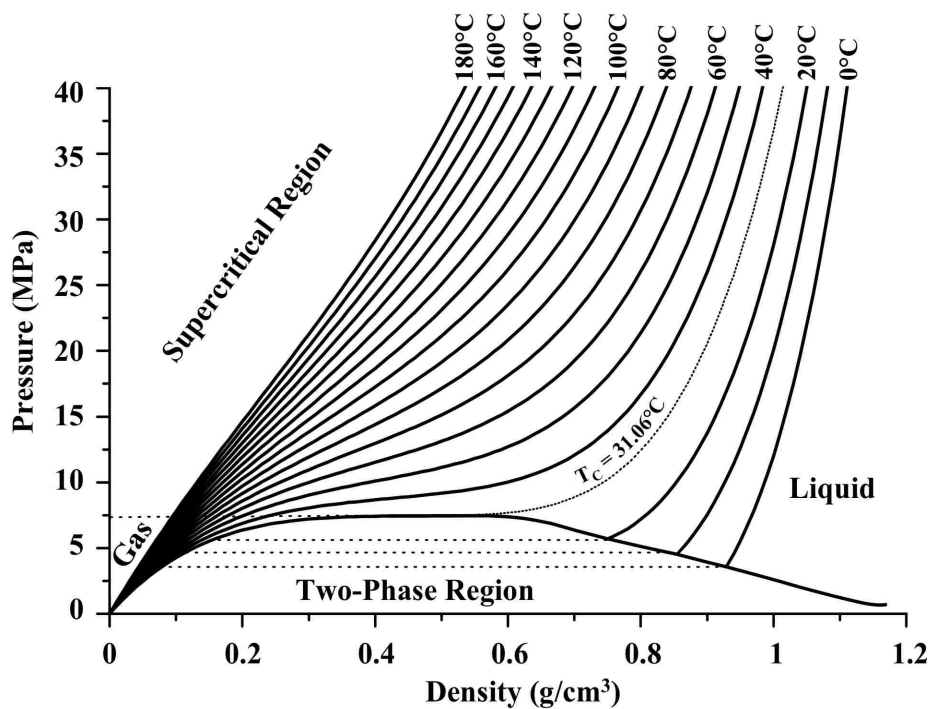


Figure 2.7. Carbon dioxide density-pressure isotherms (From Peng-Robinson equation of state with Mathias-type volume shift³¹)

2.4.2. ScCO₂ as a Solvent. Due to its properties of dissolution, scCO₂ can possess the high solvating ability of an organic liquid solvent in the presence of polymers. Carbon dioxide solubility can be greater than 30wt% in certain polymers,⁹ which can lead to significant polymer swelling depending on a variety of factors such as chemical makeup, degree of crystallinity, molecular weight, sample dimensions, etc.³² Occurring simultaneously to create a single phase, as the CO₂ dissolves in the polymer, the polymer dissolves in the CO₂. Carbon dioxide dissolution in the polymer reduces the polymer's viscosity, permitting processing at moderate temperatures. The small molecules of scCO₂ afford a low surface tension and allow it to penetrate smaller spaces than the larger molecules of liquid solvents. Furthermore, separation of scCO₂ from processed materials is easily achieved by depressurization, facilitating recycling. Making use of the attributes of scCO₂ as a solvent, fluoroalkyl substituted polythiophene semiconducting polymers were produced in scCO₂ and were observed to exhibit comparable properties to those made in the organic solvent chloroform.³³

2.4.3. ScCO₂ as a Plasticizer. By dissolving in a polymer, scCO₂ is capable of reversibly plasticizing the polymer at a low temperature, i.e., avoiding thermal degradation.^{8,34} The phenomenon of plasticization occurs when the glass transition temperature of the polymer is reduced below the processing temperature.⁹ In addition, plasticization is accompanied by a reduction in the melting temperature and viscosity of the polymer.^{8,32,34,35} Reduction in viscosity primarily occurs by increasing the free volume of the polymer,⁸ boosting polymer chain mobility.^{8,32,36} The added freedom of polymer chains can promote crystallization of the polymer,^{32,36} evidenced by a rise in the melting temperature and melting enthalpy.³² Plasticization can also reduce viscosity by

dissolved CO₂ lowering the concentration of entwined polymer chains.⁸ In terms of thermodynamics, an effective plasticizer will interact with the polymer via intermolecular forces that are on the same scale as the polymer-polymer intermolecular forces. While the size of the plasticizer molecule decreases, the plasticizer efficiency will increase.³⁴ Due to their ability to absorb more CO₂, plasticization occurs to a higher degree in amorphous polymers as compared to crystalline polymers. Polymer impregnation and foaming are some applications that benefit from the phenomenon of plasticization.

2.4.4. ScCO₂ Diffusion. The rate of CO₂ diffusion into a polymer is accelerated when CO₂ is pressurized. The diffusion rate of CO₂ is related to its small molecular size and low surface tension, facilitating its sorption into the polymer to dictate polymer free volume.^{36,37} Studies have shown that polymer sorption/desorption of CO₂ follows Fickian diffusion kinetics.^{9,36-39} Consequently, CO₂ diffusivity is related to the initial linear slope of a plot of the mass uptake of dissolved CO₂ in the polymer per total CO₂ mass uptake possible ($M(t)/M_{\infty}$) vs. the square root of desorption time divided by the initial polymer thickness ($t^{1/2}/L$). Fick's second law of diffusion (one-dimensional) for changes in concentration with respect to time is written as

$$\frac{\partial C}{\partial t} = D \frac{\partial^2 C}{\partial x^2} \quad (2)$$

Using Fick's second law, diffusion for a slab (e.g., film) of thickness L can be estimated as

$$\frac{M(t)}{M_{\infty}} = 1 - \frac{8}{\pi^2} \sum_{n=0}^{\infty} \frac{1}{(2n+1)^2} \exp\left(\frac{-D(2n+1)^2 \pi^2 t}{L^2}\right) \quad (3)$$

where $M(t)$ is the mass of the substance diffusing into the polymer at time t , M_{∞} is the mass at equilibrium sorption (after infinite time) and D is the molecular diffusivity.³⁶⁻³⁹ Equation (2) assumes the polymer thickness remains constant during CO_2 sorption. Although swelling of the polymer can occur from CO_2 sorption, studies have circumvented the issue by measuring polymer swelling to validate the assumption that it is small enough to be negligible³⁶ or have adjusted treatment conditions to ensure it is small.³⁷ The rate of diffusion increases with increasing pressure and temperature,³⁶ relying on solvent density and polymer plasticization that increase, respectively, with increasing pressure and temperature.³⁶ High diffusion rates in conjunction with its ability for polymer swelling enable compressed CO_2 to deposit additives within a polymer matrix. Berens et al. reported that the sorption rate of dimethyl phthalate (DMP) into poly(vinyl chloride) (PVC) in pressurized CO_2 could be six orders of magnitude higher than in PVC without CO_2 treatment.⁹

2.4.5. scCO_2 Intercalation/Exfoliation of Clay. Clay can also benefit from scCO_2 processing as the distance between platelets can be expanded in this environment, resulting in intercalation or exfoliation. The mechanism proceeds by CO_2 molecules, reduced in size from pressurization, entering the interlamellar galleries of the clay. Once an adequate soak period has elapsed to allow sufficient time for CO_2 to plasticize the surfactant and induce gallery expansion via surfactant conformation changes,⁴⁰ the system is catastrophically depressurized. Quickly expanding, the CO_2 molecules further separate the clay platelets to permit intercalation by plasticized polymer chains or have

the potential to bring about platelet delamination.⁴¹⁻⁴³ Mentioned above and displayed in Figure 2.4, expansion of interlamellar galleries can prompt delamination since van der Waals forces holding platelets together progressively diminish as platelets are separated.

3. EXPERIMENTAL APPARATUS

3.1. ScCO₂ PROCESSING SYSTEM

All scCO₂ infusion/dispersion experiments were conducted in a 300 mL Autoclave reactor (Autoclave Engineers) constructed of 316 stainless steel. A pneumatic motor drives the Magnedrive II magnetic mixer affixed to the reactor head that rotates the impeller within the reactor. The reactor is equipped with a stainless steel thimble to simplify insertion and extraction of processing materials. A stainless steel o-ring gasket is located between the reactor head and body to seal the vessel, and six bolts secure the reactor head to the body. Cooling coils augment the reactor head, extending into the interior of the reactor. An Omega temperature controller is manually operated to regulate reactor temperature via clamp heaters and type J thermocouples. A gas cylinder supplies the CO₂ that is further pressurized by a booster pump, stored in a vessel and transported throughout the system to the reactor via 1/8" stainless steel tubing. A pressure gauge is used to monitor the reactor pressure. Valves are located at the reactor inlet and outlet for supplying and releasing the pressurized gas. The scCO₂ processing system and reactor are shown in Figures 3.1 and 3.2.

3.2. EXTRUSION SYSTEM

Extrusion experiments were conducted with a C. W. Brabender Instruments (South Hackensack, NJ) counter-rotating twin-screw extruder and a pelletizer to produce LLDPE pellet resin containing polymer and clay. A Haake Rheocord torque rheometer drives the twin-screw extruder, and an Eurotherm 808 temperature controller heats the extruder zones and the fiber die. At the extruder feed zone, a gravity-fed hopper supplies

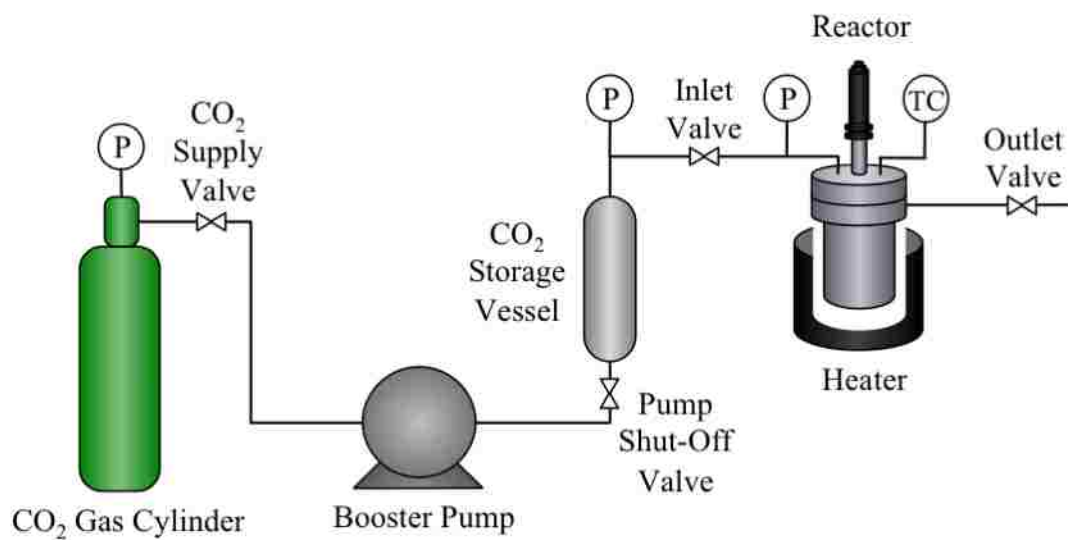


Figure 3.1. Schematic for the scCO₂ processing system

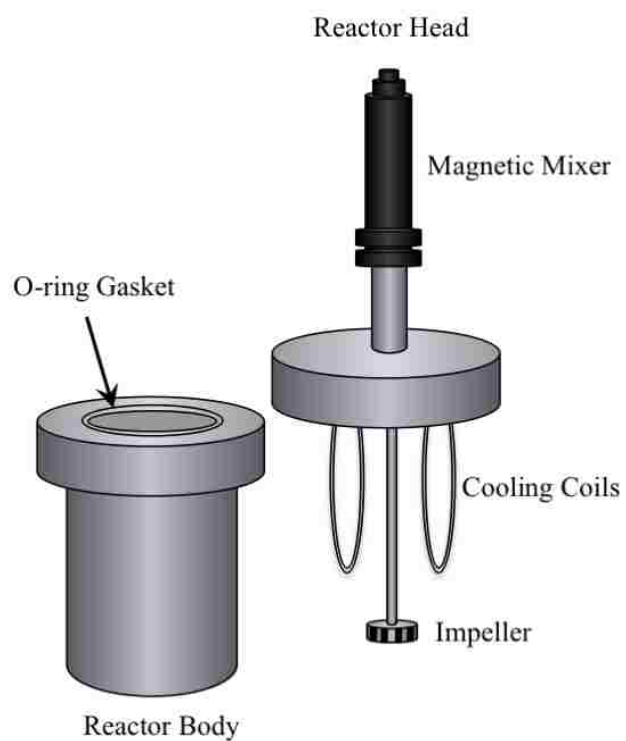


Figure 3.2. Schematic for the scCO₂ reactor

the extruder with a mixture of polymer resin and clay that is subsequently melted, mixed and extruded through the fiber die. Cooling water circulates the exterior of the extruder feed zone to curb premature polymer softening. Once extruded, the polymer-clay fiber is cooled in an ice water bath and spooled. The polymer-clay fiber is supercooled with liquid nitrogen and fed through an electric pelletizer to produce polymer-clay pellet resin. The extrusion setup is displayed in Figure 3.3.

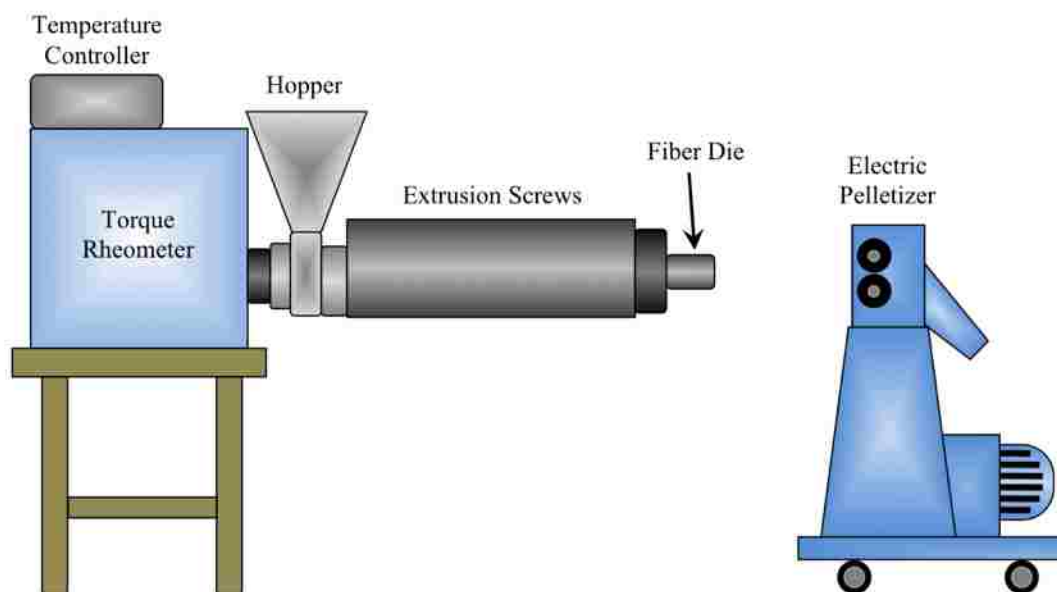


Figure 3.3. Schematic for extrusion and pelletizer system

3.3. X-RAY DIFFRACTION (XRD)

X-ray diffraction was completed with a Philips X-Pert diffractometer with a Cu- $K\alpha_1$ radiation source having a wavelength of 0.154056 nm. The generator voltage was

45 kV and the tube current was 40 mA. The XRD data angle range was from 1 to 10° with an increment of 2θ.

X-ray diffraction was conducted on polymer-clay pellet samples that were formed into 1 mm thick coins. Using a Carver Laboratory Press (Carver Model M), the polymer pellets were heated on a brass plate at 195°C until they were completely melted. Then a heated metal plate was placed on top of the lower plate with spacers in between them. The top plate was held in place until the polymer hardened and the coin could be removed.

3.4. FOURIER TRANSFORM INFRARED (FTIR) SPECTROMETRY

Fourier transform infrared analysis was conducted with a Nicolet Nexus 470 FTIR E.S.P. spectrometer (Nicolet Instrument Co., Madison, WI) that scanned the wave number range from 400 cm⁻¹ to 4,000 cm⁻¹ an average of 4 times. The spectrometer had a 4 cm⁻¹ resolution and a 1 cm absorption path length. Data from the spectrometer was collected with Omnic E.S.P. 5.1 computer software (Nicolet Instrument Co., Madison, WI) and analyzed with Spekwin32 computer software.

Heated to 185°C, a Carver Laboratory Press [Carver Model M] was used to create films for FTIR analysis by compressing polymer/clay samples to 68.9 MPa for approximately 50 s. The LLDPE/93A films had a thickness between 50 and 90 μm and the LLDPE-g-MA/93A films had a thickness ranging from 70 and 180 μm.

In order to determine the weight percent of 93A in the samples with FTIR analysis, initial calibration standards were made using a twin-screw extruder and an electric pelletizer. Used to estimate the quantity of clay in the processed samples, the first

LLDPE/clay standards contained 0, 1, 5 and 13 wt% 93A. Driven by a Haake Rheocord torque rheometer and heated with an Eurotherm 808 temperature controller, a batch mixer was used to produce LLDPE/clay calibration standards for determining precise amounts of clay within the samples that had 0.25 wt% clay and less. These LLDPE/clay standards contained 0, 0.05, 0.10, 0.15, 0.20 and 0.25 wt% 93A.

3.5. THERMOGRAVIMETRIC ANALYSIS (TGA)

Thermogravimetric analysis was conducted with samples weighing from 40 to 65 mg. The device is a Netzsch STA 409 C/CD. Samples were heated from 30 to 600°C at a rate of 10°C/min. Analyses were conducted under nitrogen atmosphere with a flow rate of 20 ml/min.

3.6. DIFFERENTIAL SCANNING CALORIMETRY (DSC)

Differential scanning calorimetry was conducted with a TA DSC 2010 on polymer-clay samples that weighed between 5 and 10 mg. Under a nitrogen atmosphere, the samples were heated from room temperature to 190°C at a rate of 10°C/min. This temperature was held for three minutes and then the samples were cooled at the same rate to about 35°C. The same heating/cooling processes were then repeated again and the data was collected. The first heating/cooling was to remove any thermal history within the sample. The second heating/cooling was to obtain the melting and crystallization temperatures. The pressure was at typical atmospheric conditions.

For DSC, polymer-clay resin samples were hermetically sealed in aluminum sample pans using a DSC sample press.

3.7. SCANNING ELECTRON MICROSCOPY (SEM)

Scanning electron microscopy was conducted on samples with a Hitachi S-4700 field emission (FE) SEM. This SEM employs a tungsten electron gun and possesses the ability for crystal orientation analysis.

Samples were cross-sectioned for SEM by supercooling them in liquid nitrogen for 2.5 h and then fracturing them with a hammer and a razorblade.

The types of LLDPE resin used in this work and their properties are listed in Table 4.1. The properties listed in Table 4.1 are the resin form, melting temperature (T_m), density and melt flow index (MFI) at 190°C. Supercritical CO₂-processing experiments involving LLDPE pellet resin were conducted with Dowlex 2517 (Dow Chemical Company, Midland, MI). The pellets are egg-shaped with 3 mm x 5 mm dimensions. Experiments requiring the processing of LLDPE granule resin in scCO₂ were undertaken with Exxon LL5100 obtained from ExxonMobil Chemical Company (Houston, TX). Most LLDPE grains were less than 0.5 mm in their largest dimension, while few were as large as 1 mm. Extruded samples undergoing scCO₂ processing utilized an extrusion grade LLDPE with trade name Dowlex 2047G (Dow Chemical Company, Midland, MI). After extrusion and pelletization, the resin was cylindrical with a diameter of 2 mm and a length of 5 mm. Used for scCO₂ processing experiments with maleated LLDPE, the pellet resin Polybond 3109 (Uniroyal Chemical Company, Middlebury, CT) has a MA graft level of 1 wt % and cylindrical dimensions of 3 mm (diameter) x 3.5 mm (length). The MA modification increases the compatibility of LLDPE with clay^{16,44-46} and CO₂.^{8,35,47}

Table 4.1. Properties of LLDPE resins used in scCO₂-processing experiments

Trade Name	Dowlex 2517	Exxon LL5100	Dowlex 2047G	Polybond 3109
Resin	Pellet	Granule	Pellet	Pellet
T_m (°C)	124	122	122	123
Density (kg/m³)	917	925	917	926
MFI (g/10min)	25	20	2.3	30

All supercritical fluid experiments used CO₂ that was obtained from Airgas (Rolla, MO). The CO₂ is research grade with a purity of 99.999%.

4.2. PROCEDURE

The procedure for preparing and processing polymer and clay in scCO₂ was comparable for all experiments and any deviations from this procedure are noted in the sections below. The processing materials, consisting of polymer and 93A, were prepared by placing them into a stainless steel thimble and mechanically mixing until the polymer was thoroughly coated with clay. All polymer resin was in pellet form unless otherwise noted as granule form. In the case of scCO₂ experiments with extruded LLDPE/93A resin, only the polymer-clay resin (no clay added) was processed in the reactor. The thimble was inserted into the reactor and the reactor was sealed. Next, the reactor was heated and pressurized. When the reactor reached the desired temperature and pressure, the experiment was deemed to have begun and was maintained in a batch mode at the prescribed conditions for a set duration. During the experiment, a constant and uniform reactor temperature was maintained by flowing water through the reactor head and driving an impeller within the reactor (~300 rpm). Once the experiment reached completion, the reactor was rapidly depressurized into an open container, and the samples were recovered.

4.2.1. Granule LLDPE Experiments. To prepare the polymer-clay mixture for scCO₂ processing experiments with LLDPE granule resin, 4.25 g of resin was mechanically mixed with 0.75 g of 93A. To observe the effect of two rapid depressurizations, the reactor was rapidly depressurized after 1 hr, allowed to cool, re-

pressurized and processed for 2 more hours before the final rapid depressurization. The samples were processed in a batch mode for a total of 3 hrs. The processing conditions and corresponding sample names for the experiments are outlined in Table 4.2.

Table 4.2. Conditions for processing 93A with LLDPE granule in scCO₂

Sample	T (°C)	P (MPa)
= +	37.8	17.2
- -	60.0	10.3
- +	60.0	17.2
- + *	60.0	17.2
+ -	98.9	10.3
+ +	98.9	17.2

* Run repeat

4.2.2. LLDPE and LLDPE-g-MA Experiments. The preparation of the polymer-clay mixture for 3-hr experimental processing times was identical for LLDPE and LLDPE-g-MA, accomplished by the mechanical mixing of 10 g of polymer with 2.5 g of 93A. The processing conditions and corresponding sample names for the experiments are outlined in Table 4.3.

4.2.3. LLDPE Experiments (1-hr). In experiments with LLDPE resin employing a 1-hr processing time, the polymer-clay mixture was prepared by mechanically mixing 5 g of LLDPE with 0.5 g of 93A. The processing conditions and corresponding sample names for the experiments are outlined in Table 4.4.

Table 4.3. Conditions for processing 93A with LLDPE and LLDPE-g-MA in scCO₂

Sample	T (°C)	P (MPa)
- -	60.0	10.3
- +	60.0	17.2
+ -	98.9	10.3
+ +	98.9	17.2

Table 4.4. Conditions for processing 93A with LLDPE in scCO₂ for 1 hr

Sample	T (°C)	P (MPa)
= -	37.8	10.3
= +	37.8	17.2
- -	60.0	10.3
- +	60.0	17.2

4.2.4. Extruded LLDPE/93A Experiments. Extruded LLDPE/93A resin was created by feeding a mixture of LLDPE and 93A through a twin-screw extruder at a temperature of 190°C. The amount of 93A in the LLDPE/93A mixture was adjusted in order to obtain nanocomposites containing 1, 5 and 13 wt% 93A. The LLDPE/93A melt was extruded through a fiber die and cooled in an ice water bath. The resultant LLDPE/93A fiber was supercooled with liquid nitrogen and pelletized.

Supercritical CO₂ experiments with extruded LLDPE/93A resin containing different amounts of clay were conducted by placing 5 g of the LLDPE/93A resin into the reactor and processing in a batch mode for 3 hrs. In an attempt to increase separation,

disruption and/or dispersion of stacked clay platelets by the rapid expansion CO₂ molecules, the reactor was quickly depressurized every half hour. The processing conditions and corresponding sample names for the experiments are outlined in Table 4.5.

Table 4.5. Conditions for processing extruded LLDPE/93A in scCO₂

93A (wt%)	T (°C)	P (MPa)
1	98.9	17.2
5	98.9	17.2
13	98.9	17.2

5. EXPERIMENTAL ANALYSIS

5.1. DISPERSION ANALYSIS BY XRD

5.1.1. Results. Samples underwent XRD analysis in order to determine if the scCO₂ processing had altered the dispersion of 93A.

5.1.1.1 Resin size experiments: granule vs. pellet. Two resin forms of LLDPE, granule and pellet, were processed in scCO₂ to investigate the dependency of clay dispersion on resin size and the associated steps of sample analysis. The d₀₀₁-spacings were determined by XRD and employed to judge the effect of processing on the clay. The presence of a peak in XRD analysis of pellet LLDPE/93A samples is indicative of the occurrence of clay infusion, and the movement in the peak position is indicative of changes in intercalation/exfoliation behavior. Determination of clay infusion into granule LLDPE was not attempted since once mixed, granule LLDPE and clay could not be readily separated due to their small particle sizes. So it would be unknown whether any clay detected by XRD could be attributed to clay mixed with LLDPE, clay infused into LLDPE or a combination of the two. However, a change in intercalation/exfoliation behavior was detected as a change in the d₀₀₁-spacing between clay platelets.

5.1.1.1.1 LLDPE granules in scCO₂. The granule LLDPE/93A samples, processed at conditions in Table 4.1, were analyzed by XRD to determine if alterations resulted from scCO₂ processing. The XRD patterns are shown in Figure 5.1. All samples exhibited peaks near that of pure 93A, which is at a Bragg angle of 3.385° and thus represents a d₀₀₁-spacing of 26.1 Å. As seen in Table 5.1, the d-spacing of 93A platelets decreased as the CO₂ processing density increased up to a certain limit. After reaching a CO₂ density of 0.656 g/cm³, the scCO₂ had no effect on the d-spacing of the clay. This is

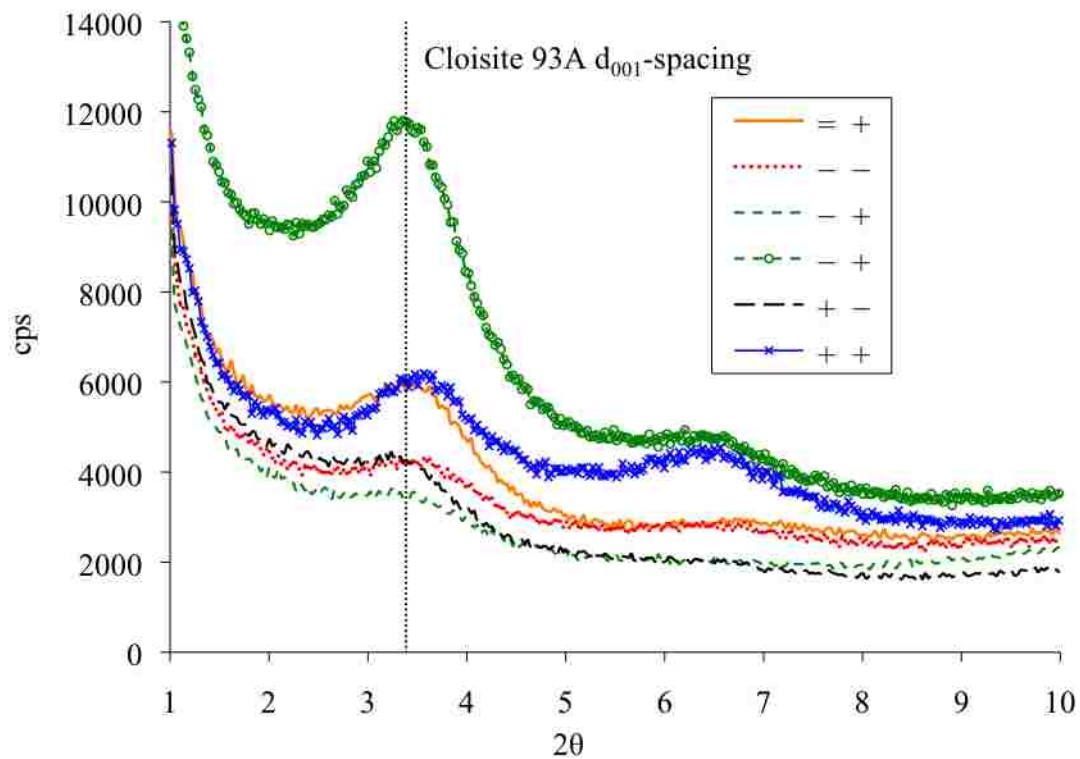


Figure 5.1. XRD patterns of granule LLDPE/93A samples

Table 5.1. CO₂ density vs. d₀₀₁-spacing of granule LLDPE/93A samples

Sample	ρ_{CO_2} (g/cm ³)	d ₀₀₁ -spacing (Å)
Pure 93A	NA	26.1
+ -	0.200	(+) 0.7
- -	0.325	(-) 0.2
+ +	0.402	(-) 0.9
- +	0.656	26.1
- +	0.656	26.1
= +	0.825	26.1

postulated to be due to the reduced temperature and elevated pressure, restricting the mobility of the surfactant and polymer chains as a result of the higher crystallinity and increased compression. The lowest density condition investigated, sample (+ -), had an increase in d-spacing, whereas the second and third lowest density conditions had decreases in d-spacing. High temperature and low pressure both improved surfactant mobility to prompt an increase in the gallery height. Losses in gallery height can be attributed to sample conditions involving a low temperature (sample (- -)) or high pressure (sample (+ +)) that individually, impeded the surfactant in such a way as to collapse the gallery.

X-ray diffraction pattern intensities are not compared due to the phenomenon of preferred orientation (especially prominent in powder samples),²¹ where crystallites are not randomly oriented within the sample and cannot produce a consistent intensity profile. The issues associated with preferred orientation are exemplified in Figure 5.1 by sample (- +) that was experimentally repeated and produced the same d-spacing, but a largely different intensity profile.

5.1.1.1.2 LLDPE pellets in scCO₂. Pellets of LLDPE were processed with 93A in scCO₂ at four different run conditions (Table 4.2). X-ray diffraction analysis was conducted on the LLDPE/93A pellets to determine if infusion had occurred and also if d₀₀₁-spacing was altered. The results are displayed in Figure 5.2. The XRD pattern reveals 93A creates a peak at a Bragg angle of 3.4° which corresponds to a d₀₀₁-spacing of 25.9 Å. All samples display similar peaks around the same angle, indicating that infusion of 93A occurred.^{20,41,44,48} The sample (- +) has the lowest almost nonexistent peak, which could indicate either the clay is well dispersed or almost no clay is in the

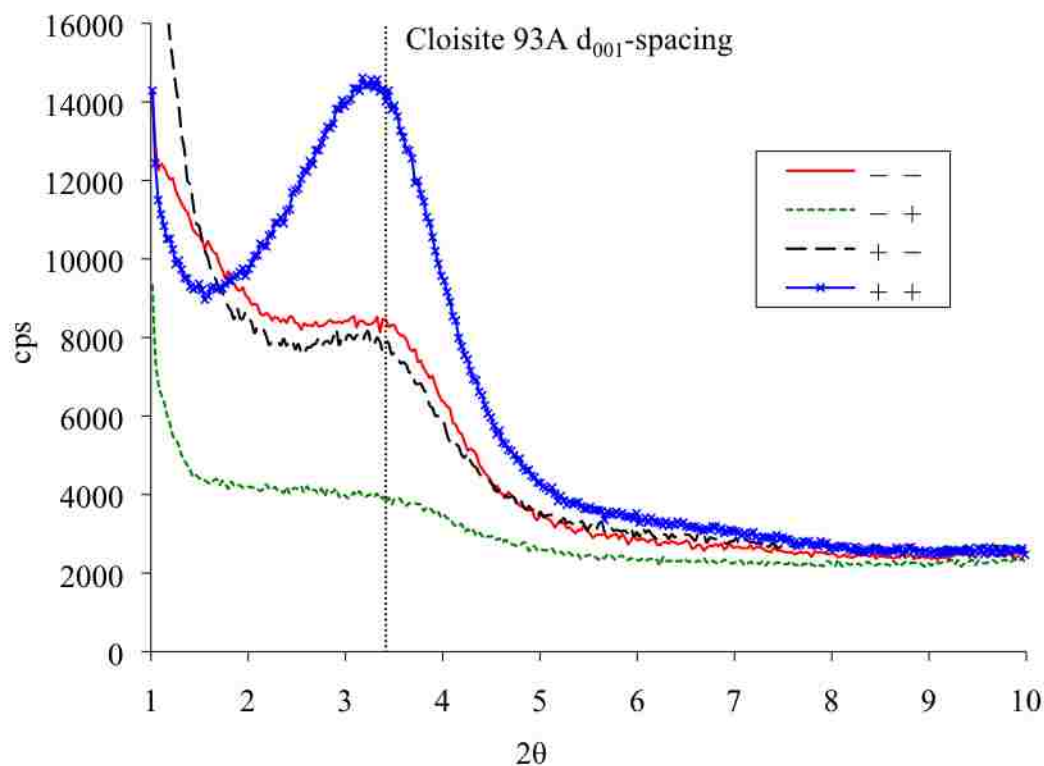


Figure 5.2. XRD patterns of pellet LLDPE/93A samples

polymer,^{16,41,44,48} most likely the latter. Presented later in this work, analysis of the quantity of clay within the sample will help to confirm which of these conjectures is correct, as XRD alone is not enough to determine if the clay is well dispersed or exfoliated.⁴⁸ Samples (– –), (+ –) and (+ +) have clear peaks from the 93A with d_{001} -spacings of 27.3, 28.1 and 27.3 Å, respectively. The increase in d_{001} -spacings as compared to pure 93A could be due to the polymer diffusing between platelets and pushing them apart or changes in conformation of the intercalated surfactant, making them closer to an exfoliated structure.^{16,41,44,46,48} As with the granule LLDPE, the low-pressure and a high-temperature sample (+ –), possessing the lowest density, had the largest increase in spacing between platelets. This sample experiences an increased

platelet spacing possibly since the CO₂ molecules, polymer chains and surfactant chains are more mobile in a low-pressure environment, making it easier for intercalation or surfactant conformation changes. And to the same end, the high temperature helps mobility by plasticizing the polymer and surfactant. Displayed in Table 5.2, d-spacing increased as the CO₂ density decreased, exhibiting the same inverse correlation between d-spacing and fluid density as the granule LLDPE/93A samples. Larger intensities in XRD peaks can indicate an increase in tactoid size and/or parallel registry of the clay.^{40,41} The run with the highest conditions, sample (+ +), had the largest peak intensity, indicating that this environment could create more uniform d-spacings of 93A within the polymer.⁴⁰

Table 5.2. CO₂ density vs. d₀₀₁-spacing of pellet LLDPE/93A samples

Sample	ρ_{CO_2} (g/cm ³)	d ₀₀₁ -spacing (Å)
Pure 93A	NA	25.9
+ -	0.200	(+) 2.2
- -	0.325	(+) 1.4
+ +	0.402	(+) 1.4

5.1.1.1.3 Summary. From the XRD results, it is apparent that 93A did not experience as large of an increase in d-spacing in processing with granule LLDPE as compared to pellet LLDPE. This is suggested to be due to the lower continuous processing time of the granule samples. Granule samples underwent two rapid

depressurizations with an interrupted processing time in comparison to one rapid depressurization with a continuous processing time for pellet samples, suggesting that a continuous processing time is more significant to intercalation/exfoliation behavior. It is possible that a continuous 3-hr processing time for granule resin could produce similar results to those obtained for the pellet resin. Also, the pellet resin showed improvement in d-spacing for three processing conditions whereas the granule resin showed improvement for one. In terms of sample analysis, as it is not the case with granule LLDPE, infusion of 93A into pellet LLDPE is determined simultaneously with the d-spacing determination by XRD, providing more information with a single analysis. In addition, the larger size of the pellet resin could enable its cross-sectioning to ascertain the depth of clay infusion. Exhibiting a greater improvement in intercalation/exfoliation behavior as well as important infusion data, pellet LLDPE samples were employed for the remainder of this work.

5.1.1.2 Processing time experiments: LLDPE in scCO₂ for 1 hr. At the processing conditions displayed in Table 4.3, LLDPE and 93A were processed in scCO₂ for a period of 1 hr in order to determine if these conditions could promote clay infusion into LLDPE. X-ray diffraction analysis was conducted on the samples and the resultant patterns were compared. Seen in Figure 5.3, there is no peak present for any of the processing conditions that can be attributed to 93A. The absence of a peak is due to the lack of clay infusion into LLDPE and was confirmed by SEM (Figure A.1). Displayed in Figure 5.4 and 5.5, XRD patterns for experiments at 60°C for 1-hr processing times were superimposed on patterns for 3-hr processing times to show the importance of the

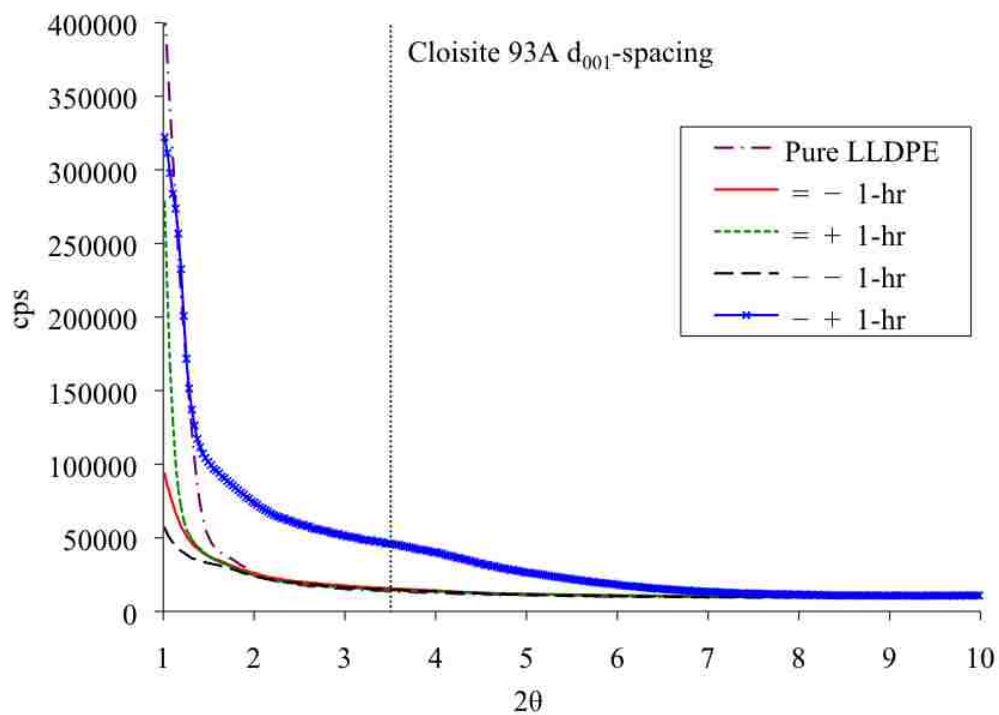


Figure 5.3. XRD patterns of LLDPE/93A samples in scCO₂ for 1 hr

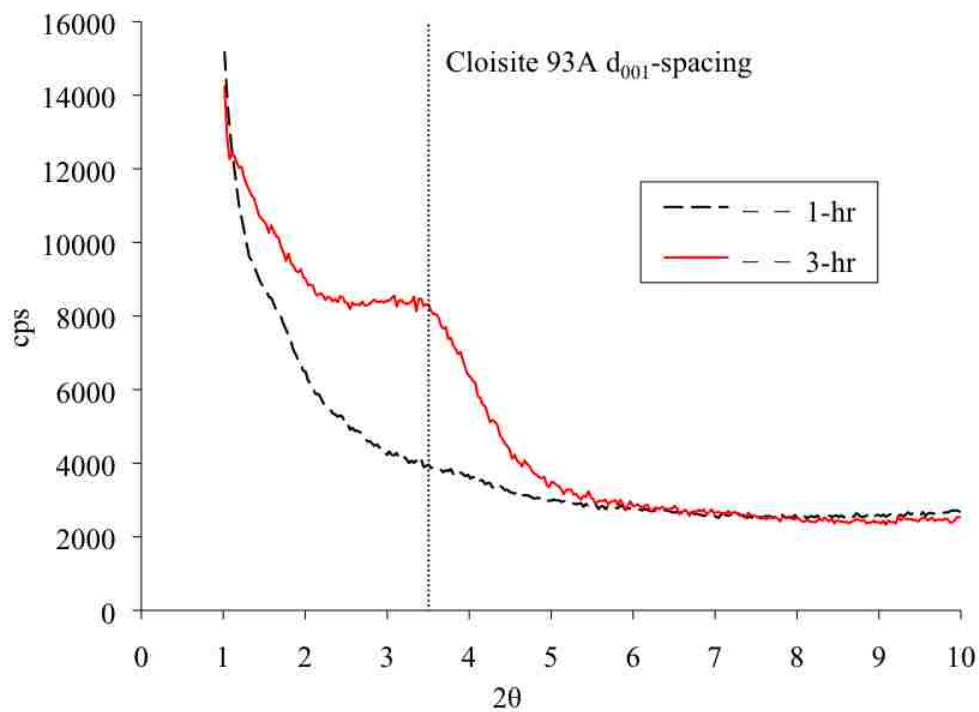


Figure 5.4. XRD patterns of LLDPE/93A samples (- -) in scCO₂ for 1 vs. 3-hr periods

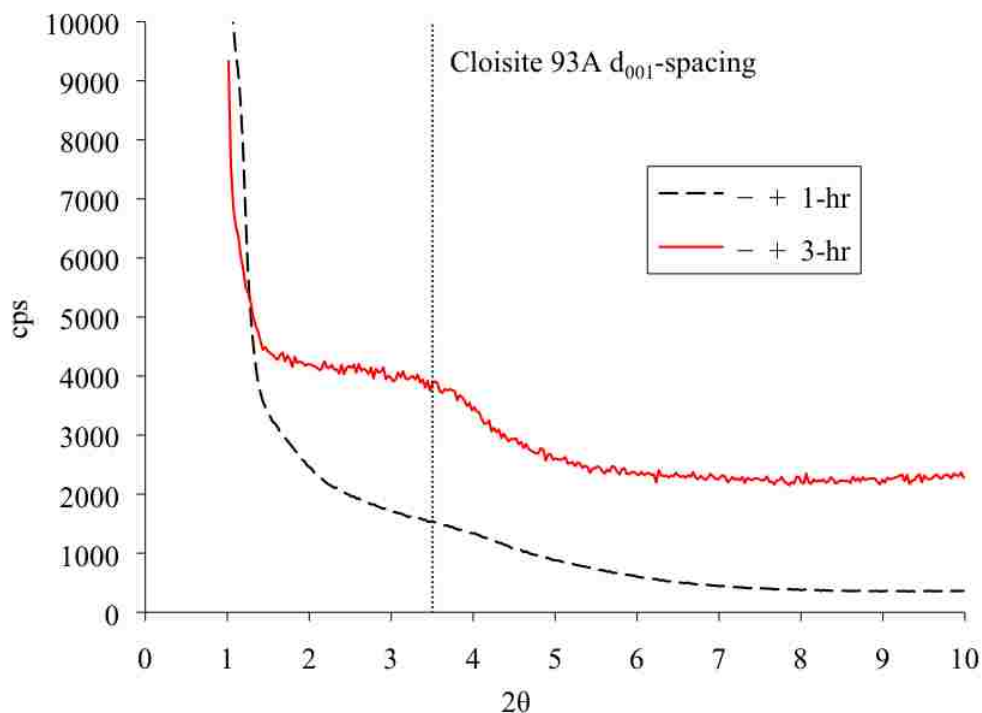


Figure 5.5. XRD patterns of LLDPE/93A samples (- +) in scCO₂ for 1 vs. 3-hr periods

extended processing to achieving clay infusion. The figures clearly indicate that at these conditions, 1 hr of scCO₂ processing is insufficient for infusing 93A into LLDPE.

5.1.1.3 ScCO₂ capability experiments: extruded LLDPE/93A. To ascertain the effect of scCO₂ processing on clay already within the polymer matrix, scCO₂ processing experiments were conducted with extruded LLDPE/93A samples containing 1, 5 and 13 wt% 93A. If scCO₂ has no effect on the clay after it is within the polymer, then it cannot be expected to aid in intercalation or exfoliation after infusion. This scenario would require the intercalation/exfoliation of clay to occur before clay infusion is undertaken. The experiments were all conducted at conditions of 210°C and 17.2MPa, ensuring that the only variation was the amount of clay within the sample. After processing, the extruded and scCO₂ processed samples (X/scCO₂) were analyzed by XRD and compared

to their parent samples that only underwent extrusion (X). The XRD patterns are displayed in Figures 5.6 and 5.7. Due to scCO₂ processing, the d-spacing for 5 and 13 wt% 93A increased, while the d-spacing stayed the same for 1wt% 93A (Figures 5.8, 5.9 and 5.10). The largest increase in spacing was observed with 5 wt% 93A, which was an increase of 11.8 Å from its extruded only counterpart (Table 5.3). Increases in the d-spacing of platelets are the result of surfactant conformation changes and/or the intercalation of polymer chains. Most likely, the 1 wt% 93A sample remained unaffected by scCO₂ processing due to the low amount of clay in the sample, corresponding to an even lower amount of clay near the surface of the LLDPE pellet capable of exposure to the scCO₂. An increase in peak intensity for samples as compared to their non-scCO₂

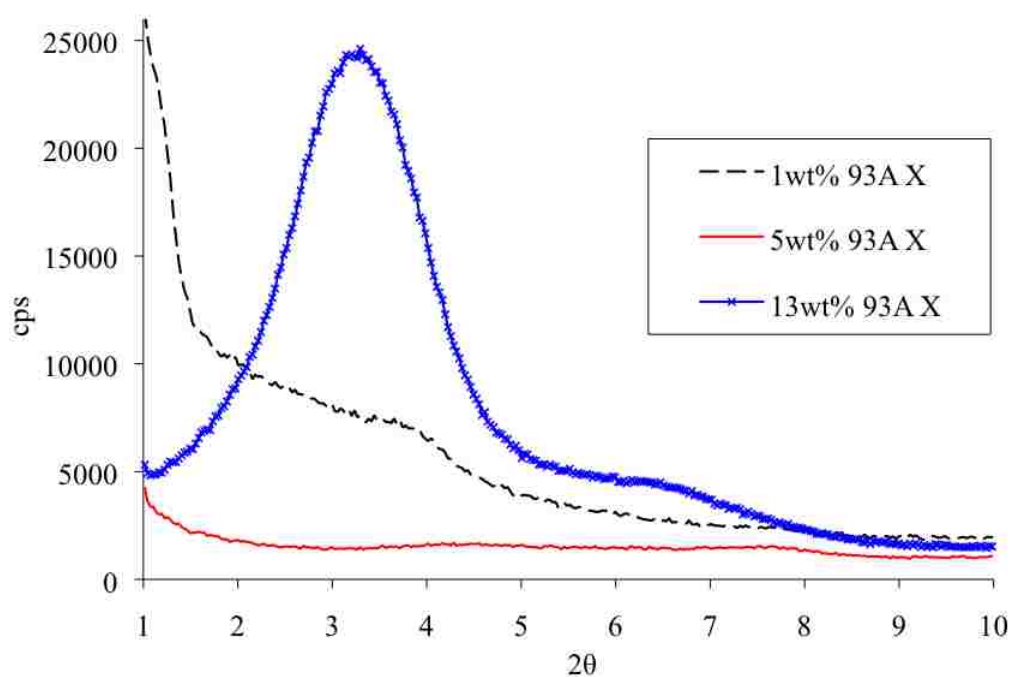


Figure 5.6. XRD patterns of X LLDPE/93A samples

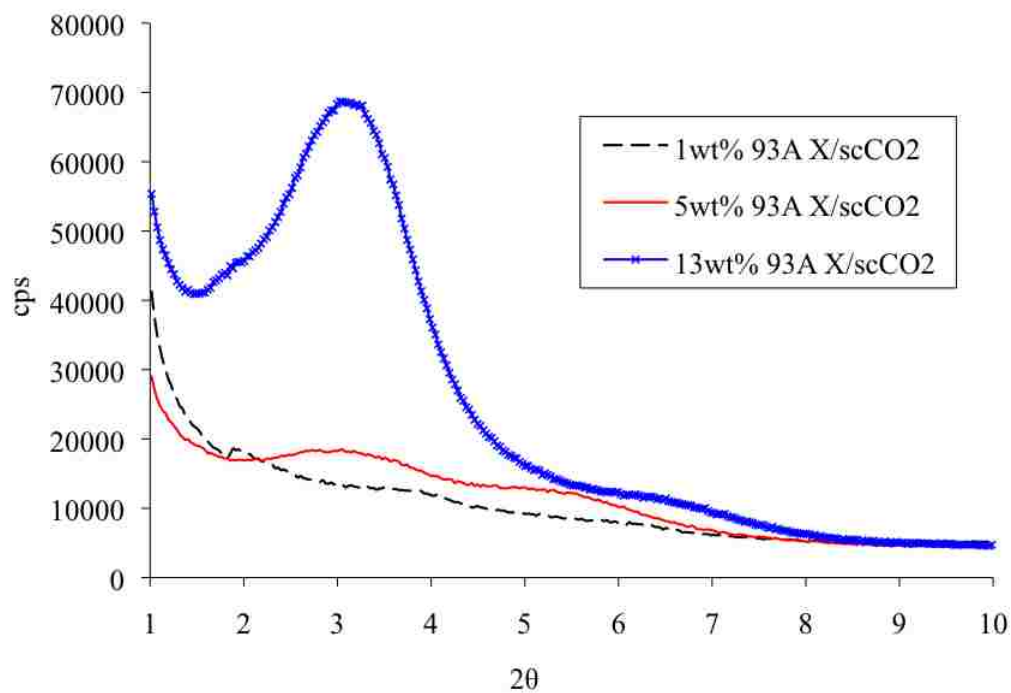


Figure 5.7. XRD patterns of X/scCO₂ LLDPE/93A samples

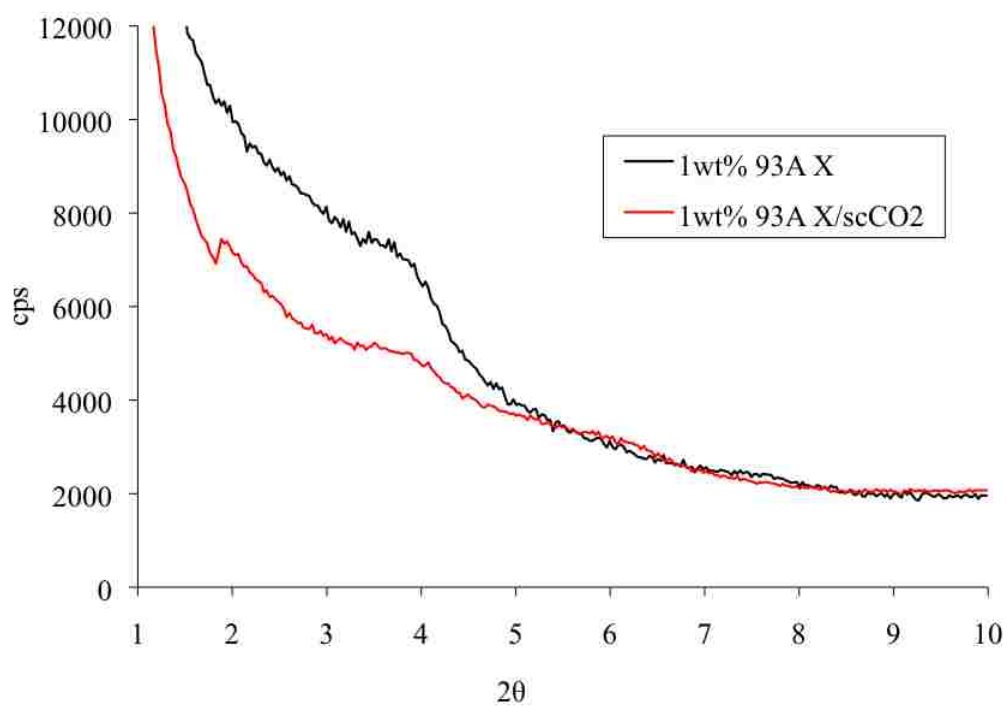


Figure 5.8. XRD patterns of LLDPE/93A samples for X vs. X/scCO₂ at 1 wt% 93A

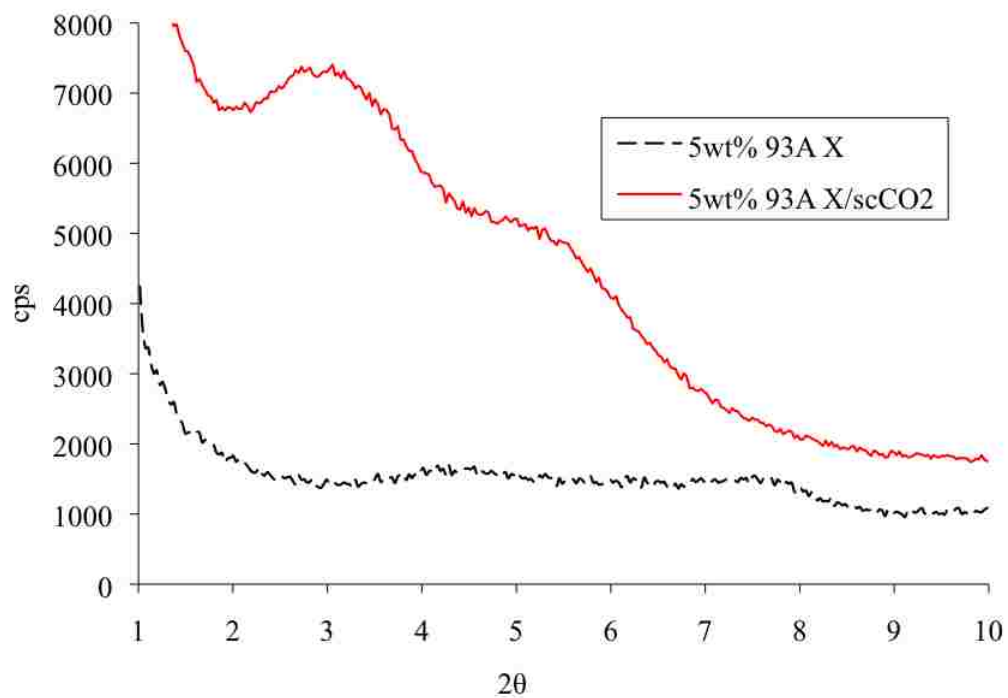


Figure 5.9. XRD patterns of LLDPE/93A samples for X vs. X/scCO₂ at 5 wt% 93A

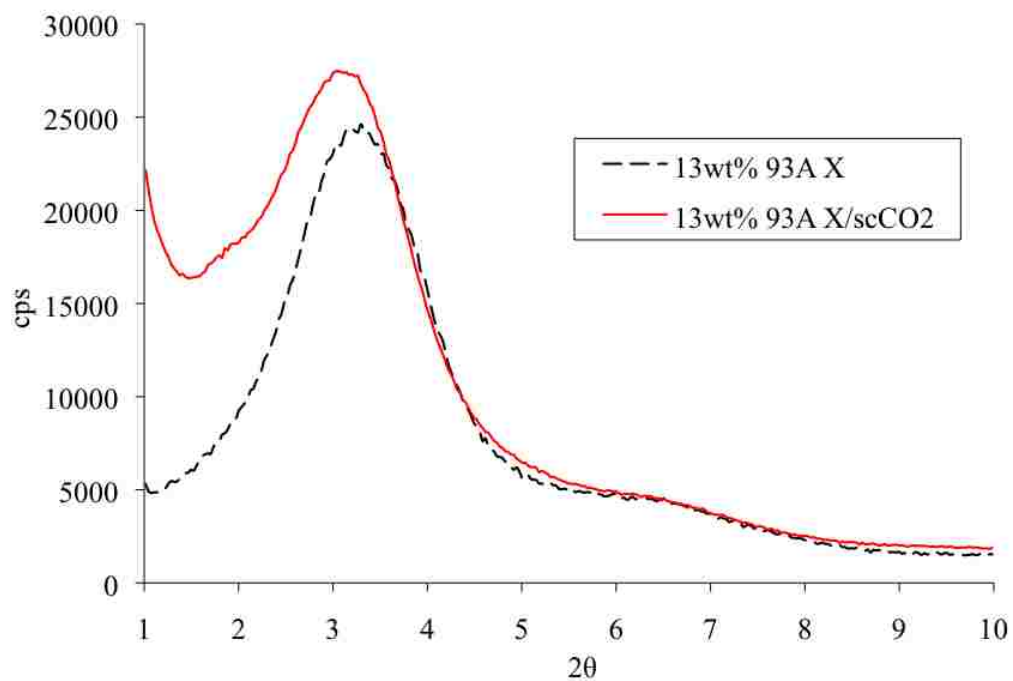


Figure 5.10. XRD patterns of LLDPE/93A samples for X vs. X/scCO₂ at 13 wt% 93A

Table 5.3. d_{001} -spacing values of LLDPE/93A samples for X vs. X/scCO₂

Sample	X (Å)	X/scCO ₂ (Å)	Δ (Å)
1wt%93A	25.4	25.4	0
5wt%93A	20.6	32.4	(+) 11.8
13wt%93A	27.0	28.6	(+) 1.6

processed counterparts could indicate an increase in the d-spacing heterogeneity of the clay.^{40,41} The treatment increases the mobility of the clay platelets by plasticizing the intercalated surfactant and surrounding polymer chains, allowing the formation of a more aligned structure.⁴⁰ The results indicate that within the LLDPE matrix, the supercritical fluid can still affect the intercalation/exfoliation behavior of 93A.

5.1.1.4 Compatibility experiments: LLDPE-g-MA. To investigate the effect of compatibility between processing components has on infusion, maleated LLDPE (LLDPE-g-MA) was processed with 93A in scCO₂ at different temperatures and pressures (Table 4.2). The polar MA modification increases the compatibility of LLDPE with the clay and the processing fluid, respectively, capable of interacting favorably with oxygen groups on the clay surface and the significant quadrupole moment of CO₂. The resultant samples were analyzed by XRD. From the XRD patterns (Figure 5.11), it is apparent that 93A was successfully infused into the LLDPE-g-MA for all run conditions since the 93A peak is present.^{20,41,44,48} Sample (- +) exhibits a less pronounced peak in comparison to the other samples in the XRD plot. A possible scenario could be that the clay is almost completely dispersed or scarcely any clay is present within the sample, giving little to no peak in the XRD pattern.^{16,41,44,48} As stated above for LLDPE (Section

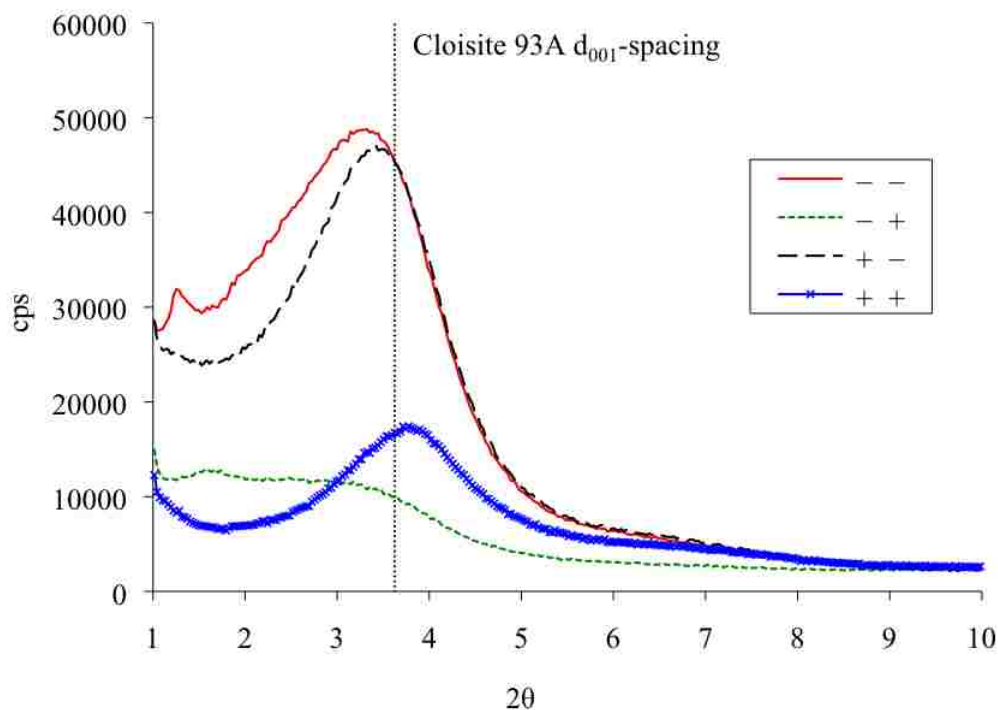


Figure 5.11. XRD patterns of LLDPE-g-MA/93A samples

5.1.1.2), this scenario can be confirmed or disproven by a quantity of clay analysis found later in this work. The d_{001} -spacings for the clay peaks found in samples (---), (+-), and (++) are, respectively, + 2.4, + 1.5 and - 1.0 Å in relation to that of 24.4 Å for 93A.

These differences in distances may not be very large, but may still be significant, as a trend seems to exist. The d-spacings indicate that in samples (---) and (+-), where the pressure was low, the spacing between clay platelets increased due to processing. In sample (---), the lowest temperature and pressure environment, the largest increase in spacing between clay platelets occurred. In this instance, the afforded chain mobility from a high temperature is less significant than from a low pressure, as the low-temperature condition was sufficient to warrant a larger increase in platelet spacing than that for the high temperature. The MA modification of the polymer could be altering the

interaction between the CO₂, organoclay and the polymer to enable greater layer separation at a lower temperature. Sample (+ -) might not have realized such a large increase in spacing because increased chain mobility from the high temperature could have resulted in a rearrangement of the surfactant in a manner to lessen the increase in layer spacing. And at a higher pressure seen in sample (+ +), the spacing between clay platelets decreased. The mobility afforded by the high temperature could have resulted in rearrangement of the surfactant chains to allow the compression by the increased pressure to reduce d-spacing.⁴⁹ In terms of a relationship between CO₂ density and d-spacing, no trend seems to exist (Table 5.4). The increase in distance between platelets is favored over a decrease because it can indicate that surfactant conformation has increased or that polymer has found its way between the platelets, enhancing the intercalation/exfoliation behavior of the clay.^{41,44,46,48}

Table 5.4. CO₂ density vs. d₀₀₁-spacing of LLDPE-g-MA/93A samples

Sample	ρ_{CO_2} (g/cm ³)	d ₀₀₁ -spacing (Å)
Pure 93A	NA	24.4
+ -	0.200	(+) 1.5
- -	0.325	(+) 2.4
+ +	0.402	(-) 1.0

Comparing LLDPE and LLDPE-g-MA, XRD analysis exhibited different relations between d-spacing and sample conditions which can be attributed to the MA modification of LLDPE-g-MA. The high-temperature and low-pressure sample for

LLDPE had the largest increase in platelet spacing, indicating preferential conditions when trying to achieve an intercalated or exfoliated clay structure. However, LLDPE-g-MA experienced the greatest intercalation/exfoliation behavior with the low-temperature and -pressure sample. It is proposed that the polar MA groups in LLDPE-g-MA alter the interaction between CO₂, organoclay and polymer to enhance intercalation/exfoliation behavior at a lower temperature than that for LLDPE.

5.1.2. Discussion. In this section, the different factors that can affect the clay gallery height are discussed, and the samples are analyzed in terms of the cause of clay gallery height changes and how the clay gallery is affected by processing conditions.

5.1.2.1 Factors affecting clay gallery. The height of the clay gallery can be affected by different factors such as the intercalant molecular size, the surfactant conformation and the interaction between the surfactant and the clay surface.

5.1.2.1.1 Molecular size. In order to determine if changes in gallery height of the clay were brought on by rearrangement of surfactant or LLDPE intercalation, the sizes of involved molecules were determined. Following the work of Xi et al.,⁵⁰ the estimated molecular size of the 93A surfactant was calculated with data for the van der Waals radius, covalent bond radius and bond angle. The size of the surfactant molecule was calculated to be 4.3 Å for the nitrogen-containing head and 23.8 Å for the length of the tail composed of 18 carbon atoms, resulting in 28.1 Å for the full length of the molecule. The molecular diameter of the surfactant tail and the LLDPE chain were assumed equivalent as they are both composed of a chain of carbon and hydrogen atoms, giving them a 4.1 Å diameter in the smallest dimension.

5.1.2.1.2 Surfactant conformation. Under certain conditions, the surfactant can undergo conformation changes within the gallery; leading to increases or decreases in gallery height. Conformation terminology is adopted from Xi et al.⁵⁰ to explain the arrangement of the surfactant from observed d-spacing values. In its initial state, the 93A surfactant was assumed to exist in a paraffin-type monomolecular conformation between the clay layers, whereby the surfactant tail is angled away from the clay surface. To make this determination, the gallery height was calculated by subtracting the thickness of a clay platelet of 9.6 Å from the d_{001} -spacing of 93A (e.g., a 93A d_{001} -spacing of 25.9 Å corresponds to a gallery height of 16.3 Å). The gallery was then used to determine the molecular packing arrangement. For a surfactant monolayer conformation, gallery height would be near 4.1 Å for the minimum dimension whereas around twice this value would indicate an assumed bilayer conformation. With greater gallery heights, the conformation is assumed to transition to the paraffin-type monomolecular arrangement that characterizes the 93A surfactant conformation. (Other conformations can exist, however, only these have been discussed to explain the methodology applied in determining the surfactant conformation.) The paraffin-type chain arrangement is altered by an increase or decrease in the tilt angle away from the clay surface. At a low enough angle, the chain will transition to a bilayer arrangement and further losses in gallery height will result in transition to a monolayer arrangement.

5.1.2.1.3 Surfactant-clay surface interaction. Changes in the gallery of 93A from scCO_2 processing can result from changes in the surfactant interaction with the clay surface. In the gallery, 93A surfactant is either tethered to the clay surface by ion-dipole interactions or bound tail-to-tail to adjacent surfactant chains by van der Waals forces.⁴⁹

During processing, the scCO₂ fluid plasticizes the surfactant, increasing its mobility. Mobilization of tail-to-tail bound chains can induce their cation exchange with residual sodium cations, tethering the surfactant chains to the clay surface via ion-dipole bonds. The increased packing from the newly bound surfactant can prompt conformation changes that lead to increases in gallery height.

5.1.2.2 Analysis of samples. The above factors were applied to sample results in order to determine the cause of changes in clay gallery height, and the effect of processing conditions on the intercalation/exfoliation behavior of samples was examined.

5.1.2.2.1 Cause of clay gallery changes. Except for the case of extruded LLDPE/93A with 5 wt% 93A in scCO₂, the maximum increase in gallery spacing considering all experiments was 2.4 Å (LLDPE-g-MA sample). Since the gallery height experienced an increase less than the diameter of a LLDPE chain (4.1 Å) and the even larger LLDPE-g-MA chain, no intercalation is postulated to have taken place and increases in spacing are due to the conditions favoring increased cation exchange of surfactant, increasing bound surfactant concentration. This expands the gallery by forcing a packing arrangement wherein the surfactant is tilted at a larger angle away from the clay surface. For extruded LLDPE/93A with 5 wt% 93A, LLDPE intercalation could have occurred since the increase in gallery height of 6.3 Å is greater than that of the diameter of a LLDPE chain. However, it is more likely intercalation did not occur, but rather the surfactant concentration increased to a level where the chain is closer to being perpendicular to the clay surface, as noted by the gallery height (22.8 Å) being near to the length of the surfactant tail (23.8 Å). Losses in gallery height, at a maximum of 1 Å (LLDPE-g-MA sample), were attributed to the processing conditions enabling the

surfactant to form a more efficient packing arrangement without further cation exchange, decreasing the angle of the surfactant chain to allow the layer to collapse.

5.1.2.2.2 Effect of processing conditions. The scCO₂ environment best suited for enhancing the intercalation/exfoliation behavior of LLDPE/93A samples was determined to result from high-temperature (98.9°C) and low-pressure (10.3 MPa) experiments. High temperatures reduce the crystallinity of the surfactant by melting, enabling increased plasticization by CO₂ to enhance chain mobility. In addition, the relatively lower experimental pressure improves chain mobility by decreasing surfactant compression. Thompson et al.⁴⁰ predominantly observed that increases in pressure led to an expansion in the gallery of organoclays. This result was due to the increase in CO₂ concentration furthering surfactant plasticization to enhance mobility. The maximum pressure employed in the Thompson et al. study of 8.4 MPa is below the minimum employed in this work of 10.3 MPa that led to improved intercalation/exfoliation behavior. It is postulated that a critical pressure exists (i.e., the solubility pressure) and above this pressure, CO₂ concentration in the surfactant remains constant, preventing increases in plasticization due to dissolving CO₂. Any further increases in pressure are detrimental to platelet separation due to compression forces brought on by the hydraulic pressure effect. It is important to note that as the CO₂ is interacting with the surfactant, it is also interacting in a similar fashion with the polymer that could alter interaction of CO₂ with the surfactant.

Intercalation/exfoliation behavior of LLDPE-g-MA samples was best enhanced with conditions employing a low temperature (60°C) and a low pressure (10.3 MPa). Mentioned above, the lower pressure is favored for gallery expansion to alleviate the

hydraulic pressure effect. In comparison to LLDPE, the reduction in temperature for increasing the gallery height can be explained by the increased compatibility of LLDPE-g-MA with the processing fluid and the clay. Greater dissolution of CO₂ occurs in the maleated polymer, enabling greater access of CO₂ to the clay galleries. Additionally, the maleated polymer allows the clay platelets to separate more easily due to attractive forces between MA and the clay surface. The combination of these factors led to a lower temperature required for mobilizing surfactant to give rise to expansion of clay galleries.

5.2. EXTENDED ANALYSIS OF 93A-INFUSED LLDPE AND LLDPE-g-MA

5.2.1. Results. Further analysis was conducted on samples of LLDPE and LLDPE-g-MA infused with 93A at scCO₂-processing conditions displayed in Table 4.2. The methods used to analyze the samples were DSC, TGA, FTIR spectrometry and SEM.

5.2.1.1 DSC. Samples of LLDPE and LLDPE-g-MA infused with 93A were analyzed by DSC to ascertain endothermic and exothermic changes attributed to the respective melting and crystallization of the PCN. Samples underwent two heating/cooling cycles during DSC, where the first cycle was used to determine changes in the polymer crystallinity induced by the scCO₂ processing. The second cycle was used to determine changes in the polymer processing conditions and crystallinity due to the infusion of clay.

The DSC analysis of LLDPE and LLDPE-g-MA samples infused with 93A produced curves that are exemplified by those displayed in Figure 5.12. The maximum

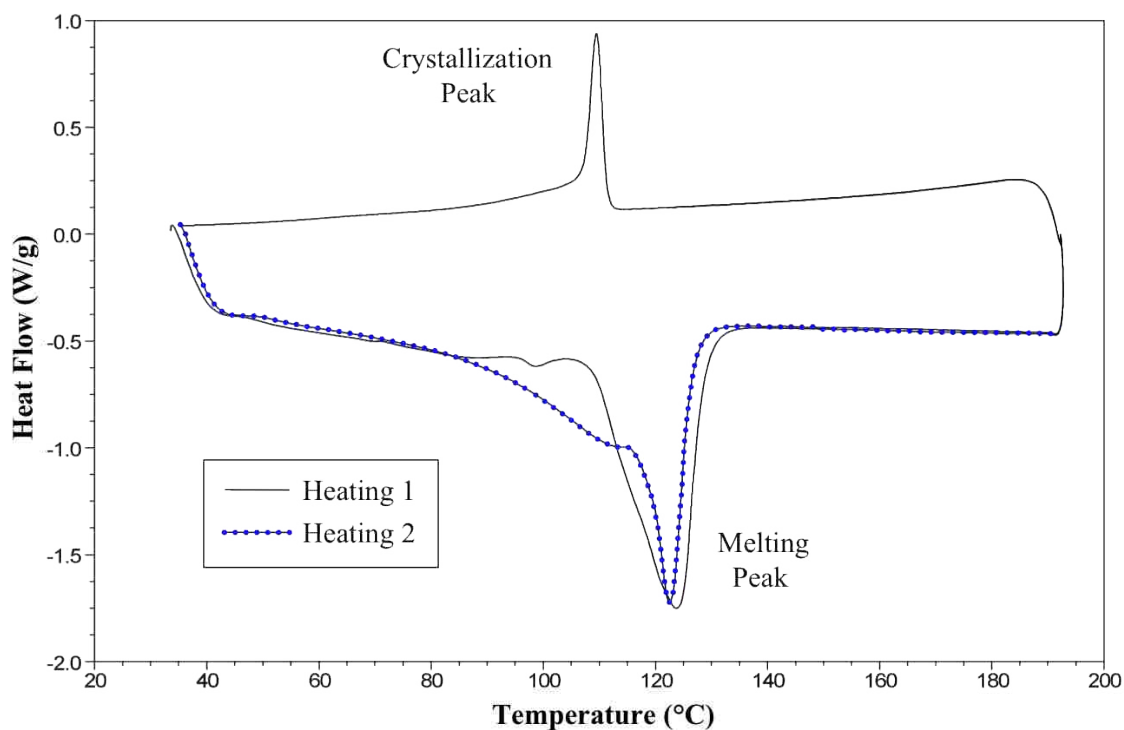


Figure 5.12. Example of DSC curves produced by LLDPE/93A and LLDPE-g-MA/93A samples

temperature variation of LLDPE/93A samples from pure LLDPE was 0.98°C for melting temperature and 1.20°C for crystallization temperature. As compared to pure LLDPE-g-MA, the melting and crystallization temperatures of the LLDPE-g-MA/93A samples deviated by a maximum of 0.46°C and 0.80°C , respectively. The changes seen from the addition of 93A to the LLDPE and LLDPE-g-MA are not very significant, leading one to infer that the processing conditions of the nanocomposite should not change much from those for their pure polymer counterparts. Melting and crystallization temperatures for the samples are summarized in Table 5.5.

Table 5.5. Melting (T_m) and crystallization (T_c) temperatures of LLDPE and LLDPE-g-MA infused with 93A as measured by DSC

Sample	LLDPE		LLDPE-g-MA	
	T_m (°C)	T_c (°C)	T_m (°C)	T_c (°C)
Pure	123.11	105.23	122.58	108.67
--	(+) 0.68	(+) 1.20	(-) 0.46	(+) 0.16
-+	(+) 0.85	(+) 1.05	(-) 0.11	(+) 0.26
+-	(+) 0.98	(+) 1.10	(-) 0.02	(+) 0.80
++	(+) 0.86	(+) 0.41	(+) 0.08	(+) 0.41

From the PCN sample melting curves, the crystallinity (α) of the polymer was calculated using the equation

$$\alpha = \frac{H_f}{H_{f100\%}} \quad (4)$$

where H_f is the melting enthalpy (aka heat of fusion) for the polymer sample and $H_{f100\%}$ is the melting enthalpy for a theoretical 100% crystalline polymer. The value of $H_{f100\%}$ for 100% crystalline polyethylene is nominally 293 J/g.⁵¹ The enthalpy of melting (H_f) for the sample is determined by integrating the area under the melting curve, as exemplified in Figure 5.13. The crystallinities of PCN samples are displayed in Table 5.6 and Table 5.7. Compared to pure LLDPE, the maximum variation in crystallinity observed for processed samples was 2.35% and 3.21% for heating 1 and heating 2, respectively. Processed samples of LLDPE-g-MA varied in crystallinity by a maximum of 3.28% for heating 1 and 1.30% for heating 2 in comparison to pure LLDPE-g-MA.

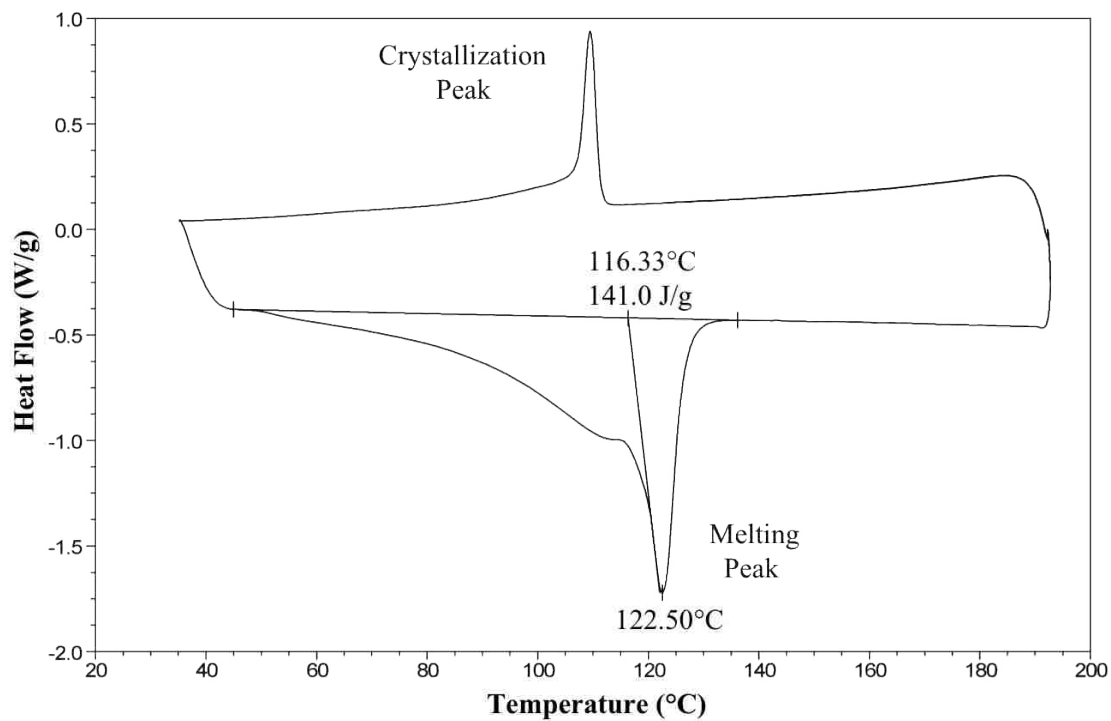


Figure 5.13. Example of integrating the area under the melting curve

Table 5.6. Crystallinity of LLDPE samples infused with 93A

Sample	Heating 1 (%)	Heating 2 (%)
LLDPE	34.64	36.11
--	(+) 0.75	(+) 3.21
-+	(-) 0.54	(-) 1.33
+-	(+) 2.29	(+) 2.12
++	(+) 2.35	(+) 1.98

Table 5.7. Crystallinity of LLDPE-g-MA samples infused with 93A

Sample	Heating 1 (%)	Heating 2 (%)
LLDPE-g-MA	47.88	49.42
--	(+) 0.34	(+) 0.65
-+	(+) 1.33	(+) 1.16
+ -	(+) 0.65	(-) 1.30
++	(+) 3.28	(+) 1.30

5.2.1.2 TGA. The TGA of PCN samples helped to determine sample composition and thermal stability. This information led to the quantification of 93A infused and the determination of the effect of scCO₂ on the polymer.

5.2.1.2.1 LLDPE. Pure LLDPE and processed LLDPE/93A samples underwent TGA to determine their thermal stability and the resultant curves are displayed in Figure 5.14. The onset temperature of the main decomposition for pure and processed samples varies between 455°C and 460°C (Table 5.8). Decomposition ends in the range of 488°C to 493°C, while weight loss is between 98.8 and 99.4%. In comparing the amount of residue remaining after polymer decomposition, processed samples left a residue from 0.61 to 0.82 wt% while pure LLDPE left a higher residue of 1.19 wt%. Residual weights for individual processing conditions are displayed in Figure 5.15. As all LLDPE/93A sample residual weights were between 30 to 50% lower than the residual weight for pure LLDPE, processing the samples in scCO₂ appears to alter the polymer in such a way that increases the degree of decomposition. An investigation by Shieh et al.³² exhibited this phenomenon to a larger extent after processing polyethylene terephthalate (PET) in a compressed CO₂ environment. Polymer weight that was not accounted for as degraded

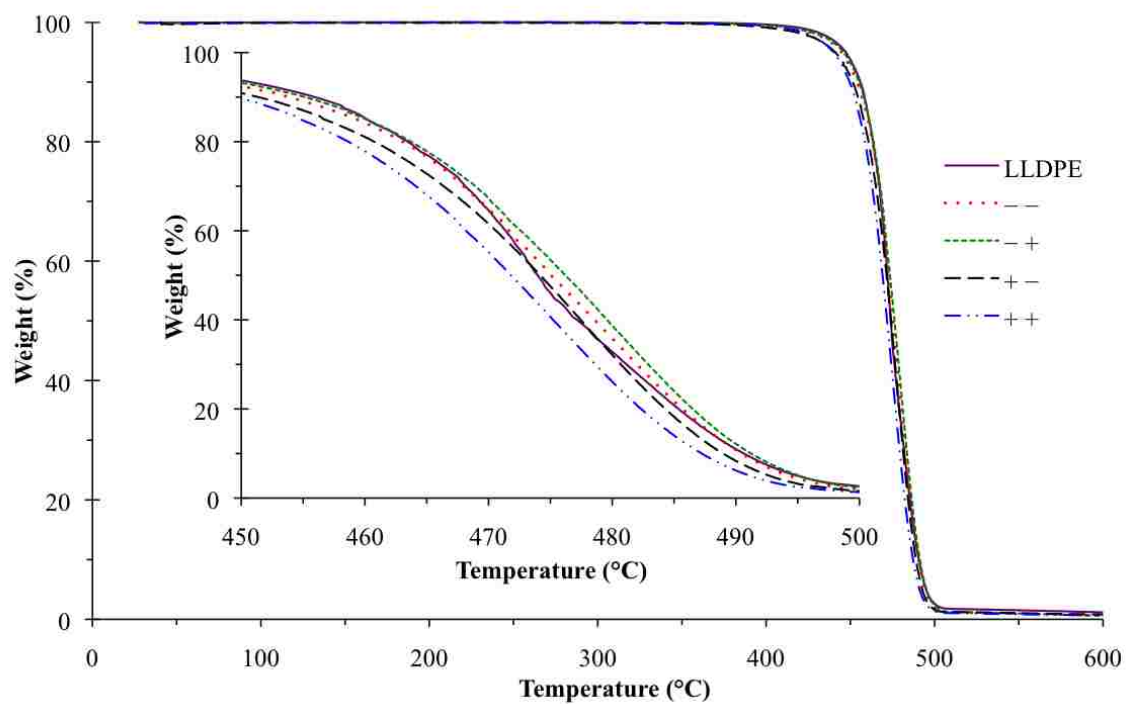


Figure 5.14. TGA of pure LLDPE and LLDPE processed with 93A in scCO_2

Table 5.8. Main decomposition for pure LLDPE and processed LLDPE/93A samples

Sample	Start T (°C)	Finish T (°C)	Weight Loss (%)
LLDPE	459.9	487.7	98.8
--	457.9	491.9	99.3
-+	459.5	492.5	99.4
+-	457.8	490.1	99.1
++	454.7	488.5	99.3

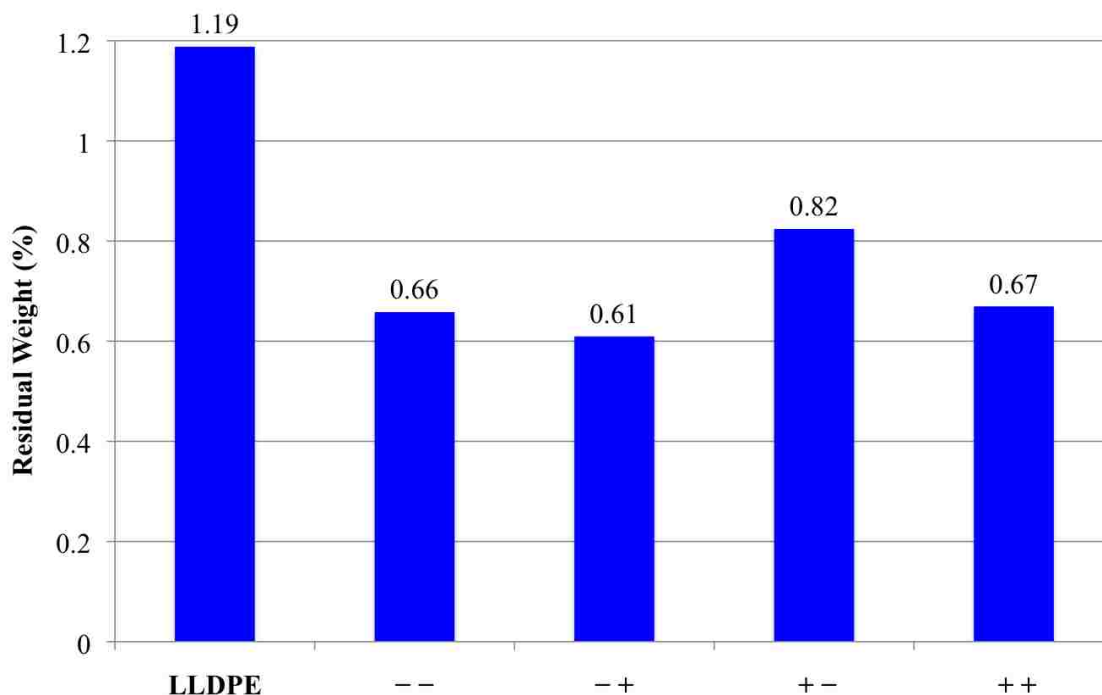


Figure 5.15. Residual weight of pure LLDPE and LLDPE processed with 93A in scCO₂

polymer or residue was attributed to water evaporation. Pure LLDPE contained no water whereas the processed samples contained between 0.01 and 0.08 wt% water, suggesting minor infusion of the hydrophilic clay.

The quantity of clay within the polymer was determined from the residual weight obtained by TGA. The quantity of clay in a PCN has been estimated to be equivalent to its residual weight after TGA,⁴⁵ assuming near complete degradation of the polymer with only clay remaining. Complete polymer degradation did not occur for pure LLDPE and LLDPE-g-MA, which both left a residual weight of 1.19 wt%. Since the quantity of clay within the polymer is expected to be small for the samples, i.e., around 1 wt% 93A and below, applying the above assumption of equivalence to the residual weight would introduce more than 100% error to the calculation. Additionally after TGA, only 76 wt%

of 93A is anticipated to remain as its residual weight due to the degradation of its organic modification.⁷ In order to increase the accuracy when calculating the quantity of 93A in samples, the residual weight left by the pure polymer and the 93A were adjusted for by applying the equation

$$93A(\text{wt}\%) = \frac{R_S - R_P}{0.76 - \frac{R_P}{100}} \quad (5)$$

where R_S and R_P are the residual weight (wt%) left by the sample and the pure polymer ($R_P = 1.19$ wt%), respectively. For LLDPE samples, the residual weights are lower than that of the pure polymer (Figure 5.16), resulting in below zero clay infusion quantities. Since such a scenario is not possible, it is proposed that no 93A was infused.

5.2.1.2.2 LLDPE-g-MA. From TGA curves for pure LLDPE-g-MA and processed LLDPE-g-MA/93A samples (Figure 5.17), it was observed that the samples began to lose weight at about 147°C, which is associated with a loss of bound water.⁷ Similar to the above TGA curves for LLDPE samples, the main decomposition for LLDPE-g-MA/93A starts at about 459°C and finishes at 492°C (Table 5.9). The residual weight left by pure and processed samples is between 0.82 and 2.19 wt%, as displayed in Figure 5.18. The higher residual weight of the LLDPE-g-MA samples as compared to the LLDPE samples is attributed to a larger amount of 93A infused into the polymer since both pure samples of LLDPE and LLDPE-g-MA left the same residual weight of 1.19 wt%. Weight loss from water and, to a much lesser extent, from degradation of the organic modifier of 93A was determined to vary from 0.14 to 0.26 wt%. The degradation

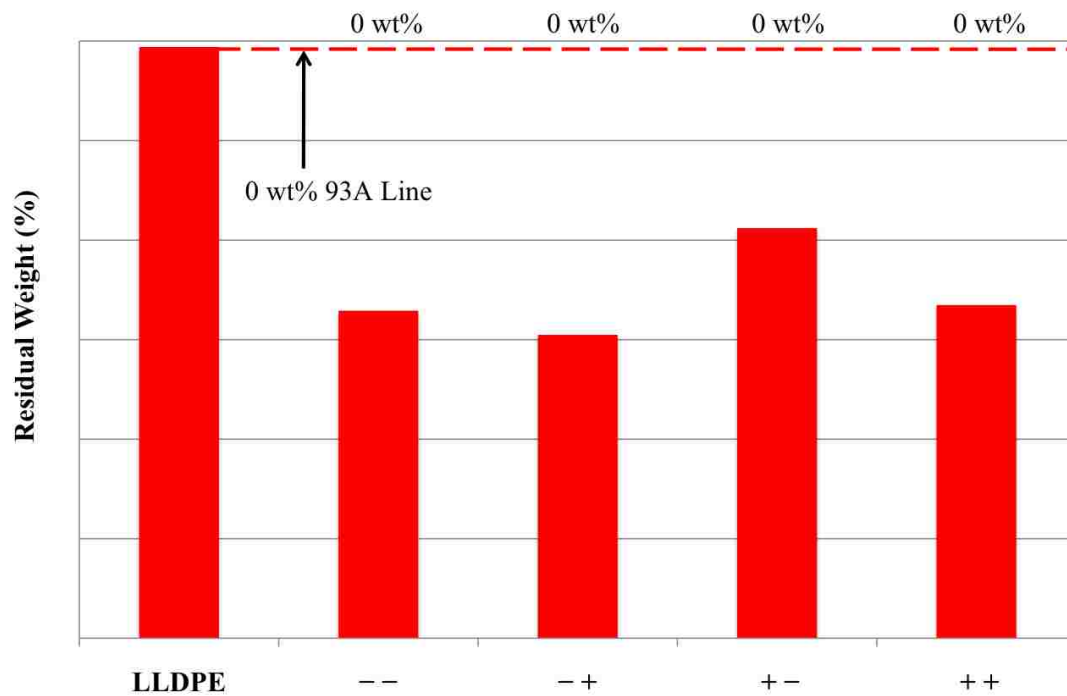


Figure 5.16. Quantity of 93A infused into LLDPE estimated from TGA residual weight

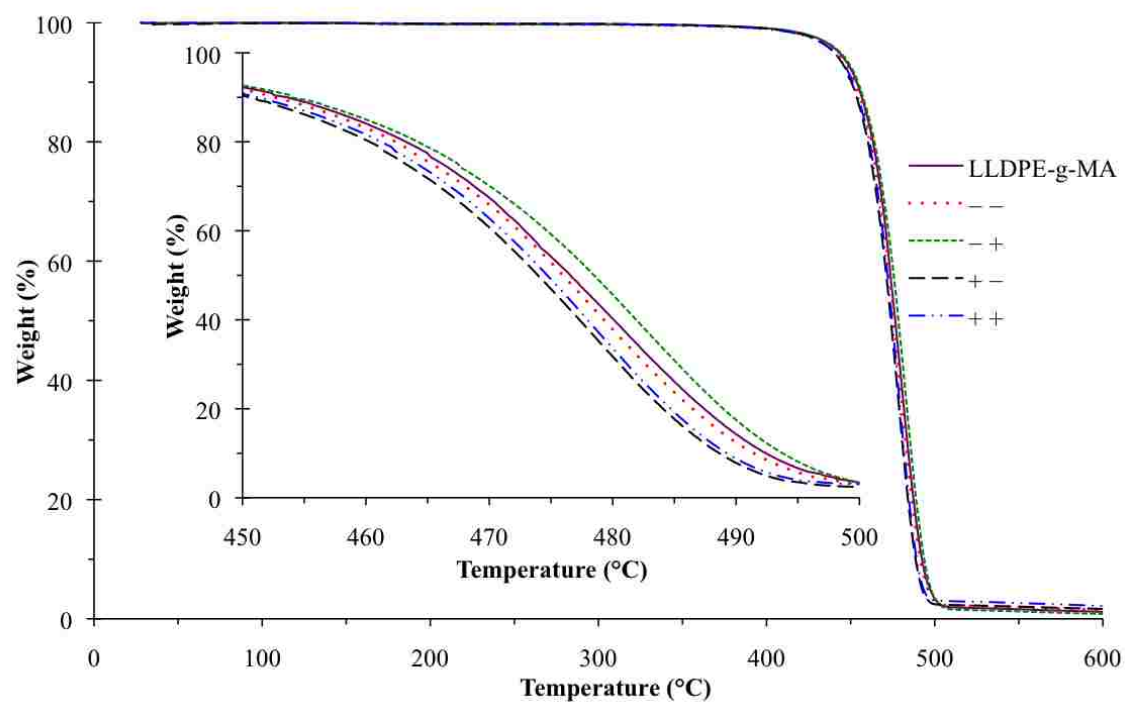


Figure 5.17. TGA of pure LLDPE-g-MA and LLDPE-g-MA processed with 93A in scCO_2

Table 5.9. Main decomposition for pure LLDPE-g-MA and processed LLDPE-g-MA/93A samples

Sample	Start T (°C)	Finish T (°C)	Weight Loss (%)
LLDPE-g-MA	459.0	493.4	98.6
--	459.3	491.9	98.2
-+	461.5	495.0	98.9
+ -	457.5	489.7	98.2
++	458.5	489.9	97.7

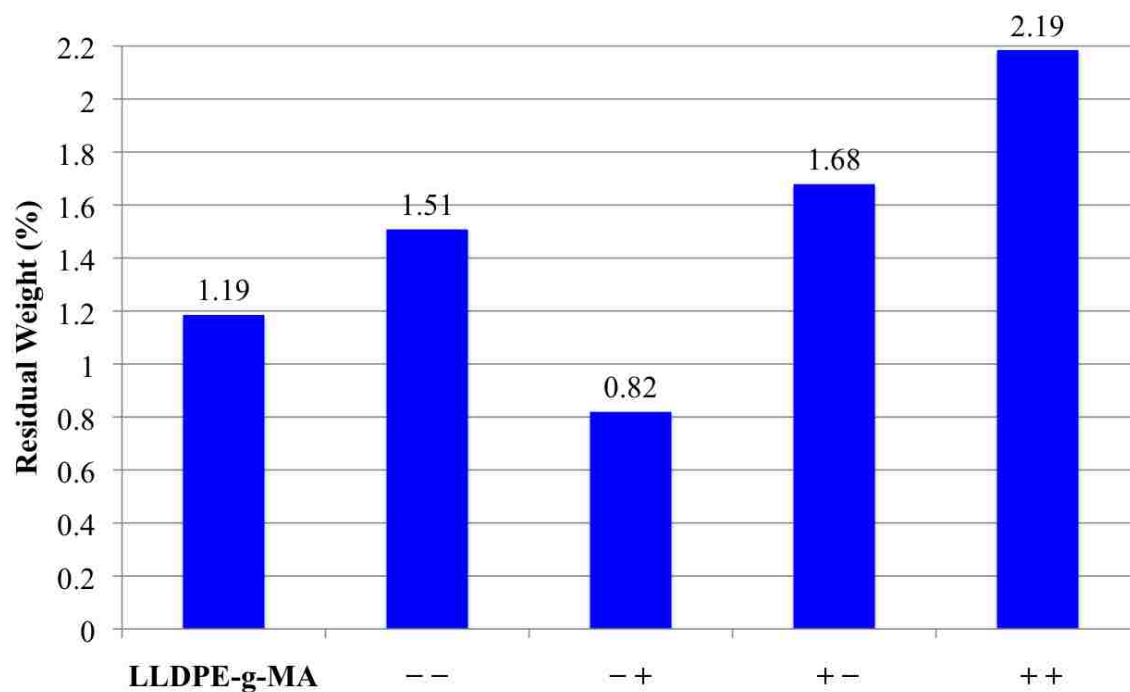


Figure 5.18. Residual weight of pure LLDPE-g-MA and LLDPE-g-MA processed with 93A in scCO₂

temperature of the organic modifier was undetectable as a result of the low weight of clay infused, corresponding to an even lower (i.e., undetectable) organic modifier weight. As

compared to LLDPE samples, LLDPE-g-MA samples contain higher water content mainly due to the polar nature of the maleic anhydride interacting favorably with the polar water molecule.

Applying the same methodology as that used for LLDPE/93A samples to LLDPE-g-MA/93A samples, the residual weight of sample (- +) is below that of pure LLDPE-g-MA, suggesting that no clay infusion occurred. In order of increasing residual weight, samples (- -), (+ -) and (+ +) have residual weights above that of pure LLDPE-g-MA, indicating that 93A was infused into the polymer. Using Equation (5), samples (- -), (+ -) and (+ +) contain 0.43, 0.66 and 1.34 wt% 93A (Figure 5.19), respectively.

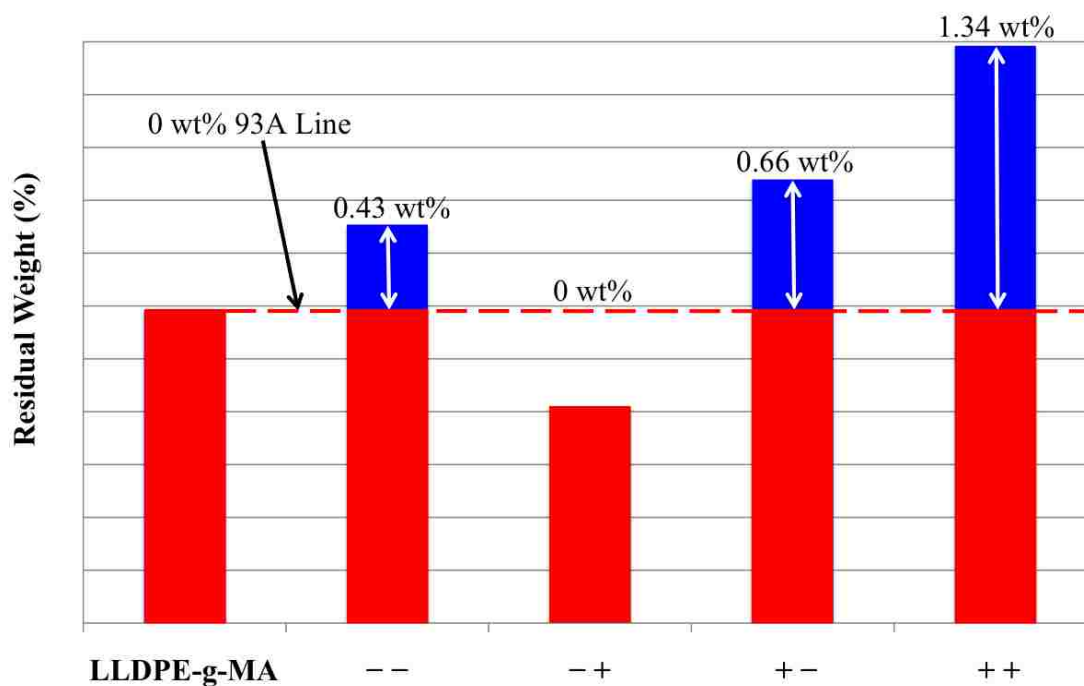


Figure 5.19. Quantity of 93A infused into LLDPE-g-MA estimated from TGA residual weight (not to scale)

5.2.1.3 FTIR. Samples of LLDPE/93A and LLDPE-g-MA/93A nanocomposites were analyzed with FTIR spectrometry. First, pellets were cleaned of residual clay on their surface by using a soft brush followed by wiping with a paper towel to ensure the only clay detected was infused clay. The clay infused from the outer polymer surface inward. Since clay infusion was assumed to be non-uniform throughout the pellets, the polymer/clay samples were melted, mixed manually, and then pressed into films for FTIR analysis. For the melt mixing, the pellets were placed on a metal plate on the heated film press platen. Once the pellets were melted, the molten polymer was mixed with a metal spatula to achieve a more uniform dispersion so an accurate bulk clay percentage in the polymer could be obtained.

Spectra obtained from the FTIR analysis of calibration standards in conjunction with the resultant calibration curve were used to determine the quantity of 93A infused into the polymer. To accomplish this, the following technique adapted from Clark et al.⁵² was employed for calculating the weight percentage from the absorbance spectra. The absorbance for small concentrations of IR-absorbing species is approximated by the Beer-Lambert law:

$$A = \log\left(\frac{I_O}{I_T}\right) = \sum_i (K_i \delta C_i) \quad (6)$$

where A, I_O, I_T, K_i, d, and C_i are the absorbance, intensity of the incident IR beam, intensity of the transmitted IR beam, absorbance coefficient, absorbing layer thickness, and absorbing species concentration, respectively. In this technique, an absorbance equation with contributions from the clay and polymer was combined with an absorbance

equation with only a polymer contribution. The Beer-Lambert law used to convey the absorbance equation for a nanocomposite of polymer (LLDPE or LLDPE-g-MA) and 93A was

$$A_1 = K_1 \delta C_{93A} + K_2 \delta C_{Polymer} \quad (7)$$

where C_{93A} and $C_{Polymer}$ are the concentrations of 93A and the polymer (either LLDPE or LLDPE-g-MA), respectively. The absorption of the polymer only was represented as

$$A_2 = K_3 \delta C_{Polymer} \quad (8)$$

To remove the absorbing layer thickness from the calculation and separate the polymer absorbance contribution from the clay absorbance contribution, a peak that had an absorbance contribution from both the polymer and 93A was divided by a peak that only had an absorbance due to the polymer. This resulted in the linear equation

$$\frac{A_1}{A_2} = \left(\frac{K_1}{K_3} \right) \frac{C_{93A}}{C_{Polymer}} + \left(\frac{K_2}{K_3} \right) \quad (9)$$

The absorption peak attributable to clay within the polymer was found at 522 cm^{-1} on the spectra⁷ and is shown in Figure 5.20. The absorption peak solely dedicated to the polymer (either LLDPE or LLDPE-g-MA) was found at 2019 cm^{-1} on all spectra and is displayed in Figure 5.21. The absorbance for each peak was determined by integration of

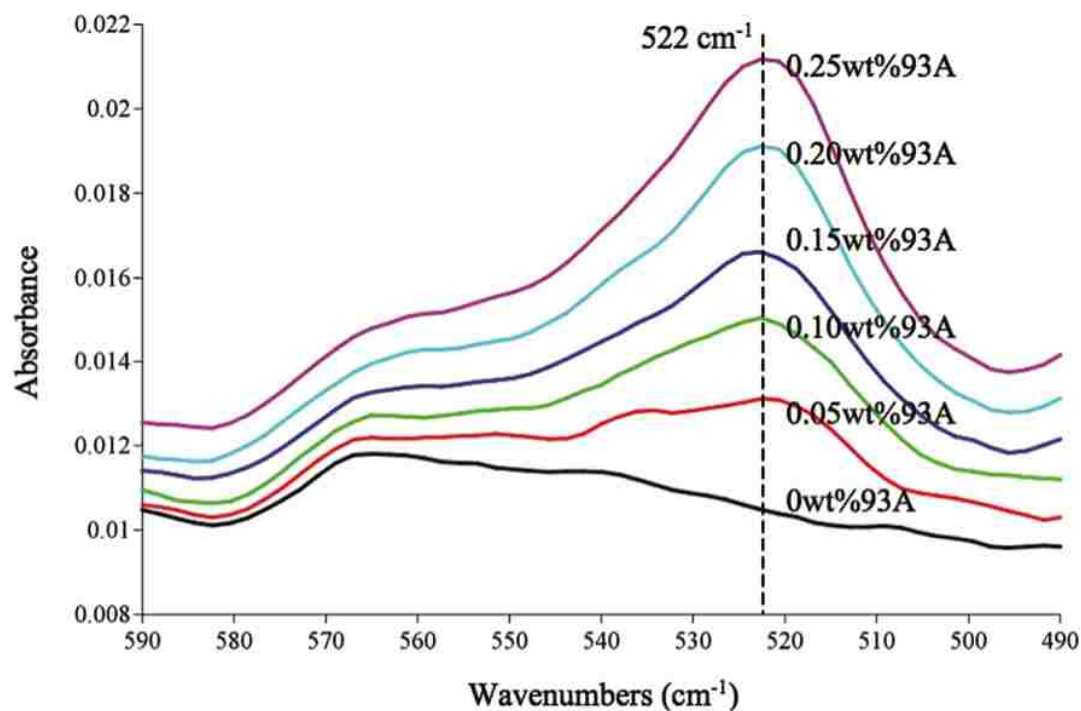


Figure 5.20. LLDPE/93A standard spectra with absorbance peak 522 cm^{-1}

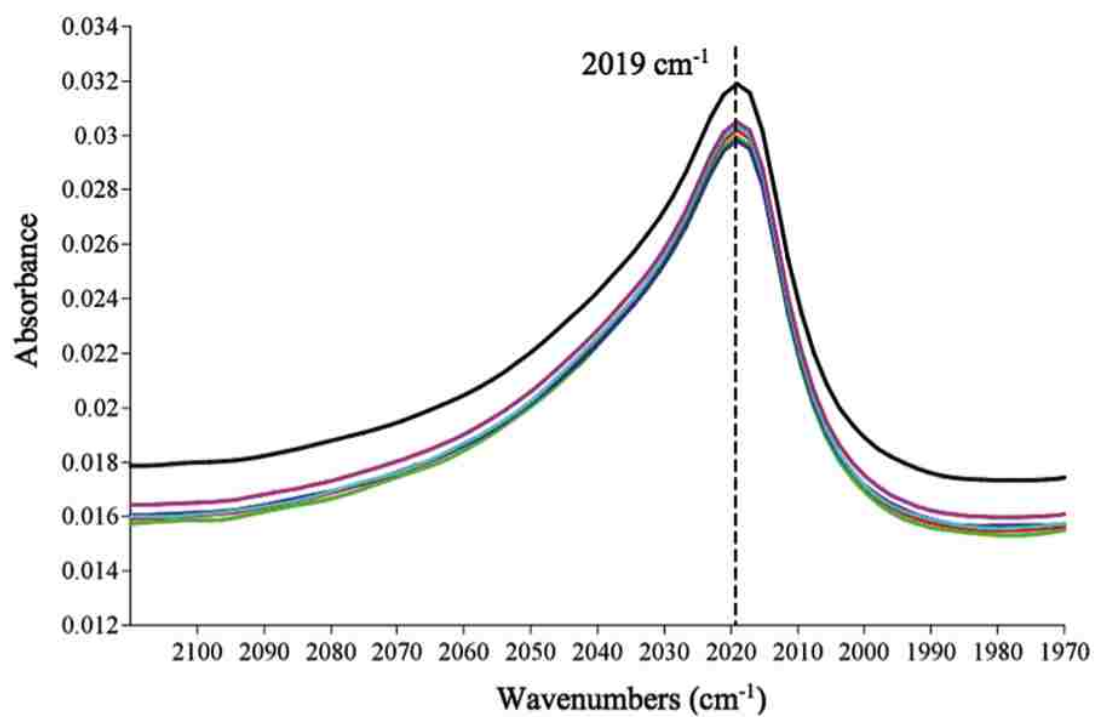


Figure 5.21. LLDPE/93A standard spectra with absorbance peak 2019 cm^{-1}

the area under the peak. Using the linear absorbance Equation (9) and the spectra obtained from the polymer/clay standards, calibration curves were regressed, that are shown, along with their corresponding squares of the Pearson autocorrelation coefficient, in Figures 5.22 and 5.23. Upon analysis, the absorbance ratios from the sample spectra were used with the calibration curves to calculate the weight percentage of 93A infused into the polymer samples. Two calibration curves were used, one for samples with clay percentages ranging from 0 to 0.25 wt% (Figure 5.22) and another for samples with clay percentages above 0.25 wt% (Figure 5.23). The larger range calibration curve used for clay amounts greater than 0.25 wt% contained a standard error of 6.3%, whereas the standard error was 2.8% for the smaller range calibration curve for 0–0.25 wt% clay.

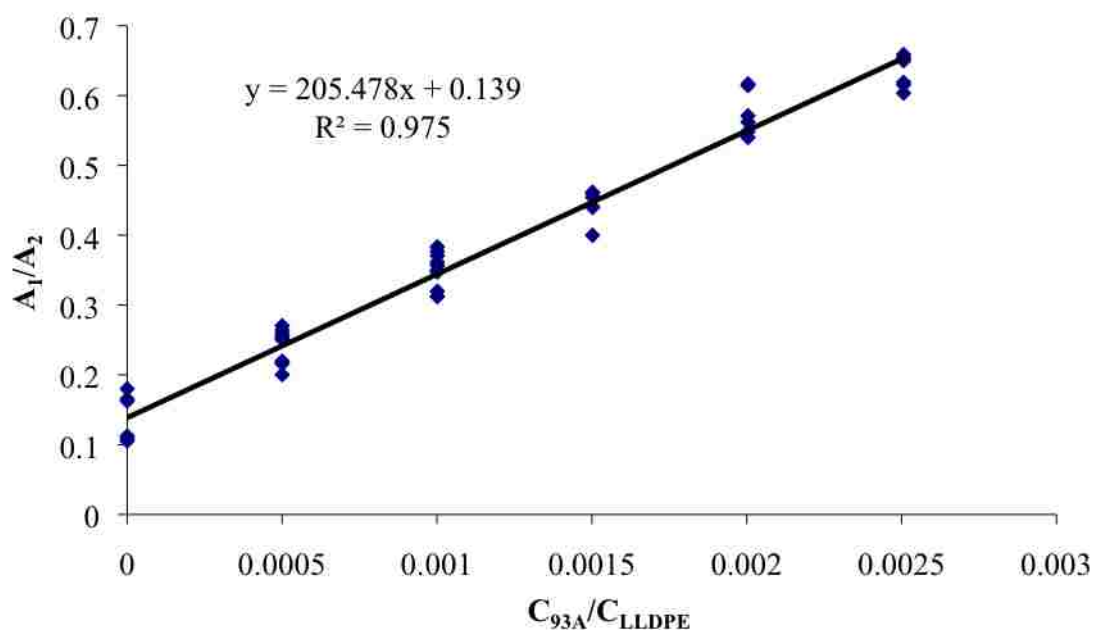


Figure 5.22. Calibration curve for LLDPE/93A nanocomposites with 0 to 0.25 wt% 93A loadings

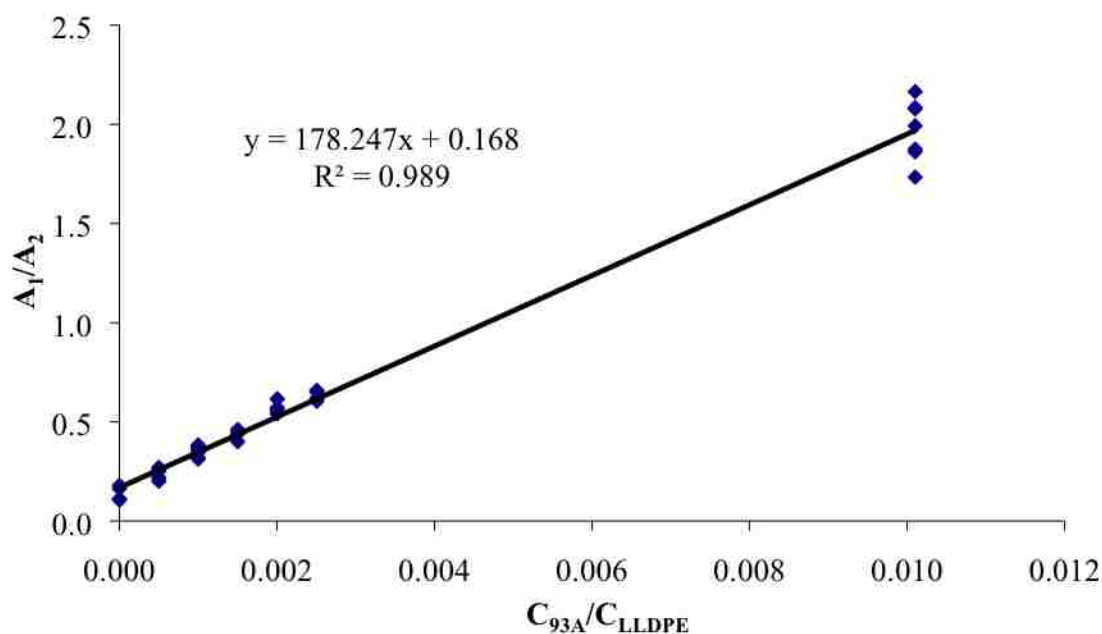


Figure 5.23. Calibration curve for LLDPE/93A nanocomposites with greater than 0.25 wt% 93A loadings

This method is applicable to different types of natural and modified clay because all clays should possess an absorption peak identifiable by FTIR analysis that will increase with clay concentration. Careful choice of the absorption peaks (for either polymer or clay) is important, as a peak can be overlapped by other peaks or can contain signal noise that could result in miscalculation of the peak absorbance and, thus, concentration. In addition, if the absorption peak chosen is indicative of the clay and not its modification, clay modifier degradation due to processing should not affect the results. However, polymer degradation could affect the results if the chosen absorption peak attributed solely to the polymer is altered by degradation. For this work, no degradation was expected because the processing conditions were below the degradation temperatures of the materials.

5.2.1.3.1 LLDPE. Nanocomposites of LLDPE/93A showed little to no clay infusion, as determined by FTIR analysis. The maximum amount of clay infusion into LLDPE was 0.16 wt%, and the minimum was 0 wt%. As displayed in Table 5.10, the lowest average clay infusion is found in the high-pressure and low-temperature run, whereas the highest average clay infusion seemed to have occurred in a low-pressure and low-temperature processing environment.

Table 5.10. Average weight percentage and standard deviation of 93A in LLDPE

Sample	Average (wt%)	Standard Deviation (wt%)
--	0.08	0.04
-+	0.04	0.06
+ -	0.05	0.04
++	0.07	0.03

5.2.1.3.2 LLDPE-g-MA. In terms of maximum clay infusion determined by FTIR analysis, nearly eight times more clay was infused into LLDPE-g-MA in comparison to pristine LLDPE. Clay infusion into LLDPE-g-MA reached a maximum at 1.27 wt% and a minimum at 0.04 wt%. The lowest average clay infusion into LLDPE-g-MA was 0.07 wt% and occurred in a high-pressure and low-temperature run, as exhibited in Table 5.11.

5.2.1.3.3 Uniform dispersion analysis. Although the aim of mixing was uniform clay dispersion, it was not achieved in most cases, as evidenced visually by white specs

Table 5.11. Average weight percentage and standard deviation of 93A in LLDPE-g-MA

Sample	Average (wt%)	Standard Deviation (wt%)
--	0.48	0.04
-+	0.07	0.02
+ -	0.73	0.20
++	0.83	0.24

in the film and analytically by the large standard deviation present throughout a single sample. This may be due to polymer pellets within the same processing environment being infused with different amounts of clay depending on their location in the reactor. To some extent, the large standard deviations in clay percentages were the cause of defects in the film samples, which resulted in oscillations or slight shifts in the spectra. The film defects, although minor, may have come from surface imperfections, i.e., scratches and divots, in the brass plates that were transferred to the film during its preparation. Furthermore, improvements in the preparation of the polymer/clay standards and samples are expected to reduce the standard error contained within the calibration curves and reduce the standard deviation within the samples, respectively.

5.2.1.4 SEM. Samples of LLDPE and LLDPE-g-MA processed with 93A in scCO₂ were cross-sectioned and then viewed via a SEM.

5.2.1.4.1 LLDPE. No clay particles were observed within the LLDPE/93A samples due to the almost nonexistent amount of clay within the samples.

5.2.1.4.2 LLDPE-g-MA. Clay particles were observed within all LLDPE-g-MA/93A samples except for sample (- +) as a result of its almost nonexistent clay

loading. For this reason, values concerning clay particles are reported on only for LLDPE-g-MA/93A samples (– –), (+ –) and (+ +). Clay particles within the samples were measured in two dimensions, consisting of a major and a minor dimension, as shown in Figure 5.24. The size of clay particles infused into LLDPE-g-MA samples ranged from 0.9 μm in the smallest dimension to 52.4 μm in the largest dimension. Clay particles were observed to predominantly exist in agglomerated configurations within the polymer matrix. In Figure 5.25, some delamination appears to have occurred, which could be due to the scCO_2 processing or due to the fracturing of the sample. In addition to the size dimensions, the location of the clay particle relative to the edge of the polymer cross-section was recorded to ascertain its depth of infusion. As the radius of the LLDPE-g-MA polymer cross-section is approximately 1500 μm , the edge, interior and

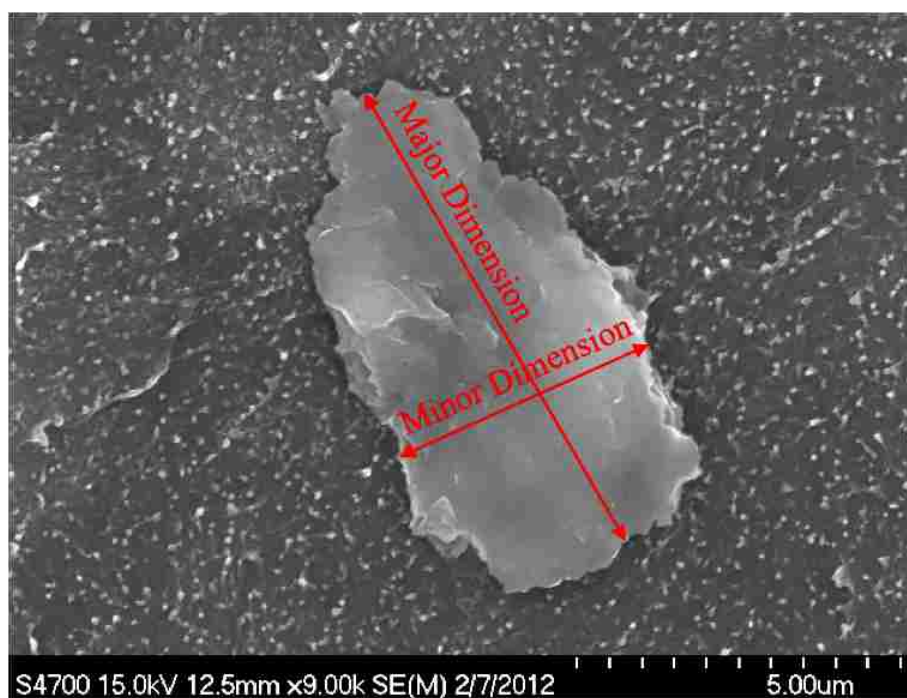


Figure 5.24. SEM of clay particle displaying its measurement dimensions

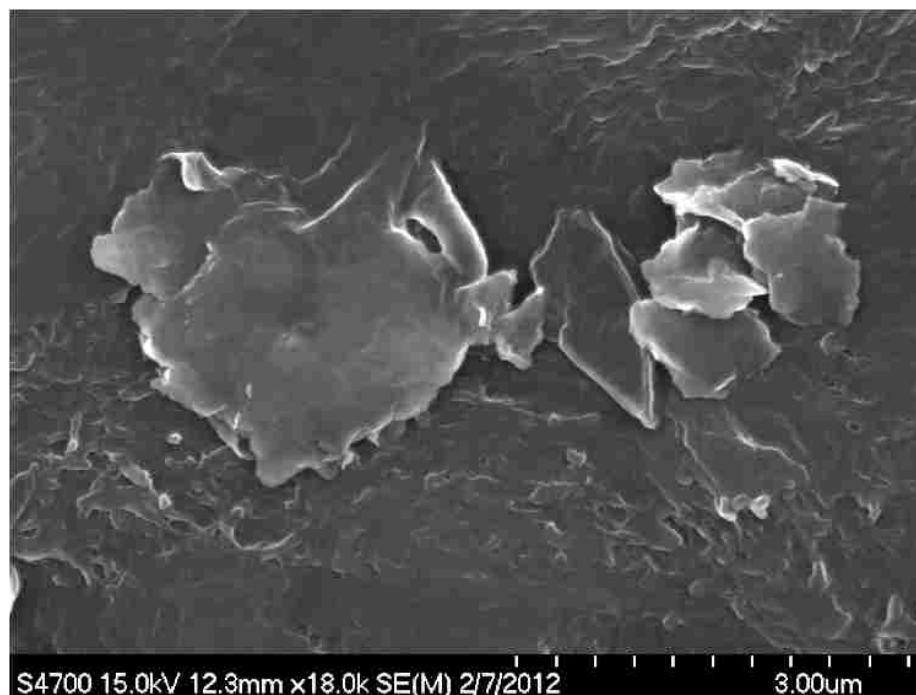


Figure 5.25. SEM of clay particle exhibiting delamination

center regions of the polymer cross-section are, respectively, defined as 0-499 μm , 500-999 μm and 1000+ μm from the edge of the cross-section. The infusion depth of 93A is significant, as it seems the 93A was successful in reaching the center region of the polymer for samples (- -), (+ -) and (+ +). However, clay particles were more readily observed near the edge region of the polymer, which could indicate a higher concentration of particles or larger particles in this region. The location, depth of infusion and size dimensions of all observed clay particles can be found in the Appendix in Tables A.5 through A.7.

5.2.2. Discussion. Using the above analyses, the effect of scCO_2 on the polymers, the quantity of 93A infused into the polymers and, from a visual inspection, the 93A size distribution and changes in the appearance of samples were determined.

5.2.2.1 Effect of scCO₂ on the polymer. Processing in scCO₂ can affect polymers by increasing their crystallinity or their thermal stability. As CO₂ dissolves and plasticizes the amorphous regions of the polymer, the mobility of the polymer chains is enhanced, which can induce them to adopt a more crystalline structure. Thermal stability of a polymer can be increased after processing with CO₂ due to the extraction of low molecular weight compounds from the polymer such as monomers, oligomers or additives.

5.2.2.1.1 DSC: crystallinity. The crystallinity of LLDPE and LLDPE-g-MA samples was calculated from DSC analysis. It was observed that the crystallinity did not significantly change due to scCO₂ processing (heating 1) or as a result of the presence of 93A in the polymer (heating 2).

Although there was not a significant change in crystallinity, some trends were observed that could be significant. For LLDPE, scCO₂-processing conditions that employed higher temperatures resulted in samples with higher crystallinities (Table 5.12). At higher temperatures, polymer chains are more mobile as the result of a more molten

Table 5.12. Influence of scCO₂-processing conditions on crystallinity (heating 1) for LLDPE/93A samples

Sample	Crystallinity (%)
- +	34.10
- -	35.39
+ -	36.93
+ +	37.00

polymer and a higher CO₂ diffusion rate that enable greater plasticization of the polymer. This higher polymer chain mobility enhances their ability to adopt a more crystalline structure. In comparison to temperature, pressure had a more significant effect on crystallinity for LLDPE-g-MA samples, as higher pressure processing environments yielded higher sample crystallinities (Table 5.13). Increased CO₂ concentration from the higher pressure could be enhancing plasticization of the polymer chains to enable crystallization. Due to the increased compatibility of LLDPE-g-MA with CO₂, pressure had a more significant effect on LLDPE-g-MA, as compared to LLDPE, since it dictates CO₂ concentration in the polymer. The low compatibility of LLDPE with CO₂ can also explain the greater influence of temperature on its crystallinity as compared to pressure. Temperature also had an effect on the crystallinity of LLDPE-g-MA as a higher temperature resulted in a higher crystallinity at constant pressure conditions.

Table 5.13. Influence of scCO₂-processing conditions on crystallinity (heating 1) for LLDPE-g-MA/93A samples

Sample	Crystallinity (%)
- -	48.23
+ -	48.53
- +	49.22
+ +	51.16

5.2.2.1.2 TGA: thermal stability. From the TGA curves displayed in Figures 5.14 and 5.17, it was observed that thermal stability during the main decomposition event

predominantly decreased for LLDPE and LLDPE-g-MA samples processed in scCO₂ as compared to their pure counterparts. Low-temperature processing conditions produced the highest thermal stability for both polymers, which is proposed to be the result of a reduction in the diffusion of CO₂ and plasticization of the polymer that inhibits the infusion of low molecular weight compounds. For both LLDPE and LLDPE-g-MA, an increase in thermal stability occurred for sample (- +) in comparison to the pure polymer, where the fluid density is the highest. Extraction ability of CO₂ increases with higher densities and these conditions could have enabled the extraction of low molecular weight compounds from the polymers, enhancing the thermal stability. In contrast, processing conditions employing a lower CO₂ fluid density and a higher temperature are typically better for infusion and could have introduced low molecular weight compounds into the polymer to result in a reduced thermal stability. The surfactant of 93A is a low molecular weight compound that could be degrading during the main PCN decomposition. This is above its typical degradation temperature of ca. 270°C and could be the result of the high level of interaction between the surfactant chain and the polymer matrix.^{18,45} In support of this, the thermal stability of LLDPE-g-MA/93A samples decreased as the quantity of 93A infused increased, keeping in mind that the quantities of 93A infused into LLDPE-g-MA/93A samples (+ -) and (+ +) can swap order due to their overlapping 93A infusion values. Thus, as the quantity of 93A increases, the quantity of surfactant will also increase, decreasing thermal stability. However, at a high enough concentration of 93A, the clay is anticipated to increase the thermal stability of the PCN.⁴⁵

5.2.2.2 Quantity of 93A infused. The quantity of 93A infused into samples was determined by TGA and FTIR analysis, and a comparison between the methods was

conducted. In addition, the effect of processing conditions on the quantity of 93A infused into samples was investigated.

5.2.2.2.1 TGA vs. FTIR: LLDPE. Samples involving the infusion of 93A into LLDPE were determined by TGA and FTIR analysis to have little to no clay infusion. The results from both methods are displayed in Figure 5.26. The results from TGA are within the range of FTIR analysis for sample (- +), whereas samples (- -), (+ -) and (+ +) are below the FTIR range by 0.04, 0.01 and 0.04 wt%, respectively. The difference in results could be due to the combination of the low quantity of clay in the samples and the error associated with the TGA and FTIR analysis methods. An alternative reasoning for the difference in results between the two methods is presented in the following section.

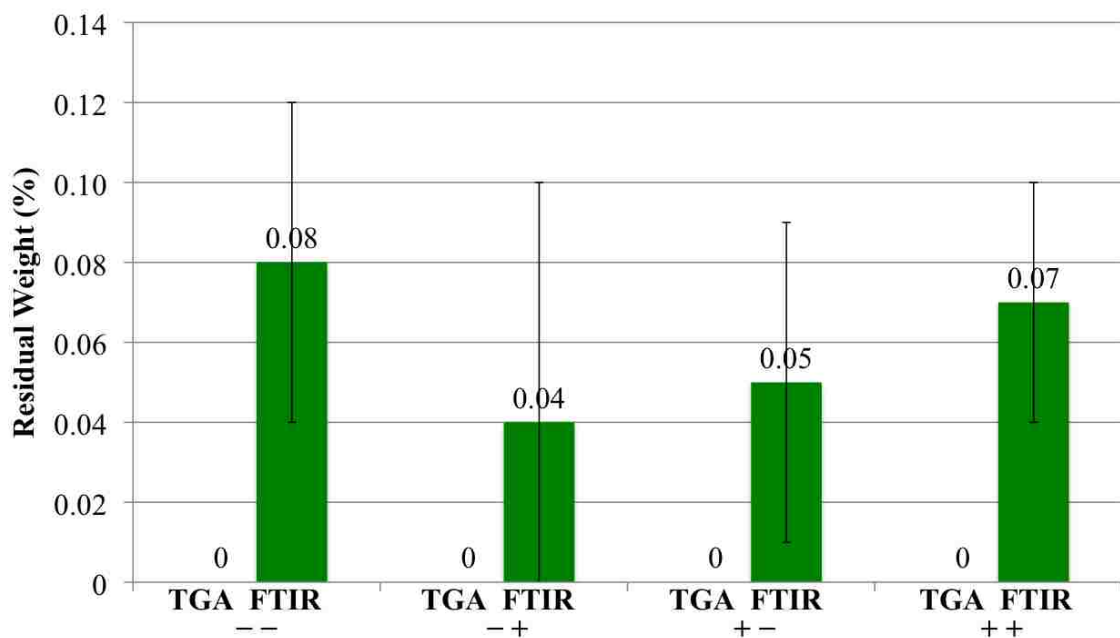


Figure 5.26. Comparison of the quantity of 93A infused into LLDPE as determined by TGA and FTIR analysis (standard deviation bars included)

5.2.2.2.2 TGA vs. FTIR: LLDPE-g-MA. Comparing 93A infusion results of FTIR analysis to TGA for LLDPE-g-MA (Figure 5.27), the FTIR analysis exhibits the same order of decreasing 93A quantity for samples (+ +), (+ -) and (- -) with sample (- +) exhibiting a near zero 93A infusion amount. Sample (+ -) for TGA is within the range of the average clay quantity attained from FTIR analysis, whereas samples (- -) and (- +) are 0.01 and 0.05 wt% below the FTIR range, respectively. Sample (+ +) is 0.27 wt% above the average FTIR range, however it is only 0.07 wt% above this sample's maximum infusion quantity of 1.27 wt% 93A. The disparity between results could be due to scCO₂ altering the samples to influence polymer degradation during TGA or due to a difference in sample preparation between the two methods. Namely, sampling

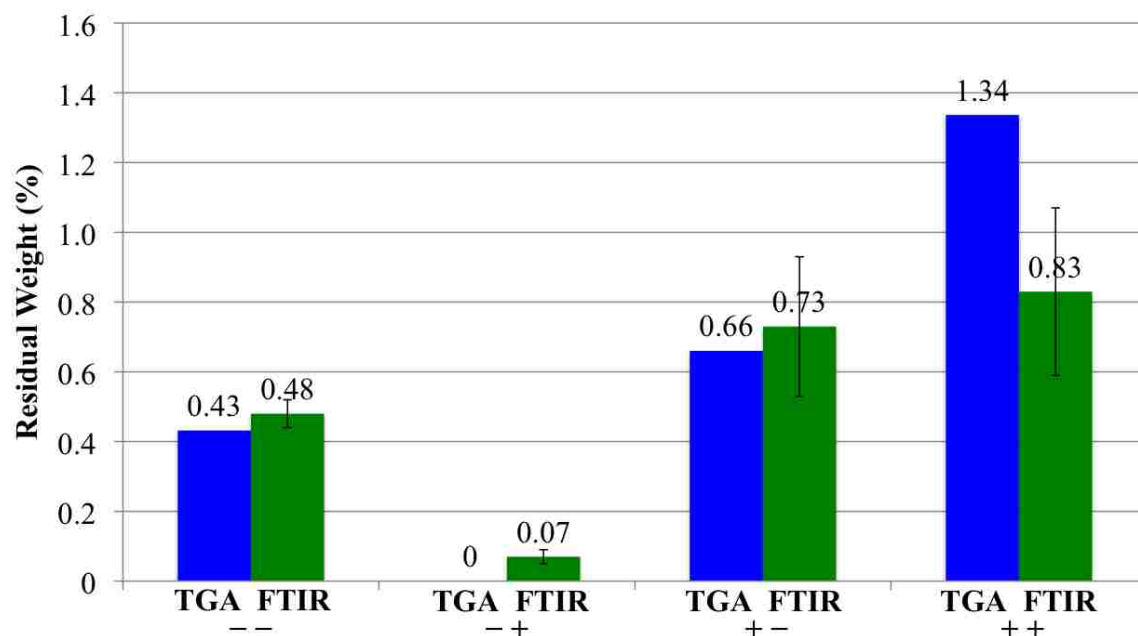


Figure 5.27. Comparison of the quantity of 93A infused into LLDPE-g-MA as determined by TGA and FTIR analysis (standard deviation bars included)

for TGA involves only one polymer pellet to contribute to clay infusion whereas FTIR analysis involves many melt-mixed polymer pellets to contribute to an average clay infusion. The higher amount of 93A in LLDPE-g-MA as compared to LLDPE is associated with the higher compatibility of the maleated polymer with both the modified clay and the scCO₂ medium.

5.2.2.2.3 TGA vs. FTIR: accuracy analysis. Once a calibration curve has been created, determination of the quantity of clay within the polymer by FTIR analysis is quick, nondestructive and potentially more accurate than TGA. It is proposed that TGA could be less accurate since scCO₂ appears to alter the polymer, decreasing the TGA residual weight in such a way that so far has been unaccountable by changes in crystallinity (DSC analysis) or thermal stability (TGA). This unaccountable change resulted in the estimation of all LLDPE/93A samples to contain zero weight percent 93A, which is not strictly true as 93A was detected by XRD analysis. The presence of 93A in LLDPE/93A samples was detected by FTIR analysis, in which the sample possessing the lowest clay infusion quantity range (sample (- +)) corresponded to the lowest almost nonexistent XRD peak (Figure 5.2). However, the difference between the results could also be attributed to the difference in sample preparation or the error associated with the two methods.

5.2.2.2.4 Effect of processing conditions: LLDPE. For LLDPE/93A samples processed in scCO₂, the processing conditions appearing to possess the least ability to infuse 93A into LLDPE employed the combination of high pressure and low temperature, which confirms that the almost nonexistent peak in the XRD plot (Figure 5.2) is from little to no 93A present within the sample. However, the pressure and temperature effects

remain elusive as a result of the TGA zero 93A infusion amount and the FTIR analysis sample standard deviations exhibiting the same order of magnitude as the average 93A infusion amount (Table 5.26); this resulted in no difference between values and an overlapping of values with the respective analytical methods.

5.2.2.2.5 Effect of processing conditions: LLDPE-g-MA. The effect of processing conditions on the quantity of 93A infused into LLDPE-g-MA is the same for TGA and FTIR analysis since both methods produced comparable results (Figure 5.27). For LLDPE-g-MA/93A sample (- +), it is proposed that the high pressure reduced mobility of carbon dioxide molecules and clay particles and that the low temperature led to a lower diffusion rate and a harder polymer; this resulted in less clay moving to a polymer interface that was too hard to permit adequate infusion. The near zero clay infusion quantity confirms that the almost nonexistent peak seen in the XRD plot (Figure 5.11) is not from a near complete exfoliation or dispersion of the clay, but from little to no clay existing in the polymer. High-pressure and high-temperature conditions produced the largest clay infusion of 1.34 wt% from TGA and the largest average clay infusion of 0.83 wt% from FTIR analysis. In actuality, these conditions could result in the same amount of clay infused as the low-pressure and high-temperature run because their standard deviations gave overlapping values during FTIR analysis. Dependent upon the critical pressure, these infusion results could suggest that the reduced mobility from high pressures was less significant at high temperatures when the fluid density was decreased, the diffusion rate was increased, and the polymer was sufficiently softened to promote infusion. In another scenario, the increased CO₂ concentration from the high pressure could have aided infusion by enhancing dissolution of LLDPE-g-MA as a result

of its compatibility with CO₂. Furthermore, the larger clay infusion amount into LLDPE-g-MA over that into pristine LLDPE was attributed to the greater compatibility of LLDPE-g-MA with the nanoclay and CO₂ offered by the MA modification.^{16,44–46}

5.2.2.3 Visual inspection. A SEM was used to visually inspect a cross-section of the samples in order to measure the size of infused clay particles. The results were used to calculate the size distribution of clay particles within samples. Additionally, changes in the appearance of samples due to scCO₂ processing were observed.

5.2.2.3.1 LLDPE. The appearance of cross-sectioned LLDPE/93A samples remained unaltered as the result of different processing conditions, which can be seen in Figures 5.28 to 5.31.

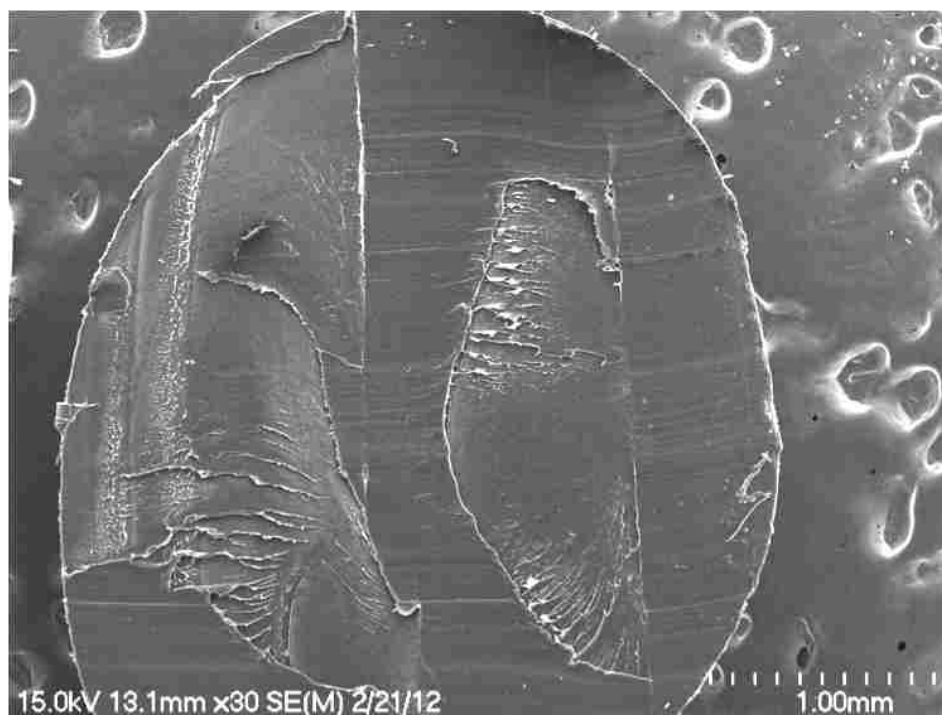


Figure 5.28. SEM of LLDPE/93A sample (– –) surface



Figure 5.29. SEM of LLDPE/93A sample (- +) surface



Figure 5.30. SEM of LLDPE/93A sample (+ -) surface

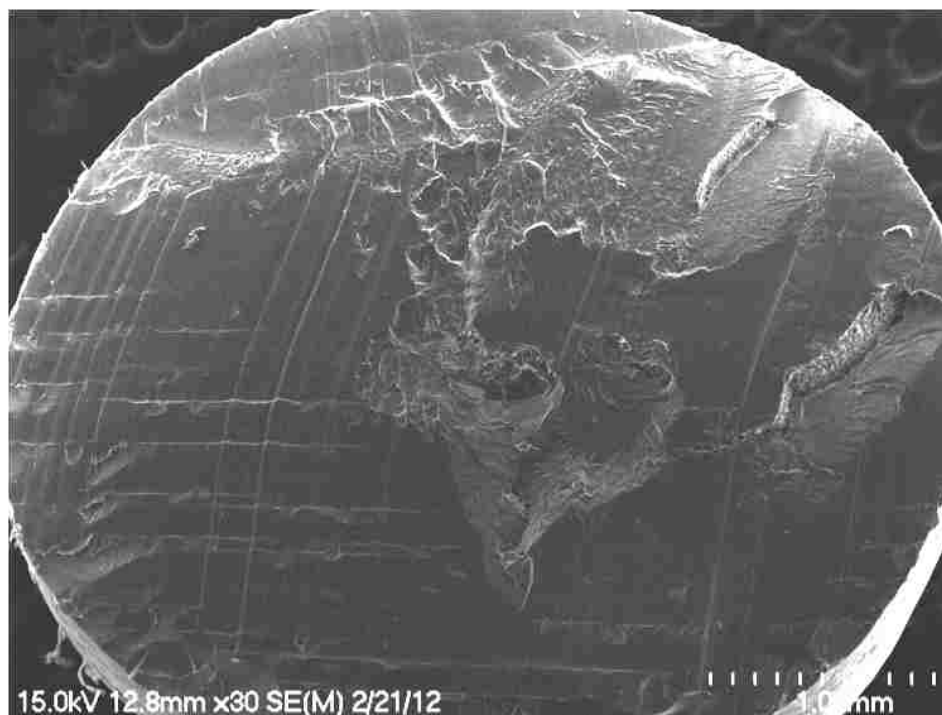


Figure 5.31. SEM of LLDPE/93A sample (+ +) surface

5.2.2.3.2 LLDPE-g-MA. After measuring the observed clay particles within LLDPE-g-MA/93A samples, the two dimensions of each particle were averaged and a size distribution of clay particles was obtained. The individual sample and total combined sample size distributions of observed clay particles for LLDPE-g-MA/93A samples (– –), (+ –) and (+ +) are displayed in Table 5.14. Since the size distribution of clay particles is relatively the same as the as-received size distribution of clay particles, it is postulated that scCO₂ processing did not significantly alter the size of the clay particles.

Different processing environments altered the appearance of the LLDPE-g-MA/93A samples differently. Samples (– –) and (– +) had relatively smooth cross-sectioned surfaces (Figures 5.32 and 5.33) since the scCO₂ processing had less of an

Table 5.14. Size distribution of clay particles in as-received 93A and LLDPE-g-MA/93A samples

Sample	Clay Particle Size		
	< 2 μm	< 6 μm	< 13 μm
As-Received	10%	50%	90%
--	8%	50%	92%
+ -	19%	48%	86%
++	10%	50%	90%
Total	14%	49%	88%

effect on the polymer. Bubbles and fissures appeared in the middle portion of sample (+ -) (Figure 5.34) as the result of CO₂ significantly infusing into the polymer. However, at the higher pressure of sample (++), fissures can be observed in the surface without bubbles (Figure 5.35). It is postulated that bubbles were unable to form due to the high pressure compressing the polymer during processing.

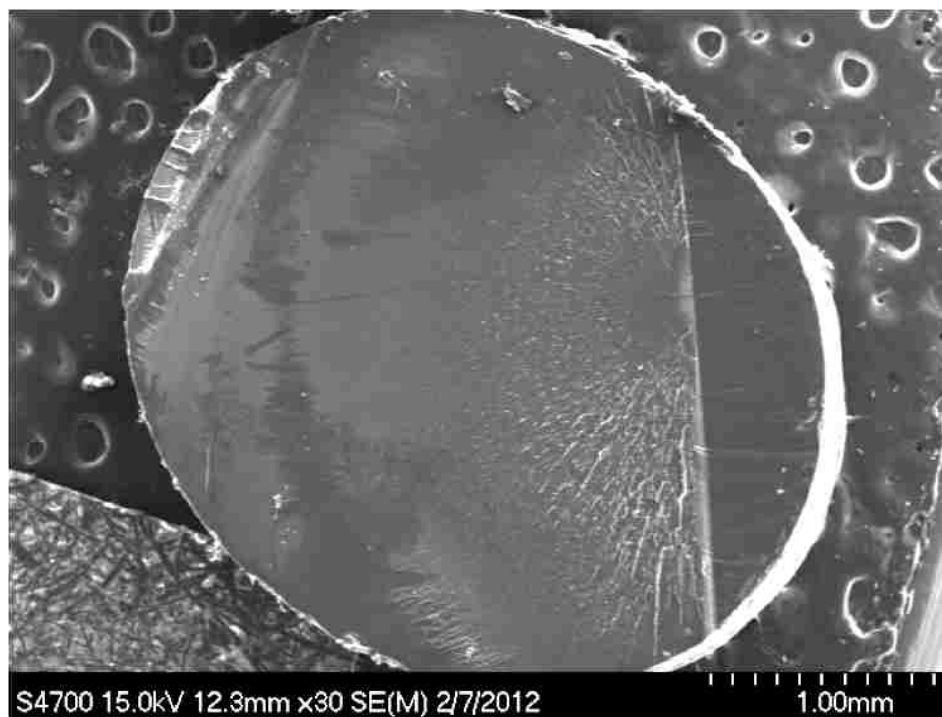


Figure 5.32. SEM of LLDPE-g-MA/93A sample (- -) surface

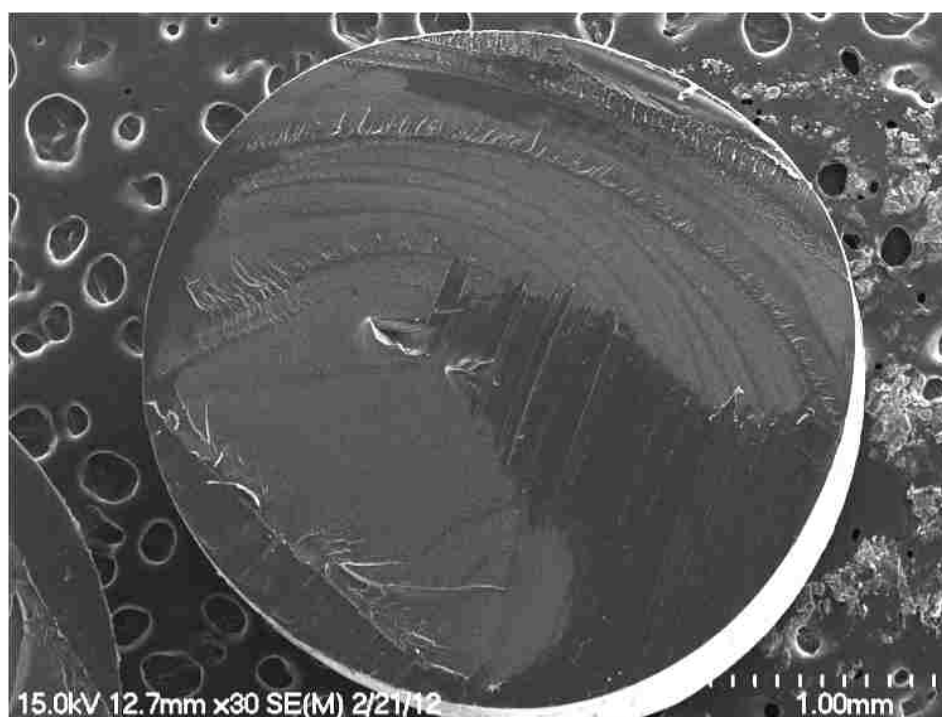


Figure 5.33. SEM of LLDPE-g-MA/93A sample (- +) surface



Figure 5.34. SEM of LLDPE-g-MA/93A sample (+ -) surface

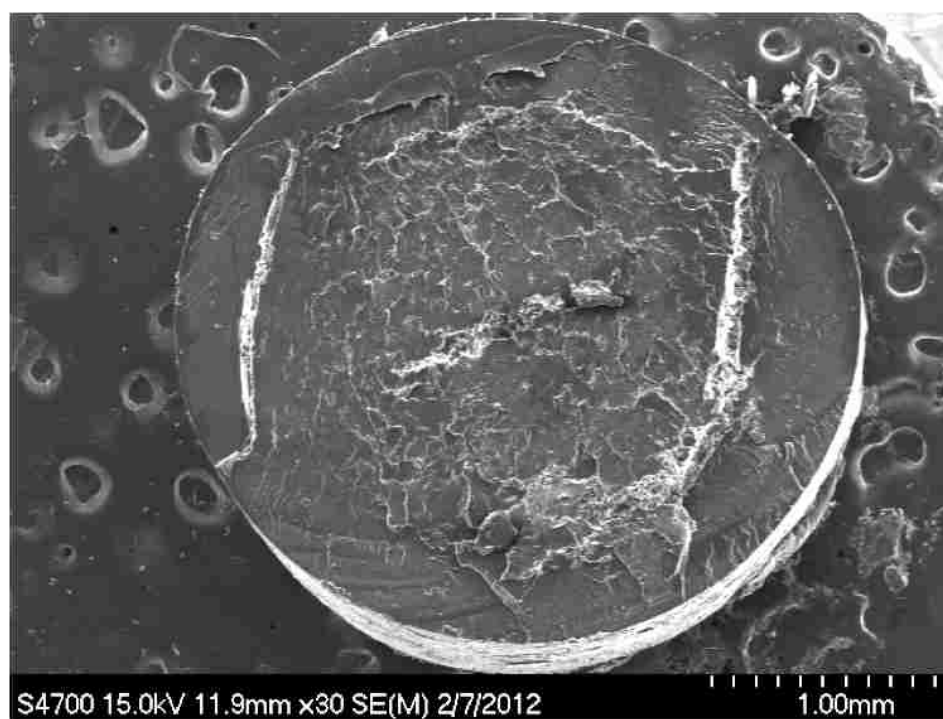


Figure 5.35. SEM of LLDPE-g-MA/93A sample (+ +) surface

6. CONCLUSIONS

Directed by XRD analysis, it was determined that a 1-hr processing time was insufficient for 93A infusion into LLDPE, scCO_2 has the capability to improve intercalation/exfoliation behavior after 93A is within LLDPE and increasing the compatibility of LLDPE affects the dispersion kinetics of 93A during scCO_2 processing. After a thorough analysis of the samples, it is proposed that intercalation by the polymer into the clay gallery did not occur and increases in the gallery height were the result of surfactant chain conformation changes. The largest conformation increases during scCO_2 processing of 93A with LLDPE were brought about by high-temperature and low-pressure conditions, improving the mobility of surfactant chains via enhancement of plasticization and reduction of compression forces. Increased packing from surfactant mobilization led to increases in the angle of tilt for surfactant chains, expanding the gallery. Considering the chemical compatibility of the processing components, the application of LLDPE-g-MA permitted the enhancement of intercalation/exfoliation behavior at a lower temperature than that for LLDPE. The reduction in processing temperature is the result of the increased affinity of the LLDPE-g-MA for CO_2 and clay, enabling greater polymer dissolution and polymer-clay interaction.

Further analysis on LLDPE and LLDPE-g-MA samples was conducted with DSC, TGA, FTIR and SEM, which were used to determine the effect of processing conditions on crystallinity, thermal stability, clay infusion quantity, clay particle size, clay morphology, and depth of clay infusion. Varying the scCO_2 -processing conditions did not significantly alter the crystallinity or thermal stability of the samples. Although, in terms of crystallinity, some trends emerged that could be significant, such as higher

crystallinities were observed with LLDPE/93A samples processed at higher temperatures and LLDPE-g-MA/93A samples processed at higher pressures. As compared to LLDPE, the increased influence of pressure on crystallinity for LLDPE-g-MA is attributed to its higher compatibility with CO₂. At low-temperature and high-pressure conditions, where the extraction potential was the highest and low molecular weight compounds could be removed, it was observed that the thermal stability for both polymers was the highest in comparison to the other conditions investigated while clay infusion quantity was observed to be almost nonexistent. For LLDPE, little to no clay infusion was achieved for all processing conditions investigated, which is postulated to be primarily due to the incompatibility between LLDPE, 93A and CO₂. However, the processing conditions did influence the amount of 93A infused into LLDPE-g-MA. The largest 93A infusion quantity was 1.34 wt%, which was observed for the high-temperature and high-pressure processing conditions. This is the result of the high temperature increasing plasticization of the polymer and diffusion rate of the CO₂. In comparison to LLDPE, LLDPE-g-MA had a greater 93A infusion quantity due to its maleic anhydride modification increasing its compatibility with 93A and CO₂. Particles of 93A were observed to predominantly exist in agglomerated configurations and their size distribution was similar to that of as-received 93A. Infusion of 93A particles was observed to have reached a depth within the center region of the polymer. In addition, the high-temperature scCO₂-processing conditions were able to significantly alter the appearance of the interior of the LLDPE-g-MA by introducing fissures and/or bubbles into the polymer.

In future work employing scCO₂ processing to disperse 93A into LLDPE and LLDPE-g-MA, experiments should be conducted with higher temperatures and lower

pressures to determine the optimum processing conditions for enhancing dispersion. Investigation of temperatures up to the surfactant degradation temperature ($\sim 212^{\circ}\text{C}^7$) would reveal the effect of molten polymer as well as the temperature dependency of the process. Experimenting with reduced pressures would lead to determination of the critical pressure, whereby the hydraulic pressure effect is minimized and CO_2 concentration is maximized, optimizing chain mobility to enhance dispersion. Employing higher temperatures in conjunction with lower pressures would also elucidate if further decreases in fluid density continue to increase gallery height, following the same trend as the results of this work. In terms of 93A infusion quantity, investigation into higher pressures with higher temperatures for LLDPE-g-MA samples would also be beneficial since high-temperature and high-pressure conditions exhibited the greatest infusion potential. After determining the optimal processing conditions, further investigation into other processing parameters such as clay particle size should be undertaken. By delaminating clay platelets prior to processing with polymer, it would be possible to determine if the smaller platelet particles allow increased clay infusion amount as compared to agglomerated stacked platelets. And if clay can be sufficiently exfoliated in scCO_2 , it is proposed that polymer and clay could undergo processing in separate but connected chambers. After the clay has been exfoliated and the polymer has been dissolved by the CO_2 , the exfoliated clay could then be injected into the polymer chamber to undergo infusion, potentially allowing the creation of exfoliated PCN's with a single working fluid.

APPENDIX

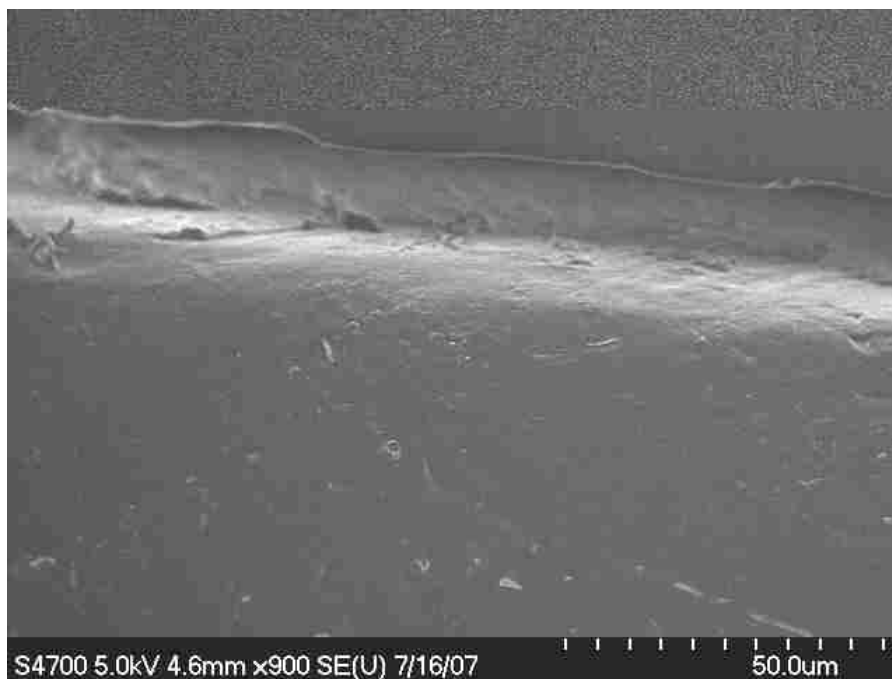


Figure A.1. SEM micrograph of 93A processed with LLDPE in scCO₂ for 1 hr

XRD

The tables below include the Bragg angle 2θ that was used to calculate the d_{001} -spacing for LLDPE/93A and LLDPE-g-MA/93A samples with Bragg's law from Equation (1).

Table A.1. CO₂ density vs. 2θ and d_{001} -spacing of pellet LLDPE/93A samples from XRD analysis

Sample	ρ_{CO_2} (g/cm ³)	2θ	d_{001} -spacing (Å)
Pure 93A	NA	3.415	25.9
+ -	0.200	3.145	2.81
- -	0.325	3.235	2.73
+ +	0.402	3.235	2.73

Table A.2. CO₂ density vs. 2θ and d_{001} -spacing of LLDPE-g-MA/93A samples from XRD analysis

Sample	ρ_{CO_2} (g/cm ³)	2θ	d_{001} -spacing (Å)
Pure 93A	NA	3.625	24.4
+ -	0.200	3.415	25.9
- -	0.325	3.295	26.8
+ +	0.402	3.775	23.4

DSC

Below are tables of the melting enthalpy obtained from DSC curves that were used to calculate the crystallinity of LLDPE/93A and LLDPE-g-MA/93A samples with Equation (4).

Table A.3. Melting enthalpy and crystallinity for heating 1 and heating 2 of LLDPE/93A samples from DSC analysis

Sample	Heating 1		Heating 2	
	H _f (J/g)	Crystallinity (%)	H _f (J/g)	Crystallinity (%)
LLDPE	101.5	34.64	105.8	36.11
--	103.7	35.39	115.2	39.32
--+	99.9	34.10	109.7	37.44
+--	108.2	36.93	112.0	38.23
+++	108.4	37.00	111.6	38.09

Table A.4. Melting enthalpy and crystallinity for heating 1 and heating 2 of LLDPE-g-MA/93A samples from DSC analysis

Sample	Heating 1		Heating 2	
	H _f (J/g)	Crystallinity (%)	H _f (J/g)	Crystallinity (%)
LLDPE-g-MA	140.3	47.88	144.8	49.42
--	141.3	48.23	146.7	50.07
--+	144.2	49.22	148.2	50.58
+--	142.2	48.53	141.0	48.12
+++	149.9	51.16	148.6	50.72

TGA

The figures below illustrate how values concerning the main decomposition of LLDPE/93A and LLDPE-g-MA/93A samples were calculated from TGA plots using Universal Analysis software from TA Instruments by employing the “Tg (Glass/Step Transition)” function.

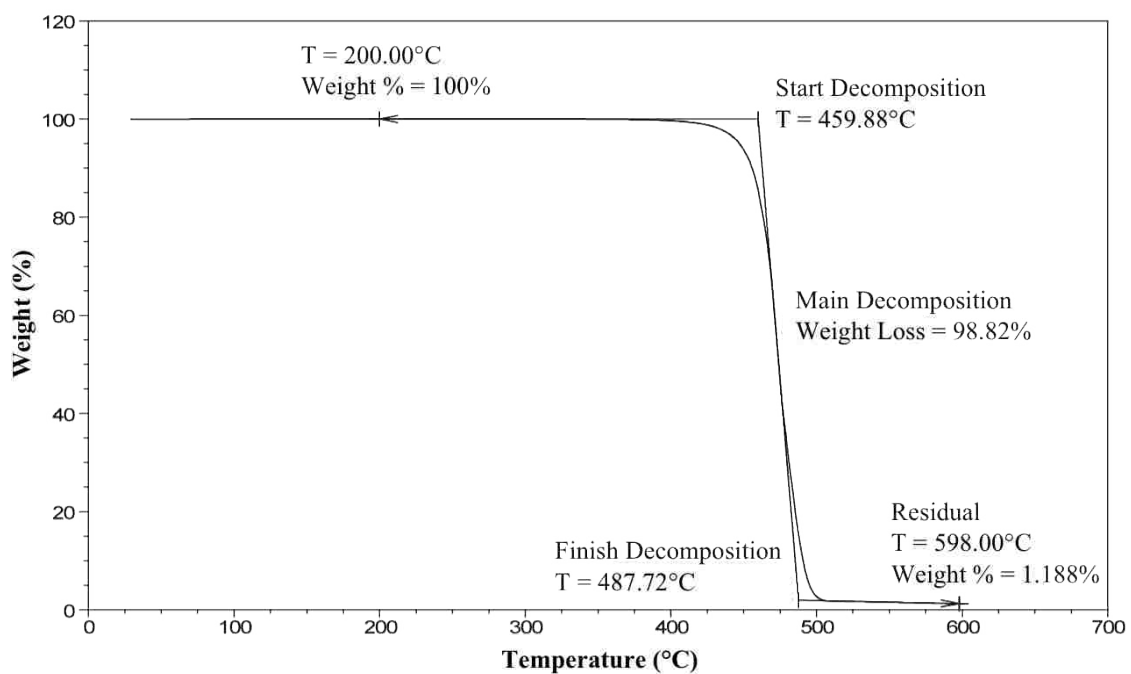


Figure A.2. Decomposition values for pure LLDPE from TGA

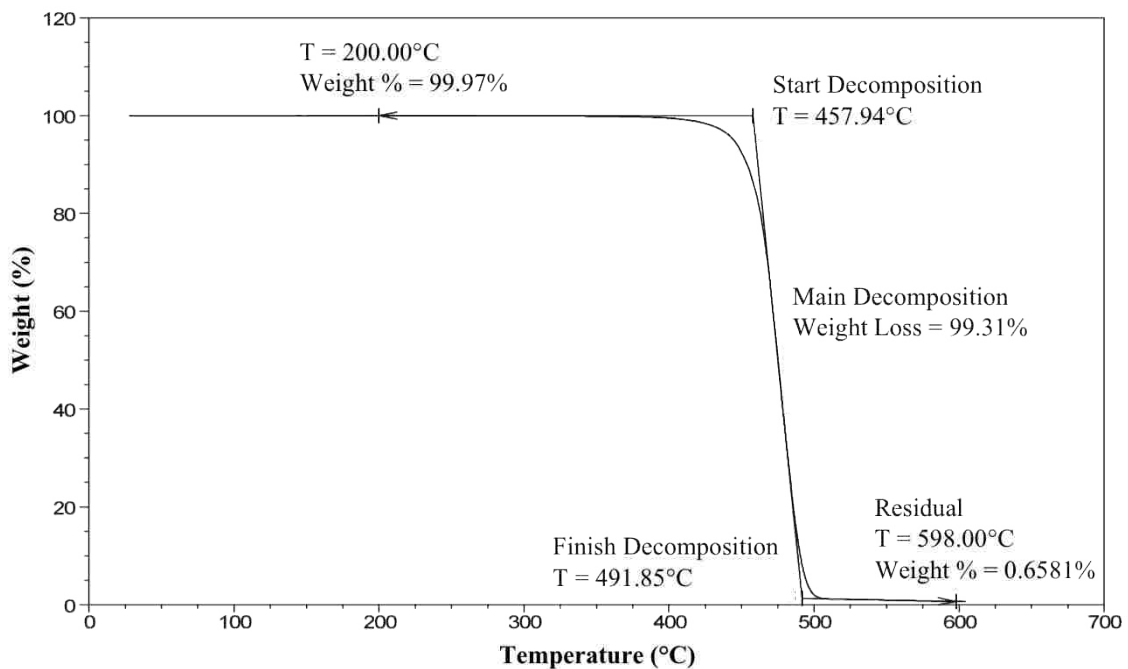


Figure A.3. Decomposition values for LLDPE/93A sample (-) from TGA

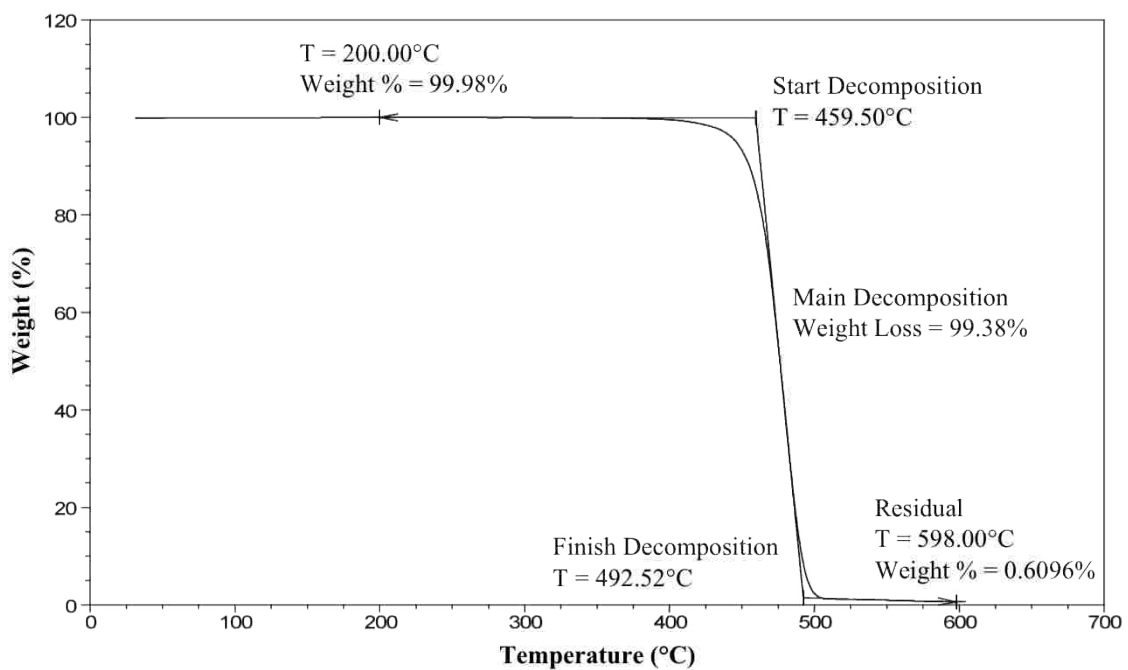


Figure A.4. Decomposition values for LLDPE/93A sample (-+) from TGA

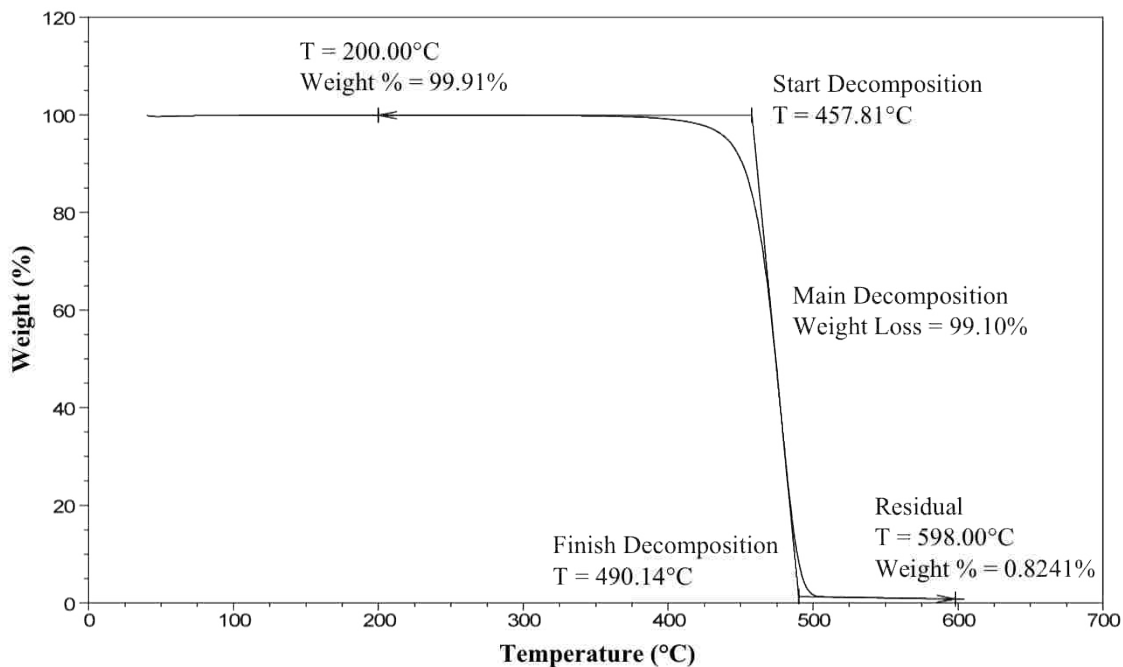


Figure A.5. Decomposition values for LLDPE/93A sample (+ -) from TGA

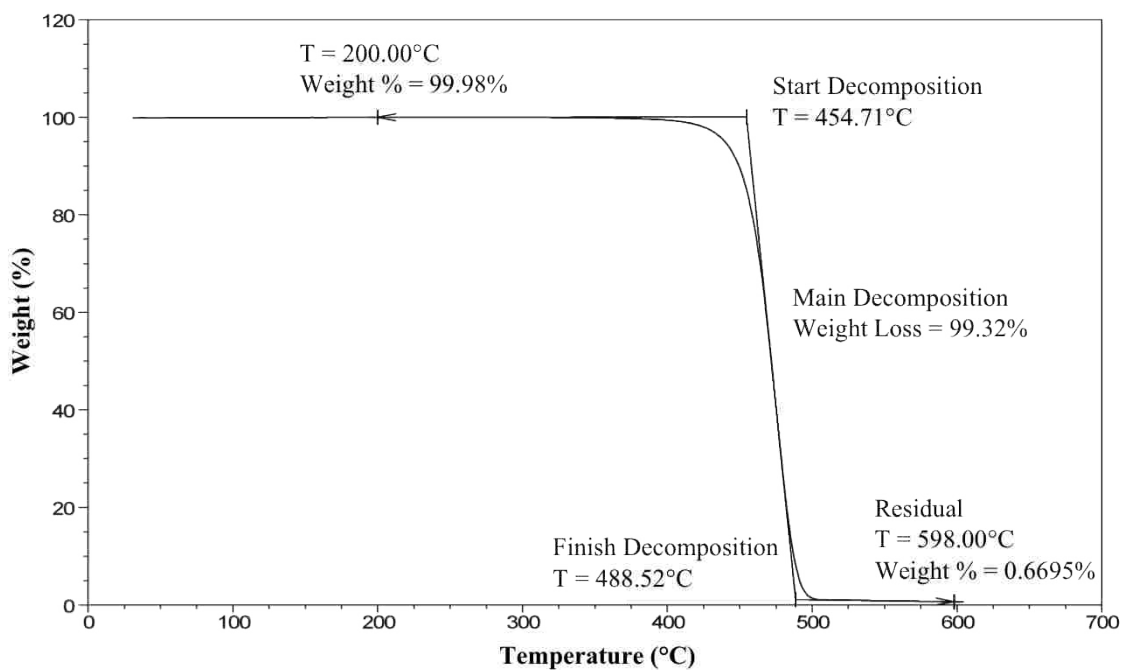


Figure A.6. Decomposition values for LLDPE/93A sample (+ +) from TGA

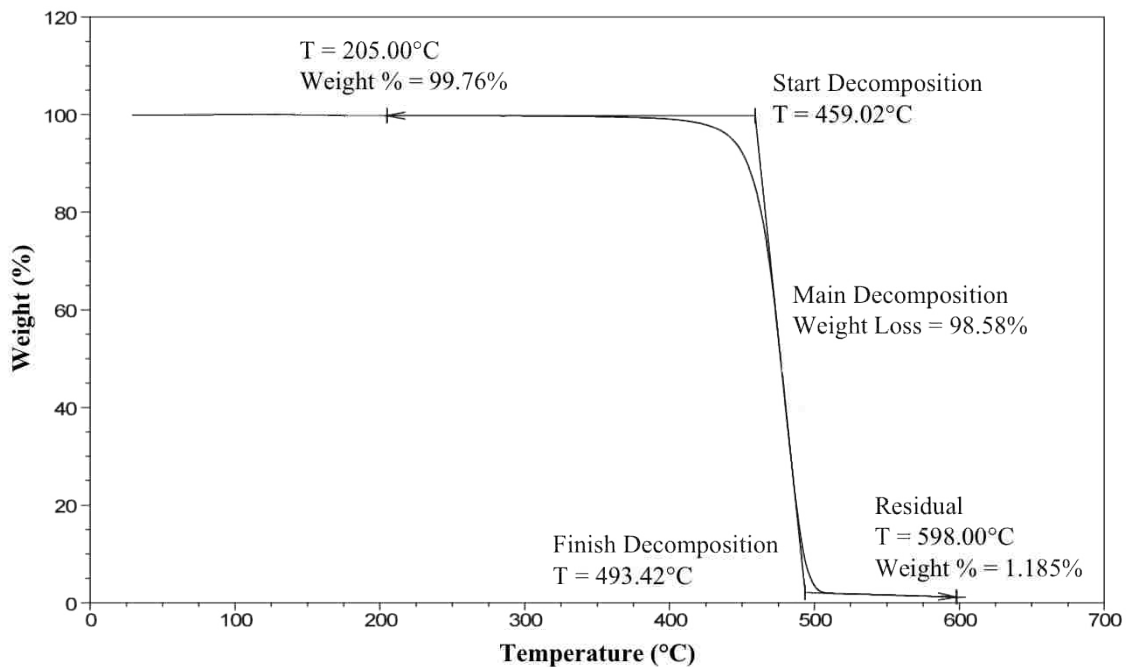


Figure A.7. Decomposition values for pure LLDPE-g-MA/93A from TGA

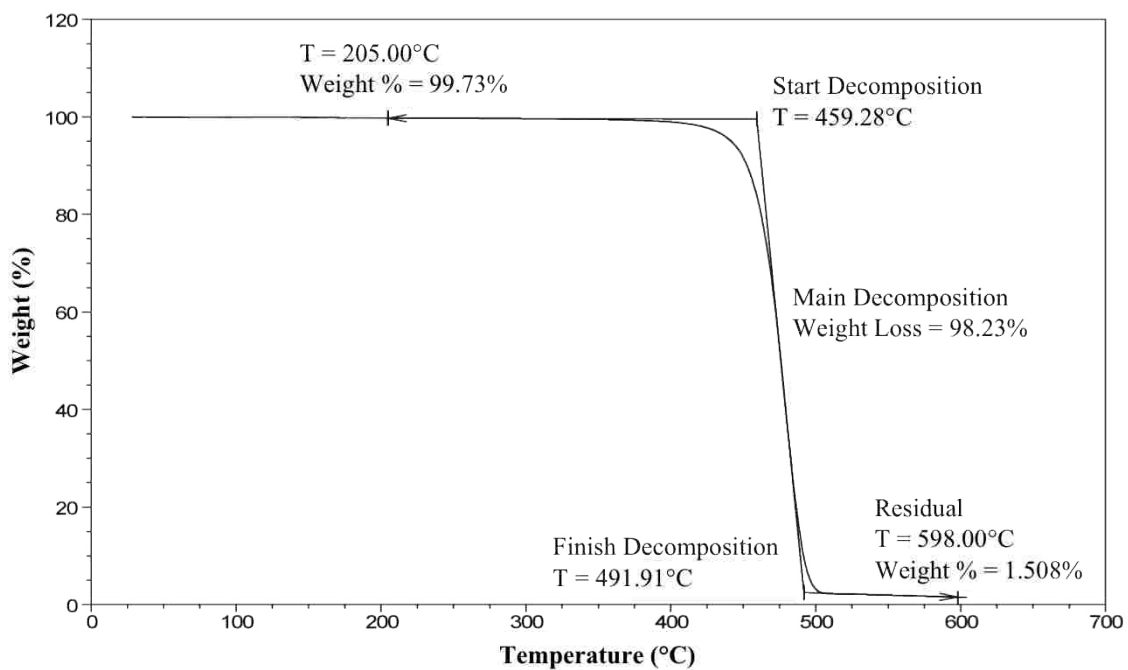


Figure A.8. Decomposition values for LLDPE-g-MA/93A sample (-) from TGA

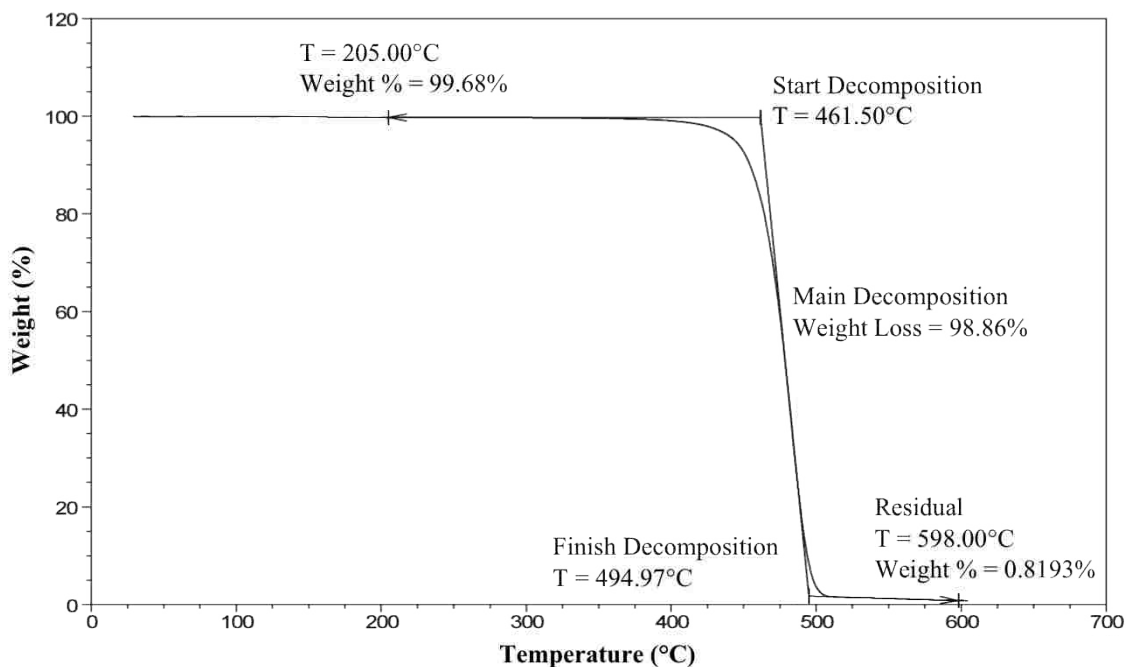


Figure A.9. Decomposition values for LLDPE-g-MA/93A sample (- +) from TGA

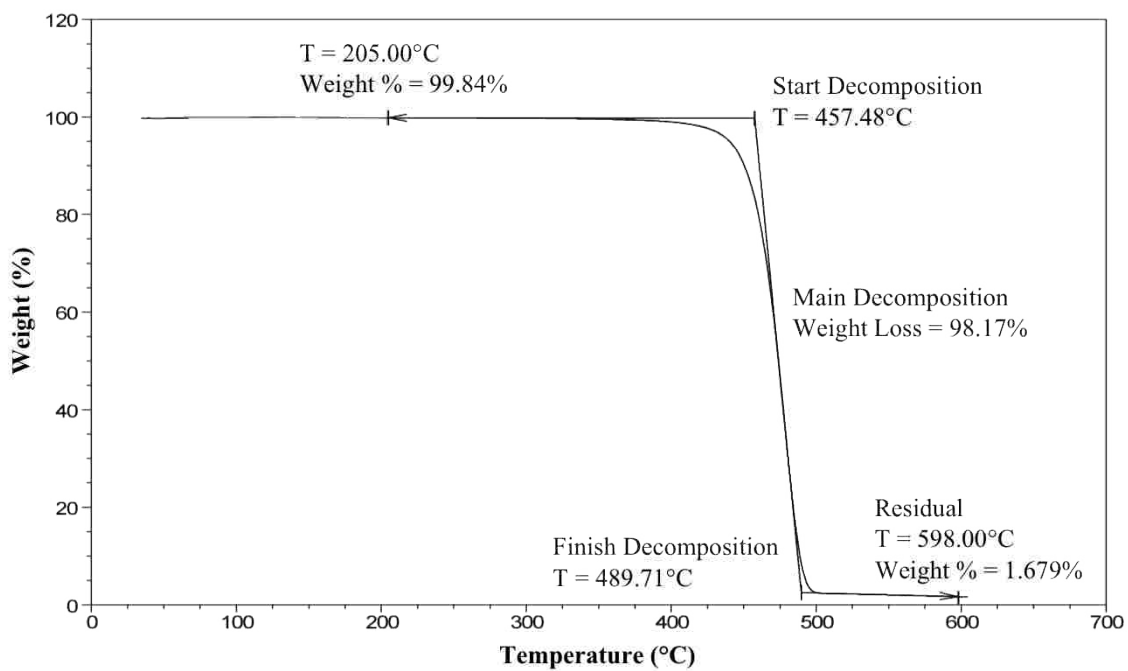


Figure A.10. Decomposition values for LLDPE-g-MA/93A sample (+ -) from TGA

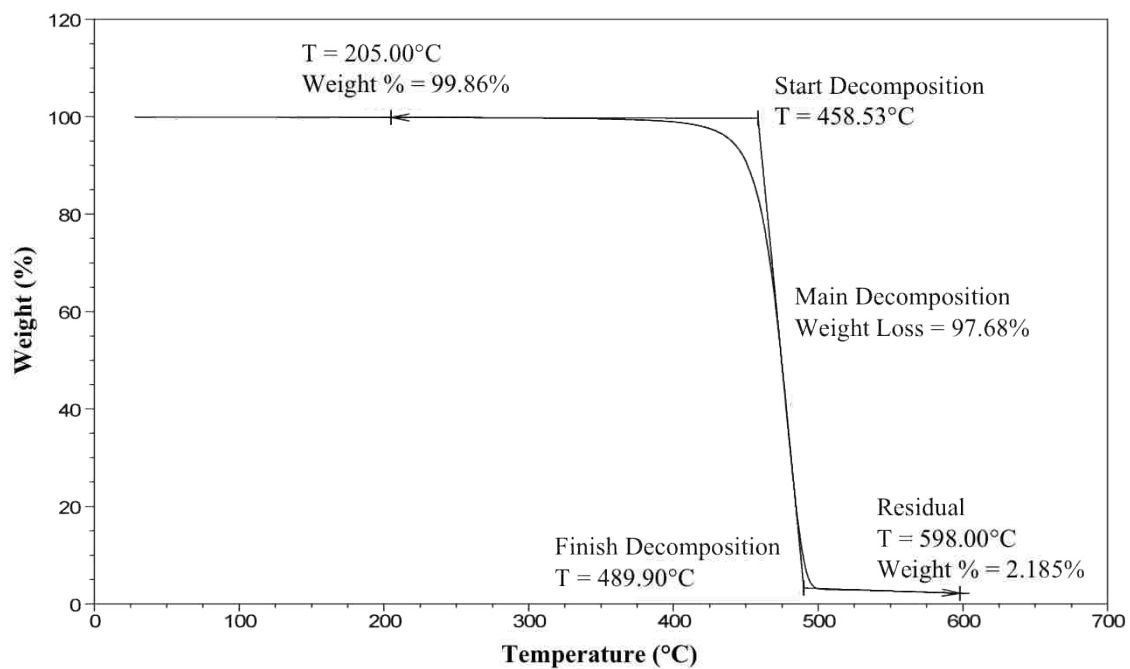


Figure A.11. Decomposition values for LLDPE-g-MA/93A sample (+ +) from TGA

FTIR

This section presents a more detailed description on using FTIR spectra to calculate the weight percent of 93A in samples by demonstrating with samples containing 0 to 0.25 wt% 93A. With FTIR spectra for standard samples, Spekwin32 software was used to obtain the absorbance for peaks at 522 cm^{-1} (A_1) and 2019 cm^{-1} (A_2) by integrating the area under the peak. The limits of integration were from 496 to 583 cm^{-1} for the peak at 522 cm^{-1} and from 1980 to 2100 cm^{-1} for the peak at 2019 cm^{-1} . Next, the ratio of the mass of 93A to the mass of LLDPE (m_{93A}/m_{LLDPE}), which is equivalent to C_{93A}/C_{LLDPE} , was plotted vs. A_1/A_2 for sample standards. A line was regressed through this data (Figure 5.22) to obtain the calibration curve (Equation (A1)) as well as the associated Pearson autocorrelation coefficient and standard error.

$$\frac{A_1}{A_2} = 205.478 \frac{C_{93A}}{C_{LLDPE}} + 0.139 \quad (\text{A1})$$

Using the absorbance ratios (A_1/A_2) obtained from sample spectra, the weight percent of 93A ($C_{93A}(\%)$) in samples was calculated with the rearranged form of Equation (A1) below:

$$C_{93A}(\%) = \left(\left(\frac{\frac{A_1}{A_2} - 0.139}{205.478} \right)^{-1} + 1 \right)^{-1} \times 100 \quad (\text{A2})$$

SEM

Table A.5. Location, depth and size dimensions of clay particles for LLDPE-g-MA/93A sample (– –)

Location	Depth (μm)	Size Dimension	
		Minor (μm)	Major (μm)
Edge	-	1.8	3.0
Edge	0	2.8	3.5
Edge	7	3.5	5.0
Edge	31	0.9	1.5
Edge	220	7.3	10.0
Interior	-	9.5	11.2
Interior	653	2.1	2.7
Interior	797	7.8	11.5
Interior	797	9.4	13.6
Center	-	23.0	43.8
Center	-	3.2	6.2
Center	1000	10.5	11.2

Table A.6. Location, depth and size dimensions of clay particles for LLDPE-g-MA/93A sample (+ -)

Location	Depth (μm)	Size Dimension	
		Minor (μm)	Major (μm)
Edge	-	15.8	20.4
Edge	119	9.5	9.7
Edge	178	8.6	9.8
Edge	178	4.6	11.0
Edge	210	3.1	4.1
Edge	210	1.4	3.2
Edge	225	11.8	13.1
Edge	261	1.3	1.9
Edge	287	8.5	11.8
Edge	311	2.3	2.4
Edge	351	10.6	15.3
Edge	362	8.2	11.7
Interior	526	10.4	16.0
Interior	834	5.4	6.9
Interior	982	4.1	6.3
Center	-	12.4	22.6
Center	-	2.4	3.5
Center	-	0.9	1.3
Center	-	3.2	4.2
Center	1180	1.4	1.5
Center	1400	1.4	1.9

Table A.7. Location, depth and size dimensions of clay particles for LLDPE-g-MA/93A sample (+ +)

Location	Depth (μm)	Size Dimension	
		Minor (μm)	Major (μm)
Edge	-	9.2	15.8
Edge	3	0.9	1.0
Edge	22	2.7	5.7
Interior	558	35.0	52.4
Interior	661	3.0	4.2
Interior	900	4.0	5.1
Interior	985	3.4	5.9
Center	-	6.0	7.7
Center	1000	9.0	15.0
Center	1280	4.2	7.9

BIBLIOGRAPHY

1. Kojima, Y.; Usuki, A.; Kawasumi, M.; Okada, A.; Fukushima, Y.; Kurauchi, T.; Kamigaito, O. Mechanical Properties of Nylon 6-Clay Hybrid. *Journal of Materials Research* **1993**, *8*, 1185-1189.
2. Kawasumi, M. The Discovery of Polymer-Clay Hybrids. *Journal of Polymer Science Part A: Polymer Chemistry* **2004**, *42*, 819-824.
3. Utracki, L. A. *Clay-Containing Polymeric Nanocomposites: Volume 1*; Rapra Technology Limited, UK, 2004.
4. Sandí, G.; Carrado, K. A.; Joachin, H.; Lu, W.; Prakash, J. Polymer Nanocomposites for Lithium Battery Applications. *Journal of Power Sources* **2003**, *119-121*, 492-496.
5. Song, M.; Park, S.; Kim, Y.; Kim, K.; Min, S.; Rhee, H. Characterization of Polymer-Layered Silicate Nanocomposite Membranes for Direct Methanol Fuel Cells. *Electrochimica Acta* **2004**, *50*, 639-643.
6. Ito, B. I.; Freitas, J. N. D.; Paoli, M.-A. D.; Nogueira, A. F. Application of a Composite Polymer Electrolyte Based on Montmorillonite in Dye-Sensitized Solar Cells. *The Journal of the Brazilian Chemical Society* **2008**, *19*, 688-696.
7. Cervantes-Uc, J. M.; Cauich-Rodriguez, J. V.; Vazquez-Torres, H.; Garfias-Mesias, L. F.; Paul, D. R. Thermal Degradation of Commercially Available Organoclays Studied by TGA–FTIR. *Thermochimica Acta* **2007**, *457*, 92-102.
8. Nalawade, S. P.; Picchioni, F.; Janssen, L. P. B. M. Supercritical Carbon Dioxide as a Green Solvent for Processing Polymer Melts: Processing Aspects and Applications. *Progress in Polymer Science* **2006**, *31*, 19-43.
9. Berens, A. R.; Huvard, G. S.; Korsmeyer, R. W.; Kunig, F. W. Application of Compressed Carbon Dioxide in the Incorporation of Additives into Polymers. *Journal of Applied Polymer Science* **1992**, *46*, 231-242.
10. Osswald, T. A.; Baur, E.; Brinkmann, S.; Oberbach, K.; Schmachtenberg, E. *International Plastics Handbook: The Resource for Plastics Engineers*; 4th ed. Hanser Gardner Publications, Inc.: Cincinnati, 2006.
11. Callister, W. D. J. Thermoplastic and Thermosetting Polymers. In *Materials Science and Engineering: An Introduction*; John Wiley & Sons, Inc.: New York, 2003; p. 467.

12. Fried, J. R. *Polymer Science and Technology*; Prentice Hall Professional Technical Reference: New Jersey, 2003.
13. Whiteley, K. S.; Heggs, T. G.; Koch, H.; Mawer, R. L.; Immel, W. *Polyolefins*; Wiley-VCH Verlag GmbH & Co. KGaA: Weinheim, 2005.
14. Carey, F. A. *Organic Chemistry*; 4th ed. McGraw Hill: Boston, 2000.
15. Fang, Y.; Liu, B.; Terano, M. Various Activation Procedures of Phillips Catalyst for Ethylene Polymerization. *Kinetics and Catalysis* **2006**, *47*, 295-302.
16. Chen, B. Polymer–Clay Nanocomposites: An Overview with Emphasis on Interaction Mechanisms. *British Ceramic Transactions* **2004**, *103*, 241-249.
17. Ngo, T.-D.; Wood-Adams, P. M.; Hoa, S. V.; Ton-That, M.-T. Modeling the Delamination Process During Shear Premixing of Nanoclay/Thermoset Polymer Nanocomposites. *Journal of Applied Polymer Science* **2011**, *122*, 561-572.
18. Peprnicek, T.; Kalendova, A.; Pavlova, E.; Simonik, J.; Duchet, J.; Gerard, J. F. Poly(Vinyl Chloride)-Paste/Clay Nanocomposites: Investigation of Thermal and Morphological Characteristics. *Polymer Degradation and Stability* **2006**, *91*, 3322-3329.
19. Lyatskaya, Y.; Balazs, A. C. Modeling the Phase Behavior of Polymer–Clay Composites. *Macromolecules* **1998**, *31*, 6676-6680.
20. Park, C. I.; Park, O. O.; Lim, J. G.; Kim, H. J. The Fabrication of Syndiotactic Polystyrene/Organophilic Clay Nanocomposites and Their Properties. *Polymer* **2001**, *42*, 7465–7475.
21. Bish, D. L.; Post, J. E. *Modern Powder Diffraction*; The Mineralogical Society of America: Washington, D.C., 1989.
22. Wachtman, J. B.; Kalman, Z. H. *Characterization of Materials*; Butterworth-Heinemann: Stoneham, 1993.
23. *Introduction to Fourier Transform Infrared Spectrometry*; Thermo Nicolet Corporation: Madison, WI, 2001.
24. Factor, M. J.; Lee, S. Quantitative Analysis of Cloisite 93A Infused into Linear Low-Density Polyethylene (LLDPE) and Maleated Linear Low-Density Polyethylene (LLDPE-g-MA) in a Supercritical Carbon Dioxide Medium. *Journal of Applied Polymer Science* **2012**, *124*, 3329-3333.
25. Egerton, R. F. *Physical Principles of Electron Microscopy: An Introduction to TEM, SEM, and AEM*; Springer: New York, 2005.

26. Wang, W. *Reverse Engineering: Technology of Reinvention*; CRC Press: Boca Raton, 2011.
27. Kaur, H. *Instrumental Methods of Chemical Analysis*; Global Media: Meerut, IND, 2010.
28. *A Beginner's Guide to Thermogravimetric Analysis (TGA)*; PerkinElmer, Inc.: Waltham, MA, 2010.
29. Hohne, G. W. H.; Hemminger, W. F.; Flammersheim, H.-J. *Differential Scanning Calorimetry*; 2nd ed. Springer: New York, 2003.
30. Lee, S.; Lanterman, H. B.; Sardesai, A.; Wenzel, J.; Marshall, B.; Yen, J.; Amin-Sanayei, R.; Moucharik, M. Polymerization of Poly(vinylidene fluoride) in a Supercritical Fluid Medium. U.S. Patent No. 7,091,288, August 15, 2006.
31. Boyle, T. B.; Carroll, J. J. Study Determines Best Methods for Calculating Acid-Gas Density. *Oil & Gas Journal* **2002**, *100*, 45-53.
32. Shieh, Y. T.; Su, J. H.; Manivannan, G.; Lee, P. H. C.; Sawan, S. P.; Spall, W. D. Interaction of Supercritical Carbon Dioxide with Polymers. I. Crystalline Polymers. *Journal of applied polymer science* **1996**, *59*, 695-705.
33. Ganapathy, H.; Yuvaraj, H.; Hwang, H.; Kim, J.; Choi, B.; Gal, Y.; Lim, K. CO₂-Soluble Semiconducting Polymers Synthesized in Supercritical Carbon Dioxide. *Synthetic Metals* **2006**, *156*, 576-581.
34. Alessi, P.; Cortesi, A.; Kikic, I.; Vecchione, F. Plasticization of Polymers with Supercritical Carbon Dioxide: Experimental Determination of Glass-Transition Temperatures. *Journal of Applied Polymer Science* **2003**, *88*, 2189-2193.
35. Shieh, Y. T.; Su, J. H.; Manivannan, G.; Lee, P. H. C.; Sawan, S. P.; Spall, W. D. Interaction of Supercritical Carbon Dioxide with Polymers. II. Amorphous Polymers. *Journal of Applied Polymer Science* **1996**, *59*, 707-717.
36. Brantley, N. H.; Kazarian, S. G.; Eckert, C. a In situ FTIR measurement of carbon dioxide sorption into poly(ethylene terephthalate) at elevated pressures. *Journal of Applied Polymer Science* **2000**, *77*, 764-775.
37. Areerat, S.; Funami, E.; Hayata, Y.; Nakagawa, D.; Ohshima, M. Measurement and Prediction of Diffusion Coefficients of Supercritical CO₂ in Molten Polymers. *Polymer Engineering and Science* **2004**, *44*, 1915-1924.
38. Duarte, A. R. C.; Martins, C.; Coimbra, P.; Gil, M. H. M.; de Sousa, H. C.; Duarte, C. M. M. Sorption and Diffusion of Dense Carbon Dioxide in a Biocompatible Polymer. *The Journal of Supercritical Fluids* **2006**, *38*, 392-398.

39. Muth, O.; Hirth, T.; Vogel, H. Investigation of Sorption and Diffusion of Supercritical Carbon Dioxide into Poly(vinyl chloride). *Journal of Supercritical Fluids* **2001**, *19*, 299- 306.
40. Thompson, M. R.; Balogh, M. P.; Speer, R. L.; Fasulo, P. D.; Rodgers, W. R. In Situ X-Ray Diffraction Studies of Alkyl Quaternary Ammonium Montmorillonite in a CO₂ Environment. *The Journal of Chemical Physics* **2009**, *130*, 1-8.
41. Horsch, S.; Serhatkulu, G.; Gulari, E.; Kannan, R. M. Supercritical CO₂ Dispersion of Nano-Clays and Clay/Polymer Nanocomposites. *Polymer* **2006**, *47*, 7485-7496.
42. Manitiu, M.; Bellair, R. J.; Horsch, S.; Gulari, E.; Kannan, R. M. Supercritical Carbon Dioxide-Processed Dispersed Polystyrene–Clay Nanocomposites. *Macromolecules* **2008**, *41*, 8038-8046.
43. Manke, C. W.; Gulari, E.; Mielewski, D. F.; Lee, E. C. C. System and Method of Delaminating a Layered Silicate Material by Supercritical Fluid Treatment. U.S. Patent No. 6,469,073 B1, October 22, 2002.
44. Wang, K. H.; Choi, M. H.; Koo, C. M.; Choi, Y. S.; Chung, I. J. Synthesis and Characterization of Maleated Polyethylene/Clay Nanocomposites. *Polymer* **2001**, *42*, 9819–9826.
45. Luyt, A. S.; Geethamma, V. G. Effect of Oxidized Paraffin Wax on the Thermal and Mechanical Properties of Linear Low-Density Polyethylene-Layered Silicate Nanocomposites. *Polymer Testing* **2007**, *26*, 461-470.
46. Ryu, S. H.; Chang, Y.-W. Factors Affecting the Dispersion of Montmorillonite in LLDPE Nanocomposite. *Polymer Bulletin* **2005**, *55*, 385-392.
47. McHugh, M. A.; Park, I.-H.; Reisinger, J. J.; Ren, Y.; Lodge, T. P.; Hillmyer, M. A. Solubility of CF₂-Modified Polybutadiene and Polyisoprene in Supercritical Carbon Dioxide. *Macromolecules* **2002**, *35*, 4653-4657.
48. Morgan, A. B.; Gilman, J. W. Characterization of polymer-layered silicate (clay) nanocomposites by transmission electron microscopy and X-ray diffraction: A comparative study. *Journal of Applied Polymer Science* **2003**, *87*, 1329–1338.
49. Thompson, M. R.; Liu, J.; Krump, H.; Kostanski, L. K.; Fasulo, P. D.; Rodgers, W. R. Interaction of Supercritical CO₂ with Alkyl-Ammonium Organoclays: Changes in Morphology. *Journal of Colloid and Interface Science* **2008**, *324*, 177-84.

50. Xi, Y.; Frost, R. L.; He, H. Modification of the Surfaces of Wyoming Montmorillonite by the Cationic Surfactants Alkyl Trimethyl, Dialkyl Dimethyl, and Trialkyl Methyl Ammonium Bromides. *Journal of Colloid and Interface Science* **2007**, *305*, 150-158.
51. Schubnell, M. Determination of Polymer Crystallinity with DSC Measurements. *UserCom* **2001**, *13*, 12-13.
52. Clark, K. Synthesis of Maleated Poly(Vinylidene Fluoride) in Supercritical Carbon Dioxide Medium. Ph. D. Dissertation, University of Missouri – Columbia, Columbia, MO, 2004.

VITA

Matthew John Factor was born in St. Louis, Missouri. His undergraduate education started in 2001 at the University of Missouri – Columbia and was completed in 2005 with the attainment of a B.S. in Chemical Engineering. In 2012, he obtained a Ph.D. in Chemical Engineering from the Missouri University of Science and Technology.

